LAWRENCE
LIVERMORE
NATIONAL
LABORATORY

LLNL-TR-623455

Exploring the plutonic crust at a fast-spreading ridge:new drilling at Hess Deep

K. M. Gillis, J. E. Snow, A. Klaus, G. Guerin, N. Abe, N. Akizawa, G. Ceuleneer, M. J. Cheadle, A. B. Adriao, K. Faak, T. J. Falloon, S. A. Friedman, M. M. Godard, Y. Harigane, A. J. Horst, T. Hoshide, B. Ildefonse, M. M. Jean, B. E. John, J. H. Koepke, S. Machi, J. Maeda, N. E. Marks, A. M. McCaig, R. Meyer, A. Morris, T. Nozaka, M. Python, A. Saha, R. P. Wintsch

February 28, 2013

Disclaimer

This work performed under the auspices of the U.S. Department of Energy by Lawrence Livermore National Laboratory under Contract DE-AC52-07NA27344.

Integrated Ocean Drilling Program
Expedition 345 Preliminary Report

Hess Deep Plutonic Crust

Exploring the plutonic crust at a fast-spreading ridge: new drilling at Hess Deep

11 December 2012–12 February 2013

Expedition 345 Scientists

Published by
Integrated Ocean Drilling Program Management International, Inc.,
for the Integrated Ocean Drilling Program

Publisher's notes

Citation:

Expedition 345 Scientists, 2013. Hess Deep plutonic crust: exploring the plutonic crust at a fast-spreading ridge: new drilling at Hess Deep. *IODP Prel. Rept.,* 345. doi:10.2204/iodp.pr.345.2014

Distribution:
Electronic copies of this series may be obtained from the Integrated Ocean Drilling Program (IODP) Scientific Publications homepage on the World Wide Web at **www.iodp.org/scientific-publications/.**

This publication was prepared by the Integrated Ocean Drilling Program U.S. Implementing Organization (IODP-USIO): Consortium for Ocean Leadership, Lamont Doherty Earth Observatory of Columbia University, and Texas A&M University, as an account of work performed under the international Integrated Ocean Drilling Program, which is managed by IODP Management International (IODP-MI), Inc. Funding for the program is provided by the following agencies:

National Science Foundation (NSF), United States

Ministry of Education, Culture, Sports, Science and Technology (MEXT), Japan

European Consortium for Ocean Research Drilling (ECORD)

Ministry of Science and Technology (MOST), People's Republic of China

Korea Institute of Geoscience and Mineral Resources (KIGAM)

Australian Research Council (ARC) and GNS Science (New Zealand), Australian/New Zealand Consortium

Ministry of Earth Sciences (MoES), India

Coordination for Improvement of Higher Education Personnel, Brazil

Disclaimer

January 2014

Expedition 345 participants

Expedition 345 scientists

Kathryn M. Gillis
Co-chief Scientist
School of Earth and Ocean Sciences
University of Victoria, B.C.
PO Box 3065 STM CSC
Victoria BC V8W 3V6
Canada
kgillis@uvic.ca

Jonathan E. Snow
Co-chief Scientist
Earth & Atmospheric Sciences
University of Houston
312 Science and Research Building 1
Houston TX 77204-5007
USA
jesnow@uh.edu

Adam Klaus
Expedition Project Manager/Staff Scientist
United States Implementing Organization
Integrated Ocean Drilling Program
Texas A&M University
1000 Discovery Drive
College Station TX 77845
USA
aklaus@iodp.tamu.edu

Gilles Guerin
Logging Staff Scientist
Borehole Research Group
Lamont-Doherty Earth Observatory of Columbia University
PO Box 1000, 61 Route 9W
Palisades NY 10964
USA
guerin@ldeo.columbia.edu

Natsue Abe
Igneous Petrologist
Institute for Research on Earth Evolution (IFREE)
Japan Agency for Marine-Earth Science and Technology (JAMSTEC)
2-15 Natsushima-cho
Yokosuka Kanagawa 237-0061
Japan
abenatsu@jamstec.go.jp

Norikatsu Akizawa
Physical Properties Specialist
Department of Earth Sciences
Kanazawa University
Kakuma-machi
Kanazawa Ishikawa 920-1192
Japan
no.no-to@stu.kanawawa-u.ac.jp

Georges Ceuleneer
Structural Geologist
Observatoire Midi-Pyrénées (UMS 831), CNRS
Université Paul Sabatier
14 Avenue Edouard Belin
Toulouse Cedex 31400
France
georges.ceuleneer@get.obs-mip.fr

Michael J. Cheadle
Structural Geologist
Department of Geology and Geophysics
University of Wyoming
1000 University Avenue
Department 3006
Laramie WY 82071
USA
cheadle@uwyo.edu

Álden de Brito Adrião
Physical Properties Specialist
IGEO (Geology Institute)
Rio Grande do Sul Federal University
Av. Bento Gonçalves, 9500 Bloco I Prédio 43113 Sala 207
Caixa Postal 15001 CEP 91501-970
Porto Alegre/RS
Brazil
ald.dba@gmail.com

Kathrin Faak
Metamorphic Petrologist
Geologisches Institut
Ruhr Universität Bochum
Universitaetsstrasse 150
Gebaeude NAF 03/167
Bochum 44780
Germany
kathrin.faak@rub.de

Trevor J. Falloon
Igneous Petrologist
Institute for Marine and Antarctic Studies
University of Tasmania
Private Bag 129
Sandy Bay
Hobart TAS 7001
Australia
trevor.falloon@utas.edu.au

Sarah A. Friedman
Paleomagnetist
Department of Geology
Southern Illinois University at Carbondale
Carbondale IL 62901
USA
safriedman@siu.edu

Marguerite M. Godard
Inorganic Geochemist
Geosciences Montpellier-UMR 5243
University Montpellier II
CC 60
Place Eugene Bataillon
Montpellier cedex 5 34095
France
marguerite.godard@um2.fr

Yumiko Harigane
Structural Geologist
Marine Geology Department
National Insitute of Advanced Industrial Science and Technology (AIST)
Geological Survey of Japan
Tsukuba Central 7, 1-1-1 Higashi
Tsukuba Ibaraki 305-8567
Japan
y-harigane@aist.go.jp

Andrew J. Horst
Paleomagnetist
Department of Earth Science
Syracuse University
204 Heroy Geology Laboratory
Syracuse NY 13210
USA
ajhorst@syr.edu

Takashi Hoshide
Igneous Petrologist
Graduate School of Science
Tohoku University
Aoba-ku
Sendai 980-8578
Japan
hoshide@m.tohoku.ac.jp

Benoit Ildefonse
Physical Properties Specialist
Laboratoire de Tectonophysique
University Montpellier II
CC49
Montpellier 34095
France
ildefonse@um2.fr

Marlon M. Jean
Igneous Petrologist
Department of Geology and Environmental Geosciences
Northern Illinois University
Davis Hall 312, Normal Road
DeKalb IL 60115
USA
mmj@niu.edu

Barbara E. John
Structural Geologist
Department of Geology and Geophysics
University of Wyoming
1000 East University
PO Box 3006
Laramie WY 82071
USA
bjohn@uwyo.edu

Juergen H. Koepke
Igneous Petrologist
Institut für Mineralogie
University of Hannover
Callinstrasse 3
Hannover 30167
Germany
koepke@mineralogie.uni-hannover.de

Sumiaki Machi
Physical Properties Specialist
Department of Earth Sciences
Kanazawa University
Kakuma-machi, Kanazawa
Ishikawa 920-1192
Japan
sumiaki@earth.s.kanazawa-u.ac.jp

Jinichiro Maeda
Igneous Petrologist
Department of Natural History Sciences
Hokkaido University
North 10, West 8, Kita-ku
Sapporo Hokkaido 060-0810
Japan
jinmaeda@mail.sci.hokudai.ac.jp

Naomi E. Marks
Metamorphic Petrologist
Chemistry and Material Sciences Department
Lawrence Livermore National Laboratory
PO Box 808, L-231
Livermore CA 94551
USA
marks23@llnl.gov

Andrew M. McCaig
Metamorphic Petrologist
School of Earth and Environment
University of Leeds
Leeds LS2 9JT
United Kingdom
A.M.McCaig@leeds.ac.uk

Romain Meyer
Inorganic Geochemist
Department of Earth Science and Centre for Geobiology
University of Bergen
Allegaten 41
Bergen 5007
Norway
romain.meyer@geo.uib.no

Antony Morris
Paleomagnetist
School of Earth, Ocean & Environmental Sciences
University of Plymouth
Drake Circus
Plymouth PL4 8AA
United Kingdom
amorris@plymouth.ac.uk

Toshio Nozaka
Metamorphic Petrologist
Department of Earth Sciences
Okayama University
3-1-1 Tsushima-naka
Okayama 700-8530
Japan
nozaka@cc.okayama-u.ac.jp

Marie Python
Metamorphic Petrologist
Department of Earth and Planetary Sciences
Hokkaido University
North 10, West 8, Kita-ku
Sapporo Hokkaido 060-0810
Japan
marie@sci.hokudai.ac.jp

Abhishek Saha
Inorganic Geochemist
Centre for Earth Sciences
Indian Institute of Science
Bangalore 560 012
India
asaha.geocal@gmail.com

Robert P. Wintsch
Metamorphic Petrologist
Department of Geological Sciences
Indiana University
1005 East 10th Street
Bloomington IN 47405
USA
wintsch@indiana.edu

SIEM Offshore AS officials

Steve Breadley
Master of the Drilling Vessel

Wayne Malone
Offshore Installation Manager

Education and outreach

Jean-Luc Berenguer
Education Officer
Centre International de Valbonne
Université de Nice Sophia Antipolis
BP 97, Valbonne
Sophia Antipolis 06902
France
jean-luc.berenguer@ac-nice.fr

Susan Gebbels
Education Officer
Craghead, Whitfield
Hexham
Northumberland NE47 8JY
United Kingdom
susan.gebbels@newcastle.ac.uk

Nicole Kurtz
Education Officer
15825 Van Aken Boulevard
Number 203
Shaker Heights OH 44120
USA
kurtz588@gmail.com

Technical support

Michael Bertoli
Chemistry Laboratory

Lisa Brandt
Chemistry Laboratory

Kristin (Hillis) Bronk
X-ray/Microbiology Laboratory

Timothy Bronk
Assistant Laboratory Officer

Chad Broyles
Curatorial Specialist

William Crawford
Imaging Specialist

Lisa Crowder
Assistant Laboratory Officer

David Fackler
Applications Developer

Emily Fisher
Downhole/Thin Section Laboratory

Tim Fulton
Publications Specialist

Clayton Furman
Logging Engineer

Randy Gjesvold
Marine Instrumentation Specialist

Thomas Gorgas
Physical Properties Laboratory

Kevin Grigar
Engineer

Margaret Hastedt
Paleomagnetism Laboratory

Michael Hodge
Marine Computer Specialist

Dwight Hornbacher
Applications Developer

William Mills
Laboratory Officer

Michael Storms
Operations Superintendent

Cruz St. Peter
Underway Geophysics Laboratory

Andrew Trefethen
Marine Computer Specialist

Garrick Van Rensburg
Marine Instrumentation Specialist

Abstract

Integrated Ocean Drilling Program (IODP) Hess Deep Expedition 345 was designed to sample lower crustal primitive gabbroic rocks that formed at the fast-spreading East Pacific Rise (EPR) in order to test models of magmatic accretion and the intensity of hydrothermal cooling at depth. The Hess Deep Rift was selected to exploit tectonic exposures of young EPR plutonic crust, building upon results from ODP Leg 147 as well as more recent submersible, remotely operated vehicle, and near-bottom surveys. The primary goal was to acquire the observations required to test end-member crustal accretion models that were in large part based on relationships from ophiolites, in combination with mid-ocean ridge geophysical studies. This goal was achieved with the recovery of primitive layered olivine gabbros and troctolites with many unexpected mineralogical and textural relationships, such as the abundance of orthopyroxene and the preservation of delicate skeletal olivine textures.

Site U1415 is located along the southern slope of an intrarift ridge within the Hess Deep Rift between 4675 and 4850 water depths. Specific hole locations were selected in the general area of the proposed drill sites (HD-01B–HD-03B) using a combination of geomorphology, seafloor observations, and shallow subsurface seismic data. A total of 16 holes were drilled. The primary science results were obtained from coring of two ~110 m deep reentry holes (U1415J and U1415P) and five single-bit holes (U1415E and U1415G–U1415I). Despite deep water depths and challenging drilling conditions, reasonable recovery for hard rock expeditions (15%–30%) was achieved at three 35–110 m deep holes (U1415I, U1415J, and U1415P). The other holes occupied during this expedition included two failed attempts to establish reentry capability (Holes U1415K and U1415M) and six jet-in tests to assess sediment thickness (Holes U1415A–U1415D, U1415F, and U1415L).

Olivine gabbro and troctolite are the dominant plutonic rock types recovered at Site U1415, with minor gabbro, clinopyroxene oikocryst-bearing troctolite, clinopyroxene oikocryst-bearing gabbro, and gabbronorite. These rocks exhibit cumulate textures similar to those found in layered basic intrusions and some ophiolite complexes. All lithologies are primitive, with Mg# between 0.76 and 0.89, falling within the global range of primitive oceanic gabbros. Spectacular modal and/or grain size layering was prevalent in >50% of the recovered core, displaying either simple or diffuse boundaries. Magmatic foliation largely defined by the shape-preferred orientation of plagioclase and olivine is moderate to strong in intervals with simple modal layering but weak to absent in the troctolite series and largely absent in the multitextured lay-

ered series. The abundance of orthopyroxene in these primitive rocks was unexpected and deviates from the standard model for mid-ocean-ridge basalt crystallization. Preservation of delicate skeletal olivine grains suggests that at least part of the recovered section of the lower crust was not subjected to significant hypersolidus or subsolidus strain.

The metamorphic mineral assemblages record the cooling of primitive gabbroic lithologies from EPR magmatic conditions (>1000°C) to zeolite facies conditions (<200°C) associated with Cocos-Nazca rifting and exposure onto the seafloor. Greenschist to subgreenschist facies alteration dominates and is most pervasive in olivine-rich lithologies and within zones of brittle fracturing and cataclasis. Amphibolite facies metamorphism is not abundant in comparison to the upper gabbros at the Hess Deep Rift.

The core recovered at Site U1415 originated at >2 km beneath the sheeted dike–plutonic transition and thus represents the lower half to a third of the EPR plutonic crust. The orientation of the magmatic fabrics and magnetic inclinations of the core suggest that Site U1415 is composed of a series of 30–65 m thick blocks that likely formed by mass wasting. Sampling three or four blocks of relatively fresh rocks proved advantageous, as it facilitated observations of two distinct types of layering and troctolite units with varying grain size, lithologic associations, and textures.

The mineralogical and textural relationships show that in several respects the Oman ophiolite is not the ideal model for fast-spreading ocean crust and call into question some aspects of both of the end-member accretion models that were to be tested. The results of the IODP Hess Deep Expedition 345 provide a reference section for primitive fast-spreading lower crust that did not exist before. This highlights the necessity of ocean drilling to address questions related to the origin and evolution of the lower ocean crust.

Introduction

The accretion of new ocean crust at mid-ocean-ridge spreading centers is one of the fundamental processes of Earth evolution. Understanding the nature of the crust and mantle and the underlying geologic processes that form them is an ongoing fundamental justification for drilling in the ocean basins (Hess, 1960; see Ocean Drilling Program [ODP] science plan at **www.odplegacy.org/program_admin/long_range.html** and Integrated Ocean Drilling Program [IODP] Initial Science Plan

at **www.iodp.org/isp**). At mid-ocean-ridge spreading centers, magmas are delivered to the base of the crust and pass through a lower crustal filter on their way to higher level magma chambers and eventual eruption as mid-ocean-ridge basalt (MORB) (see review by Klein, 2007). These melts evolve through complex processes of crystallization and deformation in the lower plutonic crust, most of which take place within the first million years of lithospheric evolution (see Coogan, 2013, for a broad overview). Our knowledge of these lower crustal processes has been strongly influenced by ophiolite studies (e.g., Pallister and Hopson, 1981; Nicolas, 1989), but only direct observation of modern ocean crust can inform a definitive understanding.

Two drilling approaches have been used to directly observe modern plutonic ocean crust: total penetration, whereby holes are initiated in the upper lavas with eventual penetration into the plutonic crust (ODP Site 1256), and off-set drilling, in which holes are directly initiated in tectonic exposures of the plutonic crust, thus bypassing the upper crust entirely (e.g., ODP Sites 735 and 894 and IODP Site U1309D). The concept of offset drilling is that by drilling relatively short holes that start at a variety of crustal levels, a composite section could be constructed that equals or even improves upon the results that could be obtained through a total crustal penetration. This approach is particularly effective for areas such as the Hess Deep Rift where use of complementary technology (remotely operated vehicles and submersibles) allows for regional-scale characterization of the crust, providing a comprehensive geological framework on which to hang the off-set sections.

The structure of the ocean crust, and in particular the nature of the plutonic sequence, varies significantly for mid-ocean ridges formed at different spreading rates (Fig. **F1**). The classic view of a layered, continuous ocean crust, the so-called Penrose model (Fig. **F1A**), is expected to be representative of fast-spreading crust (Anonymous, 1972). The structure of slow-spreading crust varies with position along the ridge, with segment centers having a thicker crustal component than segment ends (Fig. **F1B, F1C**) (Dick, 1989; Cannat et al., 1995). Ultraslow-spreading crust also shows significant variation in the thickness and rock type distribution with depth (Dick et al., 2003). To date, ocean drilling has recovered some significant sections of the ocean crust, both by total penetration holes (i.e., Deep Sea Drilling Program [DSDP] Hole 504B and ODP Hole 1256D) and offset drilling legs with numerous shallow to deep holes (e.g., ODP Legs 118, 147, 153, 176, and 209 and IODP Expedition 304/305) (Fig. **F1**).

The principal objective of IODP Expedition 345 was to sample the young primitive plutonic crust that formed at the fast-spreading East Pacific Rise (EPR), filling in a major lithologic gap in our sampling of the lower oceanic crust (blue rectangle in Fig. **F1A**). The expedition took advantage of exposed primitive gabbroic rocks at the Hess Deep Rift. Current knowledge of Hess Deep crustal sections (see **"Previous research at the Hess Deep Rift"**), in combination with geophysical studies of the EPR, drilling of the plutonic crust of slow-spread crust, and studies of ophiolite complexes, allows for the formulation of a series of specific questions that may be tested by drilling at Hess Deep.

Rationale for Hess Deep drilling

The Hess Deep Rift was selected for Expedition 345 as it is the best studied tectonic window into fast-spreading crust. An unprecedented geological framework for fast-spreading crust is available based on extensive investigation of contiguous sections of the mid- to upper crust along the Northern and Southern Escarpments and sections of the mid- to lower crust and uppermost mantle along the rift valley floor (Francheteau et al., 1990; Karson et al., 1992, 2002; MacLeod et al., unpubl. data, 2008), and Leg 147 (Gillis, Mével, Allan, et al., 1993) (see **"Previous research at the Hess Deep Rift"**). These geological relationships, coupled with investigations of recovered samples, provide a comprehensive framework for the igneous, metamorphic, and deformation processes active at the fast-spreading EPR.

Background

Crustal accretion models for fast-spreading crust

Two end-member models for crustal accretion at fast-spreading ridges have emerged from geophysical observations and geological evidence derived from the Oman and other ophiolites (e.g., Nicolas et al., 1988) (Fig. **F2**). Seismic reflection studies at the EPR identify axial melt lenses <1–2 km below the seafloor that are ~1 km wide and a few tens of meters thick (Detrick et al., 1987; Hooft et al., 1997; Kent et al., 1990; Singh et al., 1998). A low-velocity zone that underlies axial magma chambers (AMCs) is interpreted to be partially molten, containing <20% melt (e.g., Dunn et al., 2000). The internal structure of this region, such as the distribution of melt and its geometry, is not well constrained because of, for example, the uncertainties of converting compressional wave velocity with varying melt distribution. Locally, melt has been shown

to pool at or below the Mohorovicic discontinuity (Moho), both on- and off-axis, and also within the lower crust off-axis (Garmany, 1989; Crawford and Webb, 2002; Durant and Toomey, 2009; Canales et al., 2009).

The geological framework for the crustal accretion models is largely based on the Oman ophiolite, in which there are significant contrasts between upper and lower gabbros in terms of their composition and deformation fabrics (e.g., Pallister and Hobson, 1981; Nicolas et al., 1988; Coogan et al., 2002b). The lava sequence, sheeted dike complex, and upper gabbros have mafic phases and calculated melt compositions that are not consistent with direct derivation from liquids in equilibrium with the upper mantle, as expressed, for example, by their Mg#. In the lower gabbros, compositions are more primitive and range between those of the upper gabbros and melts in equilibrium with the upper mantle.

The first crustal accretion model is the gabbro glacier model (Henstock et al., 1993; Quick and Denlinger, 1993; Phipps Morgan and Chen, 1993), in which most crystallization occurs within a shallow melt lens and the resulting crystal mush subsides downward and outward by crystal sliding to generate the full thickness of the plutonic layer (Fig. **F2A**). The latent heat of the plutonic crust is largely lost to the overlying hydrothermal system through the melt lens on-axis. The sheeted sill model (Kelemen et al., 1997; Korenga and Kelemen, 1997, 1998; MacLeod and Yaouancq, 2000) predicts that almost all of the lower crust crystallizes in situ in a sheeted sill complex, such that melts pond repeatedly as they are transported through the lower crust, with crystallization occurring from the Moho to the upper melt lens (Fig. **F2C**). The amount of heat delivery to the lower crust is so high that conductive mechanisms alone cannot remove that heat, requiring extensive hydrothermal cooling along the sides of the crystal mush zone to remove the latent heat of crystallization on-axis (Chen, 2001). Hybrid models have also been proposed, in which some crystallization occurs in the AMC and some in situ within the plutonic crust (Fig. **F2B**) (Boudier et al., 1996; Coogan et al., 2002b; Maclennan et al., 2004). In fact, both end-member models require some portion of each process. In the gabbro glacier model, the melt lubricating subsiding crystals, allowing them to flow, would crystallize in the deeper crust, and in the sheeted sill model, more rapid cooling at shallow levels in the crust requires some crystal subsidence to prevent the AMC from solidifying (e.g., Maclennen et al., 2004).

Predictions for a range of chemical and physical parameters for the two end-member models are shown in Figure **F3.** The gabbro glacier model predicts nearly constant

Mg# for plutonic rocks and cumulate minerals throughout the plutonic sequence, with most crystallization occurring in a nearly steady state shallow magma chamber. The predicted increase in Mg# with depth in the sheeted sill model is based on partial in situ crystallization of magmas in the lower crust and upward migration of evolved liquids. The two models predict different changes in strain with depth, with increasing strain in the gabbro glacier model as a consequence of lower crustal flow.

Predictions for the response of the hydrothermal system are critical to the distinction of the two models. The sheeted sill lower crust requires deep, on-axis convective cooling to remove the latent heat, resulting in a higher hydrothermal fluid flux and a greater overall intensity of hydrothermal alteration in the lower crust than does the conductively cooled gabbro glacier model. Theoretical studies focusing on the axial heat budget have investigated the viability of the lower crustal accretion models (Sleep, 1975; Morton and Sleep, 1985; Chen, 2001; Cherkaoui et al., 2003; Maclennan et al., 2004). Both accretion models, as well as hybrids of the two, have been shown to be viable (e.g., Cherkaoui et al., 2003; Maclennan et al., 2004); however, the lack of observational constraint on key input parameters (e.g., permeability) make the interpretation of these thermal models uncertain.

How do the predictions of the crustal accretion models compare with our current knowledge of gabbroic sequences from fast-spreading ridges? Shallow-level gabbros sampled at Hess Deep and Pito Deep and Site 1256 all show evolved compositions (Hékinian et al., 1993; Perk et al., 2007; Wilson et al., 2006; Koepke et al., 2011). At Pito Deep, however, nearly all the gabbros from >300 m below the base of the sheeted dike complex are much more primitive than at the same structural level at Hess Deep (Hanna, 2004; Perk et al., 2007). This compositional difference suggests that primitive, mantle-derived magma may be transported to shallow depths with little fractionation occurring along the way (Pito Deep) and that crystal fractionation and postcumulus reactions may produce evolved rocks at these depths as well (Hess Deep and Site 1256) (Perk et al., 2007). Tests of the predictions for hydrothermal processes are less complete because of the absence of observations of deeper level gabbros. What has been documented to date are rapid cooling rates in the shallow-level gabbros (Coogan et al., 2007) and calculated heat fluxes across a contact aureole (Gillis, 2008) that are indicative of substantial heat loss through the axial melt lens. Collectively, observations from Site 1256 and Hess and Pito Deeps suggest that the competing accretion models may both be viable, when spatial and/or temporal variability in magmatic processes along the EPR are considered (Coogan, 2007, 2013).

Geological setting of the Hess Deep Rift

The Hess Deep Rift is located in the vicinity of the Galapagos triple junction (ridge-ridge-ridge), at the intersection of the Cocos, Nazca, and Pacific plates (Fig. **F4**) (Hey et al., 1972, 1977; Holden and Dietz, 1972). The north-south–trending EPR is spreading at 130 mm/y, and the east-west–trending Cocos-Nazca Rift is propagating westwards toward the EPR at a rate of 42 mm/y. Reconstruction of the bathymetry in this region suggests that the current configuration of the Galapagos triple junction has been active for at least 10 m.y. (Smith et al., 2011). The Galapagos microplate was initiated at ~1.5 Ma. Although the cause is not known, this initiation may be related to the formation of seamounts in the vicinity of Dietz Deep (Fig. **F4**) (Lonsdale, 1989; Smith et al., 2011; Schouten et al., 2008).

The EPR at the latitude of the Hess Deep Rift is made up of many short, first-order ridge segments separated by second-order overlapping spreading centers (Lonsdale, 1988). Thus, the crust exposed at the Hess Deep Rift likely formed within a short segment, perhaps at a segment end (Lonsdale, 1988). Reconstructions of the EPR flanks indicate several recent episodes of migrating offsets, suggesting that the crust exposed in the Hess Deep Rift could have formed on the western ridge of the EPR (Lonsdale, 1989; Smith et al., 2011; Schouten et al., 2008). This reconstruction is supported by new, highly precise zircon dates for gabbroic rocks from the intrarift ridge that place crystallization between 1.420–1.271 Ma. (Rioux et al., 2012).

The Hess Deep Rift is a complex region that formed by deep crustal extension in the wake of the westward propagation of the Cocos-Nazca spreading center. The surface expression of rifting is first evident ~30 km from the EPR where, from west to east, two 5 km wide, east–west grabens merge and the rift broadens to ~20 km and deepens to >5400 m at Hess Deep (Fig. **F5**). An intrarift ridge rises to 3000 m below sea level (mbsl) north of Hess Deep. Further to the east, the tip of the Cocos-Nazca spreading center starts to build a volcanic ridge that spreads at 55 mm/y. Uplifted rift escarpments contiguous with the EPR crust rise to depths <2200 mbsl to the north and the south of the rift.

A composite section of EPR crust and uppermost mantle is exposed along the rift escarpments and valley floor of the Hess Deep Rift. Multichannel reflection profiling along the EPR flanks north of the northern escarpment indicates a crustal thickness of 5 to 5.5 km (Zonenshain et al., 1980). The thickness of the upper crust ranges from 0.7 to 1.2 km (Karson et al., 2002), so the plutonic crust is ~3.8–4.8 km thick.

The subseafloor geology of the western end of the intrarift ridge and its southern slope has been investigated by on-bottom seismic and gravity surveys (Ballu et al., 1999; Wiggins et al., 1996). Results of these geophysical surveys, in combination with the regional geology, have led to a model whereby coherent crustal blocks were unroofed by detachment faulting and block rotation on listric normal faults (Francheteau et al., 1990; Wiggins et al., 1996; MacLeod et al., 1996b; Pariso et al., 1996). The viability of this model has been called into question based on new high-resolution bathymetric data collected as part of the JC21 site survey cruise for Expedition 345 (MacLeod et al., unpubl data, 2008). Revised models consider the role of mass failure linked with rifting (Ferrini et al., submitted) and dynamic uplift associated with the Cocos-Nazca spreading center (MacLeod et al., 2008). The results of Expedition 345 substantiate the role of mass failure as being a dominant process along the southern slope of the intrarift ridge (see below).

Previous research at the Hess Deep Rift

The Hess Deep Rift exposes contiguous sections of the mid- to upper crust along the Northern and Southern Escarpments and sections of the mid- to lower crust along the rift valley floor. The EPR upper crustal sections include laterally extensive outcrops of the lava and sheeted dike complex that are normal, depleted MORB (Stewart et al., 2002). Lateral variation in the thickness and internal structure of the volcanic sequence and sheeted dike complex are attributed to temporal variations in magma supply (Karson et al., 2002). Hydrothermal alteration of the upper crust is largely focused in the sheeted dike complex, where the dikes are variably altered to amphibole-or, locally, chlorite-dominated assemblages (Gillis, 1995; Gillis et al., 2001).

Shallow-level gabbros are exposed along the northern escarpment and at the summit of the western end of the intrarift ridge. The northern scarp exposures, which directly underlie the sheeted dike complex, are dominated by gabbronorite, with lesser amounts of Fe-Ti oxide and amphibole gabbro, varitextured gabbro, olivine gabbronorite, Fe-Ti oxide gabbronorite, and rare tonalite (Hanna, 2004; Kirchner and Gillis, 2012; Natland and Dick, 1996). The shallow-level gabbros have a wide range in Mg# (mean Mg# = 0.56; range = 0.30–0.76), with gabbronorite being the most primitive and Fe-Ti oxide ± amphibole gabbro being the most evolved end-members (Hanna, 2004; Kirchner and Gillis, 2012; Natland and Dick, 1996). The lithologies exposed at the summit of the western end of the intrarift ridge are similar to the Northern Escarpment, with gabbronorite, oxide gabbronorite, gabbro, olivine gabbro, and patches of pegmatitic amphibole gabbro (Fig. **F6**) (Gillis, Mével, Allan, et al., 1993; Hé-

kinian et al., 1993: Lissenberg et al., 2013). These shallow-level gabbros are slightly less evolved (mean Mg# = 0.58; range = 0.35–0.68) than Northern Escarpment shallow gabbros, with the most evolved samples located along the northern margin of the intrarift ridge, close to dolerites interpreted as sheeted dikes (Blum, 1991; MacLeod, unpubl. data, 2009; Pedersen et al., 1996; Gillis, Mével, Allan, et al., 1993). In both locations, shallow gabbroic rocks lack modal layering but locally contain lithologic boundaries identified by grain size variation (Gillis, Mével, Allan, et al., 1993; Hékinian et al., 1993).

Plutonic rocks exposed along the central and eastern region of the southern slope of the intrarift ridge, between 4400 and 5400 mbsl, include gabbros, gabbronorites, olivine gabbros, and lesser trocolites (Fig. **F6**) that are, on average, more primitive than the summit of the intrarift ridge (mean Mg# = 0.71; range = 0.39–0.85) (Blum, 1991; MacLeod, unpubl. data, 2009). As with the shallow-level gabbros, modal layering has not been documented for the deeper gabbros. It is important to note that the stratigraphic depth of these more primitive gabbros is not known, as these rocks likely migrated downslope by mass wasting processes.

A weak to strong magmatic foliation defined by the shape-preferred orientation of plagioclase laths is found in some samples from throughout the gabbroic sequence (Hékinian et al., 1993; Coogan et al., 2002a; Gillis, Mével, Allan, et al., 1993; MacLeod et al., 1996a). Reorientation of some sections of the shallow gabbros in Hole 894G to geographical coordinates shows that the foliations are steeply dipping (mean dip = 69°) with a nearly north–south orientation parallel to the EPR, and that there is a steeply plunging lineation (MacLeod et al., 1996b). Measurements of the anisotropy of magnetic susceptibility in samples also show that a magnetic fabric is parallel to the plagioclase fabric (Richter et al., 1996). Crystal-plastic deformation is rare throughout the gabbroic sequence, with minor undulose extinction and very rare deformation twins in plagioclase.

Hydrothermal fluid flow throughout the entire gabbroic sequence was dominated by pervasive fluid flow along grain boundaries, microfractures, and fractures. The shallow-level gabbros and the limited suite of gabbros show that incipient flow occurred at amphibolite facies (average temperature = 720°C) conditions and is manifest by amphibole veins that display no preferred orientation (Manning et al., 1996; Coogan et al., 2002a) and replacement of pyroxene by amphibole-dominated assemblages (Früh-Green et al., 1996; Gillis, 1995; Kirchner and Gillis, 2012). Whole-rock samples unaffected by a lower temperature stage of brittle deformation (see below) are de-

pleted in $\delta^{18}O$ relative to fresh values (Agrinier et al., 1995; Lécuyer and Reynard, 1996) and show minor enrichment in $^{87}Sr/^{86}Sr$ (data for the shallow-level gabbros only) (Lécuyer and Grau, 1996; Kirchner and Gillis, 2012). Calculated fluid/rock ratios using both isotopic systems range from 0.1 to 1 (Lécuyer and Grau, 1996; Lécuyer and Reynard, 1996; Kirchner and Gillis, 2012). The rate of cooling of the shallow-level gabbros is rapid (1,000 to 60,000°C/m.y.) and comparable to the upper gabbro section in the Oman ophiolite (Coogan et al., 2007; Faak et al., 2011).

When the shallow-level gabbros exposed along the intraridge rift cooled to ~450°C, they became influenced by the effects of Cocos-Nazca rifting, creating a dense array of east–west tensile fractures filled with greenschist to zeolite facies assemblages and local cataclasis cemented with the same assemblage (Früh-Green et al., 1996; Manning and MacLeod, 1996). The consequences of Cocos-Nazca rifting on the deeper gabbros have not yet been constrained.

Mantle peridotites are exposed in the vicinity of Site 895, southeast of Site 894 (Fig. **F5**). Clinopyroxene-poor harzburgites, at the most depleted end of the range for abyssal peridotites, are interpreted to be the residues of melting of an normal (N)-type MORB source (Natland and Dick, 1996). The association of dunite–troctolite-olivine gabbro with depleted harzburgite records the interaction of migrating melt with depleted harzburgite wall rock in the shallowest mantle (Natland and Dick, 1996; Arai and Matsukage, 1996; Arai et al., 1997). The geometry of these associations suggests that at least some melt transport was fracture-controlled. Significant modal layering in peridotite-hosted gabbroic rocks, a feature of the Oman mantle transition zone (Korenga and Kelemen, 1997), was not observed.

Expedition objectives

The principal objective for drilling at the Hess Deep Rift was to test competing hypotheses of magmatic accretion and hydrothermal processes in the lower ocean crust formed at the fast-spreading EPR. These hypotheses make predictions that can only be tested with drill cores, including the presence or absence of systematic variations with depth in mineral and bulk rock compositions, presence or absence of modally layered gabbro, variation of strain/deformation, and the extent and nature of hydrothermal alteration and deformation (Fig. **F3**). Specific scientific questions that address these predictions are outlined below.

1. How is melt transported from the mantle through the lower crust?

Melts erupting at mid-ocean ridges are rarely saturated in all four mantle phases at plausible segregation depths (O'Hara, 1968; Stolper and Walker, 1980). The upper mantle and crustal processes responsible for the evolution of mantle primary melts into primitive MORB are the subject of a great many studies in the geochemical literature (e.g., Kelemen et al., 1997). Melts are transported and aggregated by porous flow at both mantle and crustal levels; the latter is a process that may be identified on the basis of textural and chemical evidence. The different mechanisms of igneous differentiation (e.g., fractional crystallization, equilibrium crystallization, assimilation, and porous reactive flow) strongly influence the chemical evolution of residual liquids and host cumulates. Melt transport through the lower crust is an important boundary condition of the crustal accretion models. Is melt transported largely by porous flow through the lower crust, or is it transported in dike-like brittle fractures (Kelemen and Aharonov, 1998)? Previous studies at Hess Deep suggest that the liquid line of descent of lower crustal magmas may significantly differ from established models of MORB petrogenesis (Coogan et al., 2002a). This involves a much earlier and much more important role for orthopyroxene, such that primitive orthopyroxene is found in deeper level gabbros and in greater abundance in the Hess Deep shallow-level gabbros (Site 147) than in either the Oman ophiolite or slow-spreading ridges (i.e., Legs 118 and 176 and Expedition 304/305). Mineral and bulk chemical data for the core will provide tests for these and potentially other mechanisms of igneous differentiation and melt transport in the base of the ocean crust.

2. What is the origin and significance of layering?

Modally and compositionally layered gabbroic rocks are common in the lower crustal sections of ophiolites (e.g., Anonymous, 1972). A layered lower crust is therefore one of the key and nearly ubiquitous features of all models of fast-spreading lower crust. However, pronounced modal layering of the sort observed in major ophiolites has rarely been observed or sampled on the ocean floor so far. This may be because we have not yet drilled into the deeper levels of fast-spreading plutonic crust, commonly used sampling and observation methods are not ideal to detect such layering readily, the right areas have not been sampled, or pronounced modal layering is absent. If ophiolites indeed represent sections of normal mid-ocean-ridge crust, we expected to drill significant thicknesses of layered igneous rocks during this expedition. The rock's nature and extent is likely to have a strong bearing on the applicability of ophiolite-based accretionary models for the formation of the lower ocean crust.

3. How, and how fast, is heat extracted from the lower plutonic crust?

It is generally accepted that hydrothermal fluids initially penetrate all levels of the plutonic crust along microfracture networks at high temperatures, with fractures sealing at 600°–800°C (Alt et al., 2010; Manning et al., 1996; Coogan et al., 2002a). Initiation of incipient cracking in the upper gabbros at Hess Deep overlaps the solidus temperatures of the most evolved lithologies, as recorded in magmatic amphibole (850°–925°C) (Gillis et al., 2003) and zircon (690°–790°C) (Coogan and Hinton, 2006). Whether this is the case in the lower plutonic crust, where more primitive lithologies dominate, is not known. Penetration of fluids at high enough temperatures could promote hydrous partial melting (Koepke et al., 2007) as observed in slow spreading and ophiolitic environments. Whether and at what depths this process occurs in fast-spreading lower crust is not known. Cooling rates for upper gabbro sections from fast-spreading crust and equivalent sections from the Oman ophiolite are rapid (1,000°–60,000°C/m.y.) (Coogan et al., 2002b, 2007), indicative of significant convective cooling. Slower cooling rates in deeper level gabbros suggest that heat flow was largely conductive (Coogan et al., 2007); cooling rates for lower gabbro sections from fast-spreading crust are not known. Key questions that will be addressed include: What is the rate of cooling with depth? Is hydrothermal flow along microfracture networks an effective mechanism to cool the lower crust? When is hydrothermal cooling initiated? Does fluid penetration occur at high enough temperatures to induce hydrous partial melting? Does the lower crust cool largely by conductive or convective heat transport? This question is intimately linked to the overall crust construction models, as the glacier model is conductively cooled, while the sheeted sill model requires conductive cooling of the lower crust.

4. What are the fluid and geochemical fluxes in the East Pacific Rise lower plutonic crust?

Our understanding of the extent of fluid flow and reaction in the oceanic lower crust is presently very limited. Thermal models developed to test the crustal accretion models predict that advective cooling of the lower plutonic crust at or very close to the EPR would lead to a progressive decrease in the fluid flux and attendant fluid-rock interaction with depth, whereas more gradational conductive cooling over a broader timeframe would likely lead to lower fluid fluxes and more limited fluid-rock interaction (Fig. **F3**). Bulk rock Sr isotope data have constrained the time-integrated fluid fluxes for the upper crust (Bickle and Teagle, 1992; Gillis et al., 2005; Teagle et al., 2003; Kirchner and Gillis, 2012), and application of this approach will allow us to constrain fluid fluxes in the lower crust. Thermodynamic modeling predicts that

high-temperature fluid flow and reaction would leave little macroscopic evidence (McCollum and Shock, 1998), which is supported by $\delta^{18}O$ data for petrologically fresh samples (Alt and Bach, 2006; Gao et al., 2006). Thus, it will be critical to combine petrological and geochemical data to assess the extent of fluid-rock interaction in the lowermost plutonic crust. Key questions that will be addressed include: How does the total extent of alteration vary with depth? How does fluid flux vary with depth? What is the extent of chemical exchange between the lower crust and seawater? At what temperature is fluid-rock interaction initiated? What is the role of magmatic fluids?

Drilling strategy

The highest priority for drilling at Hess Deep was to sample one or more 100 to ≥250 m long sections of primitive gabbroic rocks. The Expedition 345 *Scientific Prospectus* (Gillis et al., 2012) identified three primary drill sites (proposed Sites HD-01B–HD-03B), with the intention that if coring was proceeding well in the first or second of these sites, it would be continued as long as possible in order to capitalize on good drilling conditions and obtain the longest possible continuous sample. Site survey data in conjunction with on-bottom observations collected during the expedition were used to plan specific hole locations in the vicinity of proposed Sites HD-01B–HD-03B.

We anticipated that drilling, coring, and logging operations in the Hess Deep Rift could be quite challenging. Thus, the operations team prepared a range of potential operational approaches that could be applied to address challenges that included water depths in excess of 4500 m, very thin sediment cover, initiating/maintaining a hole through the basement contact, and coring deeply through potentially unstable basement. These approaches included the possible deployment of a standard reentry cone, deployment of a free-fall funnel (FFF) or "nested" FFFs, bare rock hole without installation of a seafloor structure, and bare rock installation of a reentry cone with a short entry pup. In addition, the experiences of previous hard rock drilling expeditions were reviewed for best practices (see "Operations plan" in the Expedition 345 *Scientific Prospectus* [Gillis et al., 2012] for more details).

The initial focus for drilling during Expedition 345 was a flat-lying east-west–trending sedimented bench at ~4850 mbsl along the southern slope between the intrarift ridge and Hess Deep in an area dominated by primitive gabbros (Fig. **F7**). During the early stages of the expedition permission was granted by the Environmental Protection and

Safety Panel to expand the initial approved area of operations to the north of the bench to maximize drilling options along the southern slope of the intrarift ridge.

Site summary

Site U1415 is located along the southern slope of the intrarift ridge between 4675 and 4850 mbsl (Fig. F6). A series of 16 holes were drilled at Site U1415, two ~110 m below seafloor (mbsf) reentry holes (U1415J and U1415P), five single-bit holes (U1415E and U1415G–U1415I), two failed reentry holes (U1415K and U1415M), and six holes in which jet-in tests were conducted to assess sediment thickness (Holes U1415A–U1415D, U1415F, and U1415L) (Fig. F8, F9; Table T1).

Site U1415 is centered on a ~200 m wide, flat-lying east-west–trending bench at 4850 mbsl that is covered with approximately <10–30 m of largely gabbroic rubble overlain by a few meters of pelagic sediment mixed with lithic debris. Holes U1415E–U1415J are in an area where primitive (Mg# = 75–85) gabbroic rocks were recovered from above and below the bench during the JC21 site survey (see distribution of olivine gabbros in Fig. F7; see also Fig. F8). Holes U1415K–U1315N are situated along a ~100 m wide, flat-lying shoulder at ~4675 mbsl, ~160 m shallower than the bench (Fig. F8), where slightly more evolved gabbroic rocks were recovered during the JC21 site survey (Fig. F7).

Specific hole locations were selected in the general area of the proposed drill sites (HD-01B to HD-03B) using a combination of geomorphology, seafloor observations, and shallow subsurface seismic data. Early in the expedition, exploratory visual and seismic surveys, combined with jet-in tests, showed that the sediment thickness on the bench was at most a few meters. This meant deployment of a standard reentry system was not feasible; thus a hard rock reentry system–style nested free-fall funnel with casing approach was used (see **"Operations summary"**). Our early drilling results lead us to reevaluate the origin of the seafloor morphology observed in the microbathymetry of the bench area. Small-scale topography was reinterpreted to be related to mass wasting above and within the bench rather than extensional faulting along the bench, as previously thought. Thus, the strategy for placing the drill holes was modified slightly to focus on structural promontories separating areas where slumping may have dominated.

Drilling at Site U1415 also revealed that, at least locally, the bench was not a coherent fault block as originally proposed. Near-bottom 3.5 kHz seismic data suggest the pres-

ence several fault or slump blocks with a complicated structural relationship along and across strike. Variations in inclination of stable, high unblocking temperature magnetic components indicated that at least two blocks had been sampled in each hole, providing evidence of relative displacements of individual, internally coherent units. The scale of these blocks can be assessed in the two deepest holes, U1415J and U1415P (Figs. **F11, F12**). In Hole U1415J, consistency in the dip of magmatic foliation and magnetic inclinations identify two discrete blocks with vertical thicknesses of 29 and ≥50 m. In Hole U1415P, rock type and magnetic inclinations suggest two blocks of 65 and >42 m thickness. The similarity between the Troctolitic Series (see below) recovered in Holes U1415J and U1415P suggests that the blocks could originate from comparable stratigraphic levels.

The evidence of local mass wasting observed at Site U1415 and the prediction that mass wasting is a regional phenomenon (Ferrini et al., submitted) call into question the sensibility of assigning a stratigraphic position for any samples recovered along the southern slope of the intrarift ridge. The exception is the crest of the intrarift ridge. Here, the stratigraphic position of the gabbroic rocks is well constrained as being shallow gabbros, close to the sheeted dike–gabbro transition. This conclusion is based on presence of dolerites with EPR compositions interpreted as sheeted dikes along the northern slope of the intrarift ridge (Fig. **F6**) and cooling rates comparable to the uppermost gabbros along the Northern Escarpment of the Hess Deep Rift (Coogan et al., 2007). Thus, we do not present our expedition results in a depth context and strongly caution against the use of depth profiles for any samples recovered from the southern slope of the intrarift ridge (cf. Hékinian et al., 1993; Lissenberg et al., 2013).

A precise stratigraphic context for Site U1415 is not required to address most of the specific scientific objectives of Expedition 345. It is important, however, to comment on what can be constrained concerning the original depth of the Site U1415 primitive gabbros in the EPR plutonic crust. No primitive gabbros occur within 1 km of the base of the sheeted dike complex along the northern escarpment of Hess Deep Rift. Primitive olivine gabbros along the southern slope of the intrarift ridge first crop out at 3800–4000 mbsl, within 2.0 km of the inferred sheeted dike complex (Lissenberg et al., 2013) (Fig. **F6**). As these samples were recovered along a very steep slope inferred to be the head wall of a large mass wasting feature, we suggest they are in place in the context of the intrarift ridge block itself (unlike samples recovered at greater depths). Thus, we conclude that the primitive lithologies at Site U1415 formed at a minimum

of 2 km beneath the sheeted dike complex, in the lower half to one-third of the 3.8–4.8 km thick plutonic sequence.

Magmatic accretion of fast-spreading East Pacific Rise lower crust

Rock types and units

At Site U1415, igneous rocks were recovered from massive blocks and overlying surficial rubble and lithic sands and gravels. Olivine gabbro and troctolite are the major plutonic rock types at Site U1415, with minor gabbro, clinopyroxene oikocryst-bearing troctolite, clinopyroxene oikocryst-bearing gabbro, and gabbronorite (Fig. **F10**).

The primary science results were obtained from the massive blocks drilled at reentry Holes U1415J and U1415P located ~110 m apart and the single-bit Hole U1415I located ~10 m south of Hole U1415J (Figs. **F8, F9**). In the remainder of this section, only the results from the massive units from these holes are considered further (i.e., excludes the surficial rubble units).

Olivine gabbro is the dominant rock type recovered at Site U1415, occurring in both the layered series in Holes U1415I, U1415J, and U1415P and the Troctolite Series in Hole U1415P (Figs. **F11, F12**) (see below). Olivine gabbro is dominantly medium grained with equigranular–granular to granular–poikilitic textures and consists of olivine (5%–30%), plagioclase (45%–70%), and clinopyroxene (5%–45%), with trace amounts of orthopyroxene and oxides. Olivine is subhedral to euhedral with an equant to amoeboid skeletal habit, tabular plagioclase is euhedral to subhedral, and clinopyroxene is anhedral and dominantly subequant and often poikilitic. In Hole U1415P, multitextured olivine gabbros display complex variation in modal proportions of minerals, grain size, and mineral habit.

An unexpected observation is the prevalence of orthopyroxene-bearing lithologies, predominately orthopyroxene-bearing olivine gabbros and minor olivine-bearing gabbronorite (Figs. **F11, F12**). These medium- to coarse-grained, equigranular, granular rocks consist of olivine (10%–20%), plagioclase (50%–70%), clinopyroxene (15%–30%), orthopyroxene (1%–4%), and trace amounts of oxide (Cr-spinel). Olivine is subhedral to anhedral with an equant to amoeboid to skeletal habit, plagioclase is euhedral to subhedral with a tabular habit, clinopyroxene is anhedral forming interstitial grains, and orthopyroxene is euhhedral to anhedral forming subequant to equant prismatic or interstitial grains (Fig. **F13**). In some occurrences, orthopyroxene

appears as an early phase, in which it is locally intergrown with olivine, followed by late-stage clinopyroxene (Fig. **F14**).

Troctolite is the second most abundant lithology, forming decimeter-scale intervals within the layered series and the dominant lithology in the Troctolitic Series (see below). In Hole U1415J, troctolites consist of olivine (20%–80%), plagioclase (20%–5%), clinopyroxene (<1%–10%), and trace amounts of oxide (possibly Cr-spinel). In Hole U1415P, troctolites have a more consistent modal mineralogy, with olivine (35%), plagioclase (65%), and trace amounts of clinopyroxene (<1%) and oxide (<1%, Cr-spinel). In both holes, olivine is euhedral to subhedral with a subequant to amoeboid to skeletal habit, plagioclase is euhedral to anhedral with a tabular habit, and clinopyroxene is anhedral with an interstitial habit. Troctolite has an equigranular and granular texture (Fig. **F15**).

Clinopyroxene oikocryst-bearing troctolite forms decimeter-scale intervals within the layered series in Holes U1415I and U1415J. The troctolites are medium grained, seriate poikilitic-granular rocks with a strong grain size contrast between minerals in the troctolitic matrix and chadacrysts in large clinopyroxene oikocrysts (Fig. **F16A**). The troctolites consist of olivine (10%–42%), plagioclase (45%–70%), and clinopyroxene oikocrysts (3%–35%), with trace amounts of oxide (possibly Cr-spinel) and orthopyroxene. Olivine is fine grained, subhedral to anhedral with an elongated, irregular amoeboid habit. Plagioclase is fine grained, subhedral to euhedral with a tabular habit. Large clinopyroxene oikocrysts (up to 15 mm across) are anhedral and poikilitic, with a distinctive population of irregularly shaped plagioclase chadacrysts (Fig. **F17**). The plagioclase chadacrysts are oriented in a random manner within the oikocrysts, in contrast to the surrounding foliated plagioclase fabric. Many of the plagioclase chadacrysts are deformed. Olivine is absent as a chadacryst phase.

Gabbros primarly occur in centimeter-scale intervals in the layered series in Holes U1415I and U1415J (Fig. **F11**) where they are fine to medium grained, and have an equigranular/granular texture. The primary mineralogy of the gabbros is dominated by plagioclase (55%–75%) and clinopyroxene (25%–45%) with trace amounts of olivine, orthopyroxene, and oxide. Plagioclase is euhedral to subhedral with a tabular habit, whereas clinopyroxene is anhedral with a subequant habit.

The rock types recovered from Holes U1415I, U1415J, and U1415P are grouped into lithologic units based on rock type and structural constraints (Figs. **F11, F12**); these units in turn may be simplified into three lithologic series. The first lithologic series

includes the Layered Series in Holes U1415I and U1415J, which is composed of a ~30 m thick sequence of primitive olivine gabbronorites, olivine-orthopyroxene gabbros, and clinopyroxene oikocryst-bearing troctolites with moderate to strong magmatic foliation. The Layered Series is host to spectacular modal, and grain size layering. The boundaries between the layers are defined by changes in mineral modes and/or grain size and are primarily sutured such that individual mineral grains span the boundary (Fig. **F18**).

The second lithologic series is the Multitextured Layered Gabbro Series in Hole U1415P composed of a ~50 m thick sequence of olivine gabbros and orthopyroxene-bearing olivine gabbros with considerable banding, skeletal olivine textures, and occasional noritic bands (Fig. **F12**). This heterogeneous series reveals an extraordinary variety of textures that include variations in grain size, crystal morphology, and mineral fabrics and consists of a sequence of interfingered intervals that range from homogeneously textured primitive orthopyroxene-bearing olivine gabbros to dramatically banded or layered olivine gabbros. Banding can be divided into two broad categories: more common, steeply dipping, asymmetric and sometimes diffuse leucocratic banding and less common, more regular, gently dipping grain size and modal layering

The Troctolitic Series in Holes U1415J and U1415P comprise the third lithologic series (Figs. **F11, F12**). Melanocratic to leucocratic troctolites in this series are lithologically similar, commonly have a weak olivine-plagioclase foliation, and contain little modal layering (Fig. **F15**).

Basaltic and hypabyssal rocks

Basaltic and doleritic lithologies were largely recovered from the surficial rubble zone. The relationship between these rocks and the gabbroic units was only documented in the Troctolite Series in Hole U1415J where minor dikes are associated with zones of brittle deformation. The primary lithologies in Hole U1415N are moderately to highly olivine-phyric basalt and dolerite. Compositions of these basalts are at the primitive, depleted end of the EPR trend. Basalts found within the cataclastic intervals are discussed below.

Bulk chemistry

The gabbroic rocks from the layered, mutlitextured, and troctolite series are all primitive, with MgO contents ranging from ~7 to 31 wt% and $Fe_2O_3^T$ contents ranging from ~2 to 9 wt%. The olivine gabbros and gabbros have high Mg# (79–87) and Ca#

(~77–92), high Ni contents (130–570 ppm), low TiO_2 contents (0.1–0.3 wt%), and incompatible lithophile element contents (e.g., Y < 11 ppm). Five samples are distinguished by a significantly higher Cr content (~1500–2500 ppm) compared to neighboring gabbros (~36–825 ppm). Clinopyroxene oikocryst-bearing troctolites and gabbros from the Layered Series are similar in composition to the olivine gabbros. Orthopyroxene-bearing olivine gabbros have primitive compositions similar to neighboring gabbros and olivine gabbros and are characterized by high Mg# (80–85) and Ca# (77–87), high Ni (174–460 ppm) and Cr (150–2560 ppm) contents, low TiO_2 contents (0.1–0.3 wt%), and trace element contents (e.g., Y < 6 ppm).

Troctolites overlap in composition with the gabbros but have, on average, more refractory compositions with high Mg# (81–89) and Ca# (79–98), high Ni (260–1500 ppm) and Cr (365–1100 ppm) contents, low TiO_2 contents (<0.1 wt%), and incompatible lithophile element contents (e.g., Y < 3 ppm). The most refractory troctolites sampled in Hole U1415P have compositions overlapping the field of impregnated mantle peridotites. However, these samples are low in Ni relative to their high Mg#, indicating formation by a dominantly cumulate process (see below).

The gabbroic rocks at Site U1415 are far more primitive than the shallow-level gabbros at the Hess Deep Rift and are similar in bulk composition to gabbros from the shallow gabbros from Pito Deep where fast-spreading EPR crust is exposed (Perk et al., 2007). These primitive lithologies fall within the range of primitive oceanic gabbros from fast-spreading crust, as illustrated in a Mg# versus Cr content plot (Fig. **F19**). The Cr contents of these rocks likely reflect the crystallization of chrome spinel from a Cr-rich primitive parent magma.

Discussion of significant new observations

Layering

A layered lower crust is one of the key and nearly ubiquitous features of all models of the fast-spreading lower crust. Despite this, observations of modal and/or grain size layering in fast-spreading oceanic gabbros, indeed gabbros formed at all spreading rates, is rare and restricted to small intervals (e.g., Pito Deep [Perk et al., 2007], ODP Hole 735B [Dick, Natland, Miller, et al., 1999], IODP Hole U1309 [Blackman, Ildefonse, John, Ohara, Miller, MacLeod, and the Expedition 304/305 Scientists, 2006]). This lack of layering is in contrast to ophiolites where layering is nearly ubiquitous in plutonic rocks. Recovery of a wide range of layering observed in the Site U1415 gab-

broic rocks is therefore of great significance, both for confirmation of its presence in fast-spreading crust and for its variety.

Two types of layering are seen at Site U1415: (1) simple centimeter- to decimeter-scale layering defined by differences in modal mineralogy and, more rarely, by grain size and (2) asymmetric and sometimes diffuse leucocratic banding (Fig. **F20**). Regular layering is largely defined by variation in modal olivine, plagioclase, and to a lesser extent pyroxene; the layers have sharp planar boundaries on a <1 cm scale (Fig. **F20A, F20B**). In Hole U1415J, some of the boundaries show grain size variation caused by the appearance of large (2–5 mm) pyroxene crystals and others by increases in olivine grain size from 1–2 to >5 mm. This type of layering is particularly well developed in intervals of olivine gabbro and gabbro in the Layered Series in Hole U1415I and the oikocryst-bearing Layered Gabbro Series in Hole U1415J. Weak to strong magmatic foliation is common in intervals with simple layering where its orientation is generally parallel to the layers.

Diffuse layering or banding, restricted to the olivine gabbro and gabbro intervals in the Multitextured Layered Gabbro Series in Hole U1415P, is defined by modal, grain size, and shape variations in plagioclase, olivine, orthopyroxene, and clinopyroxene and mainly manifests as variably distinct leucocratic and melanocratic bands (Fig. **F20C**). Magmatic foliation areas are poorly developed to absent in the Multitextured Layered Gabbro Series.

Layer boundaries are mainly sutured (Fig. **F18**) with minor gradiation, implying that they developed at hypersolidus conditions. The simple layering observed in Holes U1415I and U1415J is reminiscent of that found in basic layered intrusions (Workshop Participants, 1986). The diffuse banding in Hole U1415P is different, with textures and modal layering suggestive of magma mixing.

Orthopyroxene in primitive gabbroic rocks

The common occurrence of orthopyroxene in the primitive gabbroic rocks at Site U1415 was not expected. Orthopyroxene is a minor (<5%) and, in some centimeter-scale domains, a major (up to 25%) phase in olivine gabbro, gabbro, troctolite, and gabbronorite (Figs. **F13, F14**). These orthopyroxene-bearing rocks have Mg# ranging from ~0.80 to 0.85. Although gabbronorites are common and expected in evolved (average Mg# = ~0.58) shallow-level gabbros at the Hess Deep Rift (Gillis, Mével, Allan, et al., 1996; Natland and Dick, 1996; Coogan et al., 2002a), orthopyroxene has only once been observed in fast-spreading primitive gabbros (Coogan et al., 2002a).

The presence of orthopyroxene as a cumulate phase at Site U1415 is significant, as it is considered to be one of the last major minerals to crystallize from mid-ocean-ridge basalt (MORB)-like tholeiitic liquids (e.g., Stolper and Walker, 1980; Grove and Bryan, 1983; Grove et al., 1992; Feig et al., 2006). One model suggests that melts crossing the Mohorovicic seismic discontinuity have variable compositions compared to those used in phase equilibria experiments and that some may be in major but not trace element equilibrium with shallow depleted mantle (Coogan et al., 2002). This model led Coogan et al. (2002) to propose that some of the melt extracted from the mantle is fully aggregated within the mantle but reacts with the shallow mantle during melt extraction. Alternatively, phase relationships derived from experimental studies cited above may be different from those observed at Site U1415 because of differing conditions, emphasizing the importance of postcruise research to address this.

Olivine textures and their significance in characterizing strain

Intrinsic to layering observed at Site U1415 is the development of dendritic, hopper, and skeletal olivine textures in the cumulate rocks (Fig. **F16B**). These types of textures have been shown to be indicative of magmatic undercooling (O'Driscoll, 2007; Donaldson et al., 1982). Importantly, the presence of these olivine textures shows that deformation subsequent to crystallization was minimal, otherwise these delicate structures would be destroyed.

Clinopyroxene oikocrysts

The textures of clinopyroxene observed in gabbroic rocks at Site U1415 are remarkable for their complexity and diversity compared to previously sampled ocean crust. Textural habits range from equant granular clinopyroxene to centimeter-scale oikocrysts of poikilitic clinopyroxene. One particular clinopyroxene texture is so distinctive that, for the purposes of description, its host rock was named "clinopyroxene oikocryst-bearing troctolite." Large poikilitic clinopyroxene oikocrysts commonly occur in a range of gabbroic lithologies recovered from elsewhere in the oceanic crust (e.g., Blackman, Ildefonse, John, Ohara, Miller, MacLeod, and the Expedition 305/305 Scientists, 2006; Cannat et al., 1995; Dick et al., 1999; Gillis, Mével, Allan, et al., 1993; Melson and Thompson, 1970); the clinopyroxene oikocrysts in the clinopyroxene oikocryst-bearing troctolites at Site U415 (Fig. **F16A**) are different. Here the clinopyroxene forms large, centimeter-scale, isolated oikocrysts contrasting strongly with a finer grained (millimeter scale) foliated troctolitic matrix. Plagioclase chadacrysts may be undeformed, bent with deformation twins and subgrains, or annealed; they may also be resorbed. No olivine chadacrysts were observed. These varying textures

record a potentially complex hypersolidus deformation history of the crystal mush. We speculate that the origin of this distinctive clinopyroxene texture is related to melt migration and reaction within the lower oceanic crust. Similar lithologies have been well documented from particular horizons in tholeiitic layered intrusions in continental settings (Olmsted, 1979; Mathison, 1987), providing evidence for a commonality between some magmatic processes occurring at both layered intrusions and mid-ocean ridges, as originally proposed by Melson and Thompson (1970).

Hydrothermal alteration of fast-spreading East Pacific Rise lower crust

The metamorphic mineral assemblages in the rocks recovered at Site U1415 record the cooling of primitive gabbroic lithologies from magmatic (>1000°C) conditions at the EPR to zeolite (<200°C) facies conditions associated with Cocos-Nazca rifting and exposure onto the seafloor. The intensity of alteration varies with igneous lithology, in particular the modal abundance of olivine, grain size, and proximity to zones of brittle fracturing and cataclasis. The metamorphic assemblages in each lithologic interval record superimposed alteration conditions, the range of which records at what stage in the cooling of the section samples encountered fluids and deformation.

Pervasive alteration

The freshest lithologies at Site U1415 are found in the Layered Series of Holes U1415I and U1415J and Multitextured Layered Olivine Gabbro Series in Hole U1415P. The average alteration intensity in these units is ~40% (<10%–90%). Olivine is the most altered primary mineral (average = 55%–65%), followed by clinopyroxene and orthopyroxene (average = 30%) and plagioclase (average = 10%–20%). The Troctolite Series in Holes U1415J and U1415P are more pervasively altered than the gabbroic series, with Hole U1415J troctolites being more altered (~80%) than in Hole U1415P (~65%). This likely reflects the presence of brittle cataclastic zones in Hole U1415J (see below). Similar to the gabbroic series, olivine is the most altered primary mineral (65%–75%), followed by plagioclase (~60%) and clinopyroxene (35%–40%). In summary, away from zones of brittle deformation, alteration intensity is largely controlled by the bulk composition of the rocks such that the most olivine rich lithologies display the most alteration.

The secondary mineral assemblages replacing primary minerals display some differences between the gabbroic lithologies in the Layered Series, Multitextured Layered Olivine Gabbro Series, and Troctolitic Series (Fig. **F21**). These differences are primarily related to the relative abundance of the secondary phases replacing olivine and pla-

gioclase. In all of the Layered Series, serpentine is slightly more abundant than talc, chlorite, and clay minerals. All assemblages have lesser amounts of amphibole, clay minerals, minor secondary oxides, and sulfides. In contrast to the Layered Series, olivine replacement in the Troctolitic Series is dominated by serpentine with lesser and varying proportions of chlorite and clay minerals and lesser talc, amphibole, minor secondary oxides, and sulfides. Similar to olivine, the relative abundance of the secondary minerals replacing plagioclase varies with rock type. The abundance of prehnite and chlorite are approximately equal in all of the gabbroic units, whereas prehnite is the most abundant secondary phase in the troctolites. In both rock types, secondary plagioclase, amphibole, and/or clay minerals also replace plagioclase. Secondary mineral assemblages replacing the other primary phases are not lithologically controlled. In all lithologies, clinopyroxene and orthopyroxene are largely replaced by amphibole and lesser chlorite.

A characteristic feature of altered olivine-rich gabbroic rocks is a concentric zonal aggregate of tremolite and chlorite that develops as a reaction product between olivine and plagioclase in oceanic gabbroic rocks (e.g., Nozaka and Fryer, 2011). Such corona textures are variably developed in all of the olivine-bearing gabbroic lithologies recovered at Site U1415 but the completion of the corona-forming action (i.e., absence of relict olivine inside a corona) appears most frequently in the Troctolitic Series in Hole U1415J.

Brittle fracturing and vein formation

Alteration veins represent a ubiquitous, although volumetrically insignificant, component of the rock types recovered at Site U1415. They reflect the later stages of cracking, fluid circulation, and fluid-rock reaction experienced by the gabbroic lithologies. Vein density is low except in the zones of extensive cataclasis found in Hole U1415J. The orientation of alteration veins is globally random; they form a network with no preferred orientation that is consistent with hydraulic fracturing.

A variety of vein mineralogies are observed at Site U1415, including amphibole, epidote, chlorite, serpentine, prehnite, carbonates, zeolite, and clay minerals. A systematic hierarchy in crosscutting relationships between veins with different fillings is hard to establish. Where present, amphibole and epidote veins are early, and mutually crosscutting relationships are observed for chlorite and prehnite. Zeolite veins are always late, crosscutting the other assemblages.

Discussion

Pervasive alteration in the gabbroic lithologies spanned amphibolite to subgreenschist facies conditions (from >700° to <200°C) (Fig. F22). Clear evidence for early high-temperature amphibolite facies is rare and is manifested by the rare occurrence of brown amphibole and green spinel associated with olivine replacement in Hole U1415J. Some of the secondary amphibole associated with pyroxene and plagioclase replacement may also record amphibolite facies, by analogy with gabbroic rocks from elsewhere at Hess Deep, but must be confirmed by postcruise analyses. Incipient alteration in the majority of the recovered core occurred at lower amphibolite (450°–650°C) facies based on corona textures and olivine alteration assemblages (e.g., Frost et al., 2008; Nozaka and Fryer, 2011). The predominant alteration occurred at greenschist (<400°C) to subgreenschist (<200°C) facies, as evidenced by serpentine, chlorite, and prehnite assemblages and zeolite and clay mineral assemblages, respectively.

Pervasive alteration in the Site U1415 primitive gabbroic rocks differs from the more evolved, shallow-level gabbros found at the crest of the intrarift ridge and northern escarpment at Hess Deep. On average, these shallow-level gabbros are fresher, particularly in comparison with the troctolites, and the dominant alteration is amphibole after pyroxene and minor secondary plagioclase and amphibole and chlorite after igneous plagioclase (Früh-Green et al., 1996; Gillis, 1995; Kirchner and Gillis, 2012). As olivine is absent or of low modal abundance in the shallow gabbros, abundant serpentine and talc would not be expected. Moreover, the lack of prehnite and chlorite replacing plagioclase may also be related to olivine abundance, as prehnite and chlorite may be by-products of the serpentinization process described above. Another feature that is ubiquitous, though with variable abundance, in the shallow gabbros and rare at Site U1415 is amphibole filling microfractures and lining grain boundaries at amphibolite facies (>700°C). An important question to address is whether incipient fracturing at amphibolite facies is rare in fast-spreading primitive gabbros, or if mineral assemblages differ because of their more evolved bulk compositions (e.g., McCollom and Shock, 1998), or if the observations at Site U1415 simply reflect local scale heterogeneity caused by, for example, proximity to a zone of focused fluid flow (Coogan et al., 2006).

Comparison with the vein types found at Site 894 provides some constraints on the evolution of fracture-controlled fluid flow. Veins in the Site 894 cores are similar to those at Site U1415, from oldest to youngest, with amphibole, chlorite ± prehnite ± epidote, chlorite–clay minerals, and zeolite veins (Früh-Green et al., 1996; Manning

and MacLeod, 1996). The chlorite and zeolite vein types have moderate to steep dips to the south that show a strong preferred east–west orientation when reoriented based on magnetic and FMS results (Manning and MacLeod, 1996). Because the EPR strikes north–south at this latitude, the veins' east–west orientations suggest formation by a mechanism unrelated to fracturing in an EPR hydrothermal system. Although the dominant fracture sets found in the Site 894 core were not observed at Site U1415, similarity in the greenschist to subgreenschist facies vein assemblages suggests a common evolution.

Evolution of cataclastic deformation, magmatism, and hydrothermal alteration

Another significant result of Expedition 345 is the recovery of blocks hosting a record of cataclasis whose development was synchronous with basaltic dike intrusion. The fault zone occurs within in the Troctolite Series of Hole U1415J, where the recovered core documents complex interactions between cataclastic faulting, fluid flow and alteration, and magmatism. Cataclasis is largely localized at two depth intervals in the Troctolite Series, where brittle fabrics range from dense-anastomosing fractures to well-developed breccias and cataclasite. Elsewhere in Holes U1415J and U1415P, only very thin (less than centimeter scale) zones of fracturing and cataclasis were recovered.

The zone of brittle deformation in Hole U1415J exhibits heterogeneous grain sizes and degree of alteration and reflects the variable intensity of cataclasis over a centimeter scale. Cataclastic fabrics are characterized by grain size reduction through microcracking and rotation of the primary igneous and metamorphic minerals. This microstructure is commonly cut by prehnite and minor chlorite veins that are in turn cut by another period of cataclastic deformation. Locally, prehnite and chlorite veins are deformed and crosscut by later prehnite and chlorite veins. These relations indicate a complex succession of vein formation and brittle deformation.

Intervals of core host evidence of localized dike intrusion synchronous with the development of fault rocks in Hole U1415J. This is based on the combined evidence from textures of several pieces of fractured dolerite, two of which have very fine grained margins adjacent to altered locally cataclasitic gabbro. As an example, microstructural observations suggest that one dolerite was likely emplaced into cohesive gabbro cataclasite hosting variable intensity prehnite/chlorite alteration. Boundaries with the cataclastite are sharp, with a distinctive increase in grain size away from the

contact. Similar to elsewhere in the zones of fracture and cataclasis, the dolerite, contact zone, and cataclastic gabbro are cut by epidote and chlorite veins that were deformed by later brittle deformation. These relationships suggest the following sequence of events: (1) localized fracture and cataclasis and fluid flow associated with faulting and low-temperature (<400°C) vein formation, (2) vein intrusion, (3) further cataclasis, (4) dolerite dike emplacement, and (5) another phase of brittle fracture.

A critical unresolved question is the timing of faulting and dike injection, as this would determine whether these processes are associated with the EPR or Cocos-Nazca Ridge. No results from the Expedition 345 can readily resolve this issue. However, comparison with the Hole 894 core may provide some constraints, as localized zones of cataclasite and vein networks with similar textures and alteration mineral assemblages to those found in Holes U1415J and U1415P were recovered. Magnetic and FMS data from Hole 894G indicate that veins and fractures show a strong preferred east–west strike and steep south-facing dips (MacLeod et al., 1996b). As discussed above, similarity in the greenschist to subgreenschist facies vein assemblages suggests that brittle deformation and alteration may be associated with Coco-Nazca rifting.

Paleomagnetism

Paleomagnetic analyses focused on determining the structural continuity of units sampled in Holes U1415J and U1415P. Variations in inclination of stable, high unblocking temperature magnetic components indicate that at least two blocks had been sampled in each hole, providing evidence of relative displacements of individual, internally coherent units (Fig. **F23**). Thermal demagnetization experiments also identified more complex remanences in some samples from Hole U1415J, indicating that magnetizations were acquired during at least two geomagnetic polarity chrons (Fig. **F24**). Postcruise paleomagnetic research will focus on understanding the origin of these multipolarity remanences.

Preliminary scientific assessment

Expedition 345 to Hess Deep Rift was remarkably successful, especially given the challenging operational conditions, which imposed less depth penetration and recovery than desired. Drilling into essentially rubble-covered fractured rock at water depths exceeding 4800 mbsl meant that our operational objective of recovering one or more 100–250 m sections was only marginally achieved. Instead, one single-bit 35 m hole

and two shallowly cased reentry 110 m holes with 14%–30% recovery were drilled. This is a remarkable achievement on the part of the operations team.

Expedition 345 achieved its primary scientific goal of recovering the first drilled sections of primitive gabbroic rocks formed at a fast-spreading ridge. Drilling at Site U1415 provided the first confirmation of predictions that fast-spreading lower oceanic crust is layered. It also revealed a diversity of layering whose characteristics have similarities and differences to both layered sequences in ophiolites and layered mafic intrusions. Moreover, the core revealed significant unexpected mineralogical and textural diversity, some of which has been rarely observed in the lower oceanic crust elsewhere or in ophiolites. The core from Expedition 345 will be a reference section, for now the only reference section, for fast-spreading primitive ocean crust, which covers about half the Earth's surface. In this way, we surpassed our scientific expectations, making Expedition 345 a milestone for ocean crustal research.

Expedition 345 was designed to address the following objectives:

- What is the origin and significance of layering?
- How is melt transported from the mantle through the lower crust?
- How, and how fast, is heat extracted from the lower plutonic crust?
- What are the fluid and geochemical fluxes in the EPR lower plutonic crust?

The primitive gabbroic core recovered at Site U1415 makes it possible to address all of these scientific objectives, as well as some unanticipated objectives, such as

- Determining the origin of orthopyroxene in primitive lower ocean crust gabbros,
- Determining how plate separation is accommodated in the crust given the evidence against high-strain flow in a partially molten or subsolidus state,
- Reconstructing parental/primary MORB melt compositions using recovered olivine-phyric basalts in Hole U1415N,
- Distinguishing an EPR versus Cocos-Nazca Ridge source for basaltic dikes that intrude the gabbroic lithologies, and
- Evaluating the fluid flux and timing of localized zones of brittle fracturing and cataclasis.

These scientific objectives will primarily be addressed using core from the two reentry holes and one 35 m deep single-bit hole at Site U1415. The relationship of each of these objectives to core is briefly commented on below.

1. What is the origin and significance of layering?

Modally layered lower crustal gabbros have been central to our models for the ocean crust since the so-called "layer cake" model of the ocean crust was first developed (Anonymous, 1972). And yet to date, evidence for modally layered crust from drill core or samples recovered by other means has been sparse, comprising a single discrete sample and a small number of short drilled intervals (Perk et al., 2007; Dick, Natland, Miller, et al., 1999; Blackman, Ildefonse, John, Ohara, Miller, MacLeod, and the Expedition 305/305 Scientists, 2006). That is why recovery of abundant modally layered gabbros from the lower ocean crust, in particular those formed at a fast-spreading ridge, is a tremendous achievement. Finally, we have unequivocal confirmation of a long-standing paradigm.

The Layered Series recovered in all holes display a remarkable variety, from simple modal layering to diffuse banding. Similarly, the recovered rocks display a spectacular variation in the development of the magmatic foliation. These differing types of magmatic foliation, magmatic layering, and their margins record complex histories of crystallization, melt migration, intrusion and mixing of melts, and deformation, to name a few of the contributing processes.

2. How is melt transported from the mantle through the lower crust?

Many aspects of the recovered primitive gabbros were unexpected and call into question our understanding of MORB crystallization at fast-spreading ridges. The modal mineralogy of the Site U1415 core, in particular the abundance of orthopyroxene, demonstrates that crystallization of MORB at fast-spreading ridges may not proceed as expected. The mineral assemblages' growth and deformation textures show a remarkable complexity that implies that no single process can explain the crystallization of these primitive rocks. The types of processes that may be operative include simple cumulus crystallization, disequilibrium crystallization caused by under-cooling of a melt, and crystallization during melt extraction and compaction and migration of melt either pervasively or in channels. Imposed on these are magmatic foliations ranging from weak to strong.

3. How, and how fast, is heat extracted from the lower plutonic crust? What are the fluid and geochemical fluxes in the East Pacific Rise lower plutonic crust?

These questions are combined here as they can primarily be addressed with postcruise research. Recovery of fresh lithologies will allow for the calculation of cooling rates

using geospeedmometric techniques and investigation of the highest temperature of fluid ingress using isotopic and thermodynamic techniques. The metamorphic assemblages and their relative age relationship in the Site U1415 core already provide some insight into the evolution of fluid-rock interaction. Some of this history is particular to the tectonic setting of Hess Deep, but much of the alteration is thought to be related to lower crustal cooling prior to tectonic disruption. Similar to primitive gabbros from slow-spreading ridges, primitive bulk compositions and the abundance of olivine lead to very different alteration histories, and it is expected that postcruise research will document the extent and nature of the resultant chemical exchange.

Operations summary

Expedition 345 occupied 16 holes in water depths ranging from 4675 to 4853 m. Seven holes were cored by rotary core barrel (RCB), recovering 55.2 m of gabbroic rock. An additional 19.8 m of core was recovered during hole-cleaning operations ("ghost cores") (Table **T1**).

Two RCB holes were cored to >100 mbsf (111.8 mbsf in Hole U1415J and 107.9 mbsf in Hole U1415P). The other five RCB holes were cored to total depths ranging between 12.9 and 37.0 mbsf. The remaining holes occupied during Expedition 345 consisted of six jet-in tests and three failed attempts to establish reentry capability.

Port call in Puntarenas, Costa Rica

Hess Deep IODP Expedition 345 officially began when the ship arrived in Puntarenas at 0500 h on 11 December 2012. All times reported in this operations section are in ship local time. Ship local time initially was Universal Time Coordinated (UTC) – 6 h. During the transit to Hess Deep, ship local time changed to UTC –7 h at 1400 h on 20 December.

After the ship was secured to the dock, we started our port call activities, including customs and immigration, IODP-United States Implementing Organization (USIO) crew change and crossover, boarding of chief scientists, and loading of airfreight. Because of shared dock space with cruise ships for the first three days of port call, most port call activities were limited to evening hours.

Activities on 12 December included the ship's crew change, offloading of temperature-controlled sample shipments and all departing sea freight and loading of three

containers of freight for the ship's crew and a hydraulic pump required to repair a crane.

Early in the morning of 13 December, we moved to anchorage because of the arrival of two cruise ships. Key USIO staff met with the chief scientists to plan initial Expedition 345 operations. Expedition 345 scientists boarded the ship by water taxi and underwent safety orientation. In the evening, the cruise ships had departed, so we returned to the dock and resumed normal port call activities, including loading of arriving shipments and preparing for loading of drilling mud on the following day.

Following the introductions of Hess Deep scientists and technical staff on 14 December, the Co-Chief Scientists presented an overview of the expedition science objectives. Scientists were given a tour of the laboratories and also underwent an orientation to shipboard computing and communications technology. Loading and storing of supplies continued, including drilling mud.

On 15 December, the Hess Deep scientists were given a presentation covering the expedition science expectations, procedures, deliverables, and obligations. Following this, the final tours of the laboratories and personal computer setup were conducted. Loading of the final drilling supplies and drilling mud were completed.

Port call operations continued on 16 December with dock cleanup after the bulk loading operation. One 40 ft container of refrigerated food was loaded along with another 20 ft container of frozen food. The drill crew also began spooling on the new aft core line.

On 17 December, the drill crew completed spooling the new drill line. This process took much longer than anticipated (>24 h) because of poor spooling of the line by the vender. The installation would not have been possible without the recent modifications to the spooling tensioner that included replacement of the drum brakes with significantly better disc brakes. The last 20 ft container of dry goods was loaded aboard along with a replacement shipment of local fresh food, as half of the original fresh food delivery was rejected due to poor quality.

Departure from Puntarenas, Costa Rica

The pilot boarded the ship at 1715 h on 17 December 2012 for the scheduled departure; however, after a captain and pilot conference, the pilot elected to delay departure until slack tide at 1800 h. In the interim, a second tug was also brought over from

the nearby container port of Caldera. All lines were singled up in preparation for an imminent departure. A few minutes before departure the Schlumberger hazmat/tools airfreight shipment arrived dockside. The tools were quickly lifted aboard with the crane and the last line was cast off at 1818 h. The pilot disembarked at 1832 h, and we got underway at full speed for Site U1415 (proposed Site HD-01B). This was 0.6 days ahead of the originally scheduled 0800 h departure on 18 December.

The transit to Site U1415 was uneventful and operations and drilling personnel and Co-Chief Scientists used the time to have multiple meetings discussing the specifics of the planned Hess Deep operations. The drill crew began testing the readiness of all drilling equipment. The 1117 nmi distance from Puntarenas to Site U1415 was covered in 4.2 days at an average speed of 11.0 nmi/h.

Arrival at Hess Deep and initial near-bottom survey

We arrived on location at Site U1415 at 2350 h on 21 December 2012 and began the process of switching from the bridge "cruise" mode to dynamic positioning control. By 0040 h, all thrusters were deployed and dynamic positioning was in full control of the ship. The drill crew spent the remainder of the day picking up drill collars and assembling the drill string. This required removing collars from the forward main deck rack and making them up into stands as well as drifting and strapping (measuring) all tubulars. After deploying 130 stands of 5 inch drill pipe, the tripping operation was suspended at 1130 h to raise the upper guide horn (UGH) and deploy the subsea camera system. We deployed the camera system, to which we had attached a seafloor positioning beacon, so that it could be released in a precise position from just above the seafloor. A 3.5 kHz subbottom pinger, for surveying the thickness of sediments, was also attached to the camera system but was not turned on. Our highest priority was to deploy the seafloor positioning beacon, and we wanted to minimize the chances another sound source (e.g., 3.5 kHz pinger) might cause problems with this.

Our initial operations were designed to verify our position relative to the site survey microbathymetric data. After arriving at Site U1415, we tripped the drill pipe to the seafloor and offset the ship 300 m south of the site coordinates. This allowed the drill string to be extended to a depth of 4886 m below rig floor (mbrf), or 20 m below the estimated seafloor depth of the first proposed drill site located on the bench. Once the vibration-isolated television (VIT) subsea camera system was in position just above the seafloor, we moved the ship to the north, upslope of the site coordinates.

From there the ship was moved an additional 35 m north where the depth began to decrease, consistent with the site survey bathymetry. By monitoring the changes in water depth we were able to confirm that the drill site was indeed located in the area of interest on the target bench. The ship was then moved back to the site coordinates and from there west 100 m, where a seafloor positioning beacon attached to the subsea camera was released without difficulty. Once again the ship returned to the site coordinates, where a drill string seafloor depth of 4850.5 mbrf was visually observed. The subsea camera was then recovered to turn on the previously mounted 3.5 kHz subbottom profiling system (pinger).

Hole U1415A

Our objective in this hole was to get an initial idea of sediment thickness in preparation for surveying. The camera system was redeployed to the seafloor with the ship positioned over the Hole U1415A coordinates (Fig. F8) and the hole was spudded at 0255 h on 23 December 2012. We conducted a jet-in test by lowering the drill string and circulating, but not rotating. This test penetrated 10.3 m into the seafloor (4848.5–4858.8 mbrf). After the test was completed, we continued the 3.5 kHz pinger and camera survey to determine sediment distribution and thickness continued along the length of the bench as per the arranged Co-Chief survey plan.

Holes U1415B and U1415C

The locations of these holes were selected to test sediment thickness and subseafloor drilling conditions, with the aim of finding a suitable site for establishing a deep hole.

Near-bottom 3.5 kHz pinger and camera survey

After pulling out of the seafloor in Hole U1415A, we continued a near-bottom survey of the bench with the 3.5 kHz pinger and camera system. At 0830 h on 23 December, we stopped the survey to conduct operations in Holes U1415B and U1415C.

Hole U1415B operations

The drill string was spaced out for a jet-in test and Hole U1415B was spudded at 0905 h on 23 December (Fig. F8). This test penetrated 11.7 m into the seafloor (4856.3–4868.0 mbrf) before the driller had to make a drill string connection to add another drilling knobby. After making the connection, the driller was unable to get back to

bottom, indicating something had fallen into the hole preventing further advancement. The drill string was pulled clear of the seafloor, ending Hole U1415B.

Hole U1415C operations

Hole U1415C was spudded at 0945 h on 23 December in the same location as Hole U1415B, only this time the driller made a connection before penetrating the seafloor. The third jet-in test extended from seafloor (4856.3 mbrf) to 76.4 mbsf (4932.7 mbrf). As it turned out, this penetration was only perceived. In reality, the BHA was most likely lying slack on the seafloor. This was discovered when the camera system was recovered and the driller found that the drill string could not be rotated. Damage to the BHA, including the bending of several collars and the tapered drill collar, were determined on recovery. This damage was attributed to the difficulty in starting a hole in unstable, rubbly basement with an unknown but likely very thin sediment cover. Drilling was further complicated by the use of drilling knobbies at the top of the drill string and significant ship heave, which led to large weight fluctuations (± 50,000 lb) on the driller's weight indicator and masked the weight change when the bit encountered hard rubble to the extent that it was not detected at the driller's console. The seafloor was cleared at 1445 h on 23 December, all 30 ft drilling knobbies in the string were laid out, and the remaining drill string was recovered. At the surface, the BHA was inspected, resulting in one joint of 5½ inch transition drill pipe, one tapered drill collar, and five control-length drill collars all being taken out of service because they were either obviously bent or suspect.

Holes U1415D and U1415E

The locations of these holes were selected to test sediment thickness and subseafloor drilling conditions, with the aim of finding a suitable site for establishing a deep hole.

Near-bottom 3.5 kHz pinger and camera survey

At the end of operations in Hole U1415C and while still at that location, we assembled a new BHA and lowered the bit to just above the seafloor. We lowered the camera system with the 3.5 kHz pinger attached and initiated a new survey of the seafloor and near-subbottom. The 3.5 kHz pinger ceased transmitting ~100 m into the survey, and we shortened the survey, which was completed using only visual observations of the seafloor.

Hole U1415D operations

A new location to drill was selected and the ship moved into position for Hole U1415D (Fig. F8). Following a routine slip and cut of the drill line, we observed the bit tag seafloor at 4850.8 mbrf. Hole U1415D was spudded at 2355 h 24 December 2012. We conducted a jet-in test that advanced 4.2 m into the seafloor. The bit was pulled clear of the seafloor at 0026 h on 25 December, ending Hole U1415D.

Hole U1415E operations

After the camera system was recovered, we installed a fresh core barrel and spudded Hole U1415E at 0330 h on 25 December. This hole was rotary cored from seafloor (4850.8 mbrf) to 22.2 mbsf (4873.0 mbrf). Cores 345-U1415E-1R and 2R were recovered (0–15.3 mbsf) with 5% recovery. Very difficult hole conditions were encountered throughout the interval, with high pump pressure, high drilling torque, and hole collapse occurring every time the bit was picked up off bottom. While cutting Core 3R (15.3–22.2 mbsf), the pump pressure dropped from 800 to 350 psi at 70 strokes/min, top drive torque dropped off significantly, and the driller noticed a string weight loss of ~10,000 lb, indicating a likely BHA failure. The drill string was recovered, and the fourth drill collar pin (first collar above the outer core barrel [OCB] stand) had broken off. Besides the inner core barrel assembly, three drill collars and the entire OCB assembly were lost in the hole. In addition, two other drill collars were bent. Only the uppermost stand was in working condition.

Holes U1415F and U1415G

The locations for these holes were selected to test sediment thickness and subseafloor drilling conditions, with the aim of finding a suitable site for establishing a deep hole.

Near-bottom 3.5 kHz pinger and camera survey

At the end of operations in Hole U1415E and while still at that location, we assembled a new BHA and lowered the bit to just above the seafloor. The previous problem with the 3.5 kHz pinger was traced to dead batteries, so the batteries were charged and the pinger was operational once again. We lowered the camera system with the 3.5 kHz pinger attached and conducted a new survey of the seafloor and near-subbottom in an attempt to locate an area on the bench with thin sediment and little or no rubble in evidence. This survey lasted from 1615 to 2000 h on 26 December 2012.

Hole U1415F operations

A new location was selected, the top drive picked up, and a jet-in test was started at 2100 h on 26 December (Fig. F8). The seafloor depth for this hole was established as 4857.0 mbrf. The bit was jetted into the formation only 1.5 m before the test was terminated. The bit was pulled clear of the seafloor and the camera system was recovered.

Hole U1415G operations

The drill string was spaced out and Hole U1415G was spudded at 2355 h on 26 December without offsetting the ship from the location of Hole U1415F. RCB coring continued to 4869.94 mbrf (12.9 mbsf) before being terminated. Core 345-U1415G-1R covered this depth interval, with 2% recovery. Hole conditions were the same as in earlier holes, making it highly risky to attempt making connections with the bit in the hole. The bit was pulled clear of the seafloor at 0445 h on 27 December, ending Hole U1415G.

Hole U1415H

The location of this hole was selected to test sediment thickness and subseafloor drilling conditions, with the aim of finding a suitable site for establishing a deep hole.

Near-bottom 3.5 kHz pinger and camera survey

At the end of operations in Hole U1415G and while still at that location, we lowered the camera system with the 3.5 kHz pinger attached and conducted a new survey of the seafloor and near-subbottom en route to Hole U1415H, located 20 m west and 15 m south of Hole U1415G.

Hole U1415H operations

After arriving at the coordinates for Hole U1415H (Fig. F8), we visually observed the drill bit tag the seafloor at 4857.6 mbrf. The camera system was recovered, and Hole U1415H was spudded at 1040 h on 27 December 2012. Rotation began after penetrating ~1.0 m of soft material, and RCB coring continued to 12.9 mbsf. Core 345-U1415H-1R covered this depth interval, with 3% recovery. Drilling conditions in this hole were vastly different than in previous holes. All drilling parameters were much smoother and less erratic; however, when preparing to make a connection, the driller raised the bit off bottom. When the driller attempted to lower the bit back to bottom, immediate formation resistance was encountered. Drilling torque became elevated

and erratic, indicating the hole had once again fallen in. Because it was considered unsafe to attempt making a connection under these circumstances, the decision was made to terminate the hole before possible loss or damage to another BHA. The bit was pulled clear of the seafloor at 0410 h on 28 December, ending Hole U1415H.

Hole U1415I

The location for this RCB-cored pilot hole was selected using 3.5 kHz data that indicated a thin sediment cover and bottom images that showed a flat-lying sedimented seafloor free of rock fragments.

Near-bottom camera survey

At the end of operations in Hole U1415H and while still at that location, we deployed the camera system, without the 3.5 kHz pinger, and moved the ship ~50 m northwest to the next potential site for a pilot hole. Once on location, a brief visual survey was conducted with the subsea camera confined to a ~5 m radius around the target coordinates. The area appeared to be relatively free of boulders or any indications of rubble.

Hole U1415I operations

After the camera system was recovered, we started Hole U1415I at 1110 h on 28 December 2012. Drilling proceeded much the same as in Hole U1415H, albeit with a slower rate of penetration (ROP). After penetrating ~6 m, drilling was halted, the drill string was picked up a few meters off bottom, and the circulating pumps were reduced. This initial test indicated that the hole was remaining stable. The test was repeated the following morning at ~9 mbsf with the same result, although once back on bottom, the drilling torque temporarily increased slightly as if something was being ground up below the bit. Associated with this increase in torque was an increase in ROP from 0.4 to 0.8 m/h. Slow penetration rates were to be expected given that we were applying a very light weight on bit (5 klb), as the majority of the BHA was still unsupported above seafloor. By mid-morning on 29 December, enough penetration had been achieved to allow the core barrel to be recovered and a drill pipe connection to be attempted. We deployed the sinker bars and Core 1R was recovered at 0945 h on 29 December. The core contained 0.16 m of gabbroic rocks from 0 to 11.7 mbsf. A drill pipe connection was made, the bit was run back to bottom, and coring resumed after circulating ~3.0 m of fill out of the bottom of the hole.

RCB coring continued in Hole U1415I to 35.2 mbsf under challenging conditions. Cores 1R through 4R extended from 0 to 35.2 mbsf, with 7.12 m of recovered core. The overall recovery includes three sections of coarse sand–sized gabbro particles (Sections 345-U1415I-3R-1, 3R-2, and 3R-3). One interpretation of the presence of these particles is that were simply cuttings. Later examination showed them to be more highly altered and fractured gabbroic material than the recovered core, suggesting that a zone of cataclasis was being drilled. We spent many hours attempting to stabilize the hole so that we could hang the drill pipe off at the rig floor to deploy a FFF, but we were unable to get the bit below 8 mbsf. We eventually abandoned the effort to deploy a FFF because of the excessive risk to the BHA. We pulled the bit out of the seafloor and retrieved a core barrel (Core 5G) that contained 0.21 m of gabbroic rocks inferred to have come from no deeper than ~5 mbsf. The RCB coring assembly was changed out for a 14.75 inch tri-cone drilling assembly and deployed back to the seafloor. When the camera system reached bottom, we easily found the mound of cuttings around Hole U1415I; however, the hole appeared to be collapsed, precluding a bare-hole reentry. We decided to abandon Hole U1415I and drill a new hole nearby instead.

Hole U1415J

Hole U1415J was sited in close proximity to Hole U1415I because of the nature of the significant layered gabbroic series recovered at the bottom of Hole U1415I. From the beginning, Hole U1415J was established as a reentry hole, in a nested FFF configuration with casing.

Hole U1415J operations

After our last operation in Hole U1415I, a failed attempt to reenter the hole with a 14.75 inch tri-cone bit, we offset the ship 10 m to the north, verified that the seafloor was free of any boulders, and observed the bit tag the seafloor at 4850.0 mbrf. After we recovered the camera system, Hole U1415J was spudded at 1855 h on 31 December 2012 using a 14.75 inch tri-cone bit. Drilling proceeded at ~1.2 m/h from 0 to 7 mbsf and then slowed to ~0.6 m/h until total depth of 4865 mbrf (15 mbsf).

After three wiper trips to clean the hole, we assembled a FFF around the drill string in the moonpool. The base of the FFF has an opening of 16 inches, and we did not attach a casing stinger below the FFF. We dropped the FFF and the drill string began taking weight soon after the FFF was deployed. We then spent 11.25 h washing and reaming

the bottom 10 m of the hole. After one last wiper trip, the drill string and the 14.75 inch bit were recovered to the rig floor at 1400 h on 2 January 2013.

A 15 m string of 10.75 inch casing was made up and hung off the moonpool doors for free-fall deployment. A new 9.875 inch RCB BHA was made up and lowered through the casing to the seafloor for reentry. The 16 inch FFF was found buried upright in the cuttings pile of Hole U1415J; only the upper part of the rim and deployment shackles were visible. The FFF was reentered at 0420 h on 3 January and the camera system was retrieved. The drill string began taking weight at 9 mbsf and was easily washed down one more meter to 10 mbsf. The cone of a FFF was assembled around the drill string in the moonpool and connected to the cut-off joint of the 10.75 inch casing that had been previously hung off in the moonpool. The total length of the casing was 15.0 m from the cone base to the end of the casing shoe. The assembly was free-fall deployed at 0730 h on 3 January.

The hole was washed and reamed to total depth (15 mbsf) and circulated clean with two 25 bbl mud sweeps. Ghost Core 2G, containing 0.2 m of rock fragments and two buckets full of coarse sand, interpreted to be drill cuttings, was recovered from the cleaned interval at 1045 h. We resumed RCB coring and Cores 3R through 5R were retrieved. Hole problems required washing and reaming at ~32 and 35 mbsf, during which ghost Cores 6G and 7G were recovered by 0100 h on 5 January. Another fresh core barrel was dropped, and on this attempt the bit made it easily to total depth (34.9 mbsf) and RCB coring resumed. The hole drilled smoothly and Core 8R was recovered from 34.9 to 45.2 mbsf at 0805 h. During retrieval, the area between 4878 and 4882 mbrf (28 and 32 mbsf) remained problematic and was once again reamed and conditioned multiple times. RCB coring resumed at 0900 h, and Core 9R was cut from 45.2 to 55.3 mbsf and arrived on deck at 1200 h on 5 January.

Coring continued through Core 13R, which extended the hole to 79.4 mbsf. A wiper trip was conducted, and the bit was raised to 6.5 mbsf without encountering any problems. The bit was then lowered back into the hole and took weight at ~37 mbsf. The driller was able to wash and ream to 45 mbsf. The bit was lowered and encountered weight again at 57 mbsf. The driller washed and reamed the hole to total depth at 79.4 mbsf. The bit was raised off the bottom of the hole and became stuck at 72 mbsf with high circulation pressure, no rotation, and no ability to move the bit up or down. The pipe was worked for 2.5 h before it was pulled free with 100 klb overpull. The bit was pulled up to 6 mbsf inside the 10.75 inch casing. The core barrel that was

in place during this wiper trip was recovered (Core 14G), and a new core barrel was dropped.

We decided to use cement to help stabilize the hole. However, we had not yet observed the nested FFFs and therefore did not know how far the 15 m of casing attached to the FFF extended into the borehole. We raised the bit back up into the 10.75 inch casing and deployed the camera system to constrain the height of the FFF above seafloor. The top of the second, "upper" funnel appeared to be ~2 m above the rim of the first, leaving the casing shoe at ~13 mbsf. After retrieving the camera system, we wanted to get the bit as deep as possible before cementing. After passing a tight spot at 38 mbsf, we were able to wash and ream to 57 mbsf. However, we could not get past this depth and stopped trying at 0800 h on 7 January. At this time, the core barrel that was in place during this washing and reaming was retrieved (Core 15G). We deployed a new core barrel, washed and reamed back down to 57 mbsf, and pumped 25 bbl of cement that contained 0.25 lb/sack of lost-circulation material. After the cement was in place, we raised the bit up to 15 mbsf and the 10.75 inch casing was flushed to remove any cement from this area. The bit was then pulled out of the hole, and the drill string was flushed to clear out any remaining cement residue. We slipped and cut 115 ft of drill line and then retrieved the drill string. The bit was back on the rig floor at 2315 h on 7 January.

We then assembled a new BHA with a 9.875 inch tri-cone bit for drilling out the cement. This bit does not recover core but has a more robust cutting structure for reaming and clearing operations. The drill string was lowered to the seafloor and we reentered Hole U1415J at 1130 h on 8 January. After recovering the camera system, the bit was run to 57 mbsf before encountering fill, without any evidence of cement. The hole was reamed once again to 77 mbsf and swept with high-viscosity mud. The bit was pulled up to 14 mbsf for a wiper trip and then lowered back down to 76 mbsf. The bit was then positioned at 63 mbsf, and a second remedial cement job was performed using 35 bbl of cement. During the cement job, the bit was lowered to 71 mbsf. After the cement was pumped, the bit was raised up to the casing shoe, and the 10.75 inch casing was flushed to ensure that no cement remained in this interval. The bit was pulled clear of the seafloor, and the drill string was circulated to flush any remaining cement from the pipe.

Because we wanted to drill out the cement with the same bit, we had to wait for the cement to harden. While waiting for this to happen, we conducted a near-bottom camera and 3.5 kHz pinger survey of two other potential drill sites. At the completion

of the survey, we reentered Hole U1415J at 2215 h on 9 January. We felt that the cement still needed a little more time to harden, so we kept the bit in the 10.75 inch casing until 0630 h. On lowering the bit into the hole, we encountered the same obstruction at ~35 mbsf, but it was easily passed. This time, the bit encountered cement at 63 mbsf, which we drilled out to 73 mbsf. Several hours were required to drill back down to the total depth of the hole (79.4 mbsf). Little advancement could be made until we significantly reduced the pump strokes to ~30 strokes/min, which allowed the bit to advance to the bottom of the hole. Each time a mud sweep was pumped, clear pump pressure changes were observed suggesting that the cuttings might now be getting circulated out of the hole. We then drilled 5 m of new hole (to 84.4 mbsf) without coring in an unsuccessful attempt to reach a more competent formation. At this point, we decided to retrieve the drill string to switch back to a RCB coring BHA. The bit was back on the rig floor at 0600 h on 11 January.

We assembled a new BHA with a 9.875 inch RCB coring bit, lowered it to the seafloor, and reentered Hole U1415J at 1700 h on 11 January. The bit began to take weight at the normal 35 mbsf but was able to pass through quickly. The hole was then washed and reamed, reaching the bottom of the hole (84.4 mbsf) at 0130 h on 12 January. The core barrel used during this reaming (Core 17G) was recovered and on deck at 0230 h on 12 January. We dropped a new core barrel and resumed RCB coring. Core 18R advanced from 84.4 to 89.1 mbsf. All drilling parameters appeared stable and good. Initial indications were that the two remedial cement jobs were successful and that the cuttings were now being expelled from the hole. New fill on bottom between cores appears to be from the immediate formation being drilled into and not from uphole. Core 19R was advanced from 89.1 to 94.1 mbsf. Coring parameters remained reasonably constant and the penetration rate was initially 2.5 m/h but jumped to 5.0 m/h midway through cutting Core 19R.

After recovering Core 19R, we encountered challenges getting back to the bottom of the hole. Once we did, however, Cores 20R and 21R were cut from 94.1 to 101.8 mbsf and recovered 1.58 m (21%) of rocks. The hole conditions continued to be problematic, and we conducted a wiper trip up to 74 mbsf that encountered tight spots at 82 and 86 mbsf. Core 22G was recovered from this reamed interval. After eventually getting back to bottom, Core 23R extended 2 m into new formation (101.8–103.8 mbsf). Once again, we had challenges washing and reaming back to the bottom of the hole (103.8 mbsf). In the end, we were unable to get completely back to bottom and our pump pressures remained abnormally high, leading us to suspect that one or more bit nozzles were plugged. We decided to attempt cementing the lower 20 m of the hole

(our third cement job in this hole) and then retrieve the drill string to replace the bit while the cement hardened. Before pumping the cement, we retrieved Core 24G. After positioning the bit at 96 mbsf, we pumped 12.5 bbl of cement. The bit was raised up to 76 mbsf while pumping the cement. The bit was then pulled to 15 mbsf so that any cement remaining in the casing/FFF could be circulated out. We pulled the bit out of the hole at 1605 h on 13 January. The drill string was then flushed of any remaining cement, and the bit was back on the rig floor at 0135 h on 14 January.

A new RCB (C-7) bit with a mechanical bit release (MBR) was assembled to the bottom of the BHA. We also added a fourth stand of drill collars to the BHA. After tripping to the seafloor, operations were put on hold while a slip and cut of the drill line was completed. We reentered Hole U1415J at 1542 h on 14 January. Once the camera system was back on board, the driller commenced lowering the pipe into the hole. The drill string took weight at 36 mbsf but was able to pass this interval relatively easily. The bit encountered cement at 78 mbsf and was drilled out to 99 mbsf (3 m below the bit depth when cementing). We washed and reamed the rest of the way back down to the bottom of the hole (103.8 mbsf). After we retrieved the core barrel that was in place while washing and reaming from 99.0 to 103.8 mbsf (Core 25G; 0.48 m recovered), we resumed RCB coring. While cutting Core 26R (103.8–111.8 mbsf), the first 4.2 m drilled at a slow 1.3 m/h, but the last 3.8 m was penetrated in <3 min. Core 26R was recovered on-deck at 0830 h on 15 January. While retrieving the core, the drill pipe became stuck. We tried to free the drill string for over an hour before deciding release the bit as the next step in freeing the drill string. When lowering the MBR shifting tool with the sinker bars to release the bit, we attached the core orientation (FlexIt) tool so we could determine the hole inclination. We had to offset the ship ~260 m (~5% of water depth) to lower a tool joint down nearly 8 m to the rig floor so that the core barrels could be removed and the shifting/FlexIt tools deployed. Our attempt to shift the MBR sleeve and release the bit was unsuccessful, so we retrieved the shifting tool. Data from the FlexIt tool indicated the hole was ±3° from vertical. This put to rest one proposed theory that we had been tracking down a high angle fault and might never drill out of the fractured material. On our second attempt to release the bit, we added a core barrel to the shifting tool and pumped it down to the bit at 70 strokes/min. The sinker bars were then run into the hole to retrieve the shifting tool and release the bit. However, before the sinker bars reached the core barrel, the drill string worked itself free. The sinker bars were recovered, leaving the core barrel and shifting tool in place. If we had recovered the core barrel, the sleeve would have shifted, leaving the bit and MBR in the hole. Once the pipe was free, we were able to pull the drill string, and the bit was back on the rig floor at 0130 h on 16 January.

Because of the continually problematic and deteriorating hole conditions and the diminishing return on recovering core samples for science, the decision was made to abandon Hole U1415J and move to a different location.

Holes U1415K–U1415N

Hole U1415K consisted of a failed attempt to establish reentry capability that penetrated to 35.3 mbsf without any coring except for a single ghost core (345-U1415K-2G) that recovered 4.72 m of surficial mud, gravel, and rocks. Hole U1415L consisted of a jet-in to 4 mbsf; no cores were recovered. Hole U1415M was a failed attempt to establish reentry capability that penetrated to 25.9 mbsf without any coring except for a single ghost core (345-U1415M-2G) containing 5.87 m of surface gravel and mud. Hole U1415N consisted of RCB coring that penetrated to 37.0 mbsf and recovered a total of 1.56 m (4%) of olivine-phyric basalt and gabbro.

Hole U1415K operations

After moving ~400 m northwest of Hole U1415J, we lowered a new BHA with a 14.75 inch tri-cone bit to the seafloor and prepared to conduct a short camera survey prior to spudding the hole. However, the camera developed problems during the trip in and had to be recovered. A spare camera was installed before it was redeployed. We conducted an expanding box survey extending out 10 m, and a location to start Hole U1415K was chosen. We verified the seafloor depth (4698.4 mbrf) by tagging the seafloor with the bit, retrieved the camera system, and started Hole U1415K at 2155 h on 16 January 2013. The 14.75 inch hole reached a total depth of 35.3 mbsf by 0400 h on 17 January. A wiper trip was performed, and the bit pulled back to 6.6 mbsf. A 16 inch FFF without any stinger was deployed to facilitate subsequent reentries. The driller waited 1.25 h before pulling out of the hole to allow time for the FFF to reach the seafloor. The bit was then pulled clear of the seafloor at 2310 h on 17 January. We deployed the camera to observe the FFF cone; the cone was not upright and appeared to be nearly on its side. We felt that the base of the FFF cone was still in or immediately adjacent to the hole. We decided to retrieve the bit, change to an RCB BHA, and attempt to reenter the hole (either through the FFF cone or by a bare rock reentry). The ultimate goal was to deploy a second FFF with 10.75 inch casing to stabilize the upper ~35 m of hole and allow deeper coring. The 14.75 inch bit arrived back on the rig floor at 1110 h on 18 January. A 36 m length of 10.75 inch casing string was assembled and hung off in the moonpool doors using C-plates and casing elevators. The RCB BHA was assembled and lowered through the casing and back to the seafloor. The

camera was deployed, and a seafloor survey was conducted from 2333 h on 18 January until 0051 h on 19 January in an attempt to locate Hole U1415K. No discernible hole or cuttings mound could be identified during the survey, and it was decided that the hole was located at the base of the leaning FFF cone. A reentry was attempted by placing the bit at the base of the cone. This was accomplished relatively quickly (~45 min) and the bit was lowered into the seafloor, penetrating 1–2 m before taking weight. We decided to retrieve the camera and to attempt to walk the bit into the hole using light bit weight and low rpm. A perceived reentry into Hole U1415K occurred at 0140 h. Rotation was applied for ~2 h without any luck in penetrating further into the hole. We decided to abandon our attempts to continue operations in Hole U1415K, retrieve the RCB BHA, and start a new hole with a 14.75 inch tri-cone bit. As of 1200 h on 19 January, the RCB BHA was still being recovered back to the surface. The RCB BHA and coring bit was back on the rig floor at 1510 h on 19 January. The seafloor positioning beacon deployed at the start of our Hess Deep operations on 22 December 2012 was nearing the expected lifetime of its batteries, so we commanded it to release at 1503 h and it was back aboard at 1639 h.

Hole U1415L operations

We assembled a 14.75 inch tri-cone bit and drilling BHA with three stands of drill collars and lowered it to the seafloor. While the BHA was being lowered, we also deployed the camera system with the same positioning beacon (with new batteries) and the 3.5 kHz pinger. The seafloor positioning beacon was commanded to release at the Hole U1415K coordinates, but it did not immediately fall to the seafloor. After 40 minutes of working the camera system up and down, the beacon eventually came loose. At 0515 h on 20 January, we started a visual and 3.5 kHz subbottom seafloor survey by moving the ship 95 m east of Hole U1415K. Unfortunately, the 3.5 kHz pinger ceased working before the survey commenced, but we continued with the visual inspection of the seafloor. After we arrived at the target location, we conducted a box survey extending out 10 m to ensure that no large boulders or rubble were in close proximity. We also tagged the seafloor with the bit, revealing an approximate seafloor slope of ~14° to the south. Hole U1415L consisted of a 1 h jet-in test that penetrated to 4 mbsf through sediment and soft rubble. Hole U1415L was spudded at 0845 h on 20 January, and the bit was pulled clear of the seafloor at 0900 h.

Hole U1415M operations

After recovering the camera system, Hole U1415M was started at 1240 h on 20 January. The initial penetration from seafloor to 5 mbsf went relatively quickly, indicating

that the formation was sediment/soft rubble. From ~5 to 9 mbsf, the formation became hard with a significantly slower ROP (0.5–1.0 m/h) and smooth torque, as is typical of massive hard rock. The ROP increased again to ~4.0 m/h from 9.0 to 11.0 mbsf. A hard rock reentry system (HRRS)-style FFF with a 26 inch opening was assembled around the drill string in the moonpool. We did not attach a stinger or base plate. The funnel was deployed at 2100 h on 20 January. We then deepened the hole to 19.6 mbsf, where the hole began to pack off. We spent the next 4 h washing and reaming the hole and circulating high-viscosity mud. Eventually the hole was stabilized, and we continued drilling down to 25.9 mbsf. At that depth, the bottom of the hole became problematic and the bit was unable to penetrate deeper than 24 mbsf, so we conducted a wiper trip by raising the bit up to 8 mbsf and then lowering it to the bottom of the hole. However, the bit still could not penetrate past 24 mbsf. Another high-viscosity mud sweep was pumped. The camera system was lowered to observe the orientation of the FFF cone, but it was obscured by clouds of mud and cuttings coming from the hole. Portions of the rim of the FFF cone, however, were discernible at times buried in cuttings. We pulled the bit out of the hole at 1602 h on 21 January and then waited for 1 h to let cuttings settle for better visibility. The top of the FFF cone was clearly visible in the cuttings mound. The camera was retrieved, the drill string raised to 4660 mbrf, the top drive set back, and we performed a slip and cut of 115 ft of drill line. After the slip and cut, the drill string was recovered, and the bit arrived back on the rig floor at 0330 h on 22 January. Our next step was to assemble 25 m of 10.75 inch casing and hang it off on the moonpool doors. We assembled a RCB BHA with a used C-7 core bit (2 h rotating time in Hole U1415K) and lowered it and the camera system to the seafloor. The top drive was installed and the drill string spaced out for reentry into Hole U1415M. An attempt was made to maneuver the vessel for reentry; however, because of the drill string space out, the bit was positioned nearly at the seafloor, and the driller was unable to raise the bit any higher. This resulted in the bit repeatedly tagging the cuttings mound and the FFF, creating clouds of debris in the water column and completely obscuring the FFF cone. We offset the ship south to slightly deeper water while a 30 ft knobby was laid out and a 20 ft knobby was picked up, giving an additional 3 m of room in the derrick. We moved back over Hole U1415M and reentered the FFF cone at 1645 h on 22 January. The cone appeared to tip/shift as the bit made contact with the inner surface. Circulation along with slow rotation was used in an unsuccessful attempt to find the 14.75 inch hole. No progress was made, and we retrieved the camera system so we could use more rotation. This also was not successful, so we redeployed the camera system and offset the ship in an attempt to drag the funnel out of the way. This also did not work,

and the FFF cone appeared to be solidly in place in the cuttings mound, wedged sideways into a large boulder that had been hidden beneath the seafloor sediment. We reentered the FFF cone for one last failed attempt to find the hole below the FFF cone. We then decided to abandon Hole U1415M at 0000 h on 23 January. Ghost Core 2G (assumed to be from 0 to 3.5 mbsf) was recovered at 0230 h on 23 January containing 5.87 m of surface gravel and mud from the multiple failed reentry attempts.

Hole U1415N operations

Because we had the RCB coring system in place, we decided to offset the ship to immediately spud a single-bit unsupported hole. The vessel was moved 15 m west of Hole U1415M. We recovered the camera system, dropped a new core barrel, and started Hole U1415N at 0340 h on 23 January. Core 1R was cut from 0 to 14.9 mbsf and was recovered at 1315 h on 23 January with 0.45 m of roller rocks. After retrieving Core 2R (14.9–18.9 mbsf; 0.15 m recovery), 4.75 h were spent to work the bit down to bottom before beginning to cut the next core at 2330 h on 23 January. Core 3R was a full 9 m advance (18.9–27.9 mbsf; 0.50 m recovered), and then the ROP for Core 4R (29.7–37.0 mbsf; 0.46 m recovered) was very high. After recovering Core 4R, the drillers were never able to work the bit back down to bottom. The hole continued to pack off (high pump pressures) and had high/erratic torque, as seen during the expedition associated with the unstable/rapidly drilled intervals. We decided to abandon Hole U1415N at 1700 h on 24 January. The bit cleared the seafloor at 1740 h and was back on the rig floor at 0145 h on 25 January. The core barrel that was in place during the final attempts to clean out the hole back to bottom (Core 5G) was recovered at 0125 h on 25 January. The four cores recovered from Hole U1415N extended from 0 to 37.0 mbsf and recovered 1.56 m (4%) of basement rocks.

Hole U1415O

Our only operation here consisted of drilling a 14.75 inch hole to 17.0 mbsf. After reaching this depth, we prepared to establish reentry capability but had to abandon the hole because of poor hole conditions.

Hole U1415O operations

Following unsuccessful operations at Holes U1415K–U1415N on the shoulder, we decided to move back to the bench. The BHA was changed to a drilling assembly with a 14.75 inch tri-cone bit and lowered to the seafloor. While the BHA was being deployed, a new FFF cone was prepared for deployment. We deployed the camera system

with the 3.5 kHz pinger attached and conducted a seafloor survey around the target drilling location. We also observed the bit tag the seafloor at 4861.0 mbrf. The survey was completed at 1536 h on 25 January 2013 and the camera system was back on board at 1815 h. Drilling in Hole U1415O started at 1900 h. The bit was washed down 1.5 mbsf and then drilled in a massive, hard formation to 5 mbsf. At 5 mbsf, the bit penetrated 10 m (to 15 mbsf) in only 15 min. The formation firmed up from 15.0 to 17.0 mbsf by 0345 h on 26 January. We then successfully conducted a wiper trip and started to prepare to deploy the FFF cone. At this time, the hole began to collapse, and our attempts to drill and ream back down to bottom failed; we could only get back to ~8 mbsf. We decided to abandon Hole U1415O at 0700 h on 26 January. The bit cleared the seafloor at 0710 h, ending Hole U1415O.

Hole U1415P

Hole U1415P was sited on the southern margin of a small promontory, between Holes U1415G and U1415O. From the onset, Hole U1415P was established as a reentry hole and was intended to be a nested FFF configuration with casing similar to that at Hole U1415J. However, after deployment the initial FFF cone tipped over and could not be used. Instead, we successfully reentered the bare hole and installed a FFF with 12.5 m of 10.75 inch casing.

The primary accomplishment in Hole U1415P was RCB coring that extended from 12.5 to 107.9 mbsf and recovered 30.57 m (32%) of gabbroic rocks. In addition, material was recovered in five ghost cores obtained during hole cleaning operations in previously drilled portions of the hole.

Hole U1415P operations

After conducting a visual survey and selecting the position for Hole U1415P, we recovered the camera system, installed the top drive, spaced out the drill string, and started Hole U1415P at 1255 h on 26 January 2013. The 14.75 inch bit was washed without rotating to 2.0 mbsf (4866.0 mbrf), and drilling proceeded to 11.0 mbsf (4875.0 mbrf). We then assembled a HRRS-style FFF cone. The 26 inch interior diameter of this cone was reduced to 16 inches by attaching portions of a CORK fishing tool funnel (OF3620). In contrast to our previous FFF cone deployments, this time we attached a base plate to the bottom of the FFF. After the FFF cone was deployed to the seafloor, we continued drilling the hole to 12.5 mbsf. The camera was deployed to observe the orientation of the FFF cone and the bit pulling out of it. However, the FFF was very difficult to see through clouds of sediment. Eventually, we decided not to

wait and pulled the bit out of the hole and through the FFF cone at 1545 h on 27 January. The bit appeared to heave down on the cone at least twice in the process. The bit was back on the rig floor at 0105 h on 28 January. We assembled 12.5 m of 10.75 inch casing and hung it off on the moonpool doors. Next, we assembled an RCB BHA, lowered it through the casing in the moonpool, and lowered it to the seafloor. The camera system was also lowered to the seafloor. Before we prepared to locate and reenter Hole U1415P, we had to slip and cut the drill line for the fourth time this expedition. After installing the top drive and spacing out for reentry, it was immediately apparent that the FFF cone was not sitting upright. Some camera perspectives looked as if the FFF cone was leaning to one side, whereas in other perspectives it appeared to be lying fully on its side. At the base of the FFF cone was a dark spot that appeared to be the top of the hole. Discussions alternated between attempting to reenter the cone or the hole. Eventually the pipe was maneuvered close enough to take a stab at cone reentry. The cone was indeed lying on its side at too high an angle for reentry, and this attempt failed. We then moved the bit over the dark area at the base of the FFF cone and successfully reentered Hole U1415P at 1450 h on 28 January. The total time expended after starting to search for the FFF cone was 2.6 h. The reentry of the bit into the open 14.75 inch hole with >4800 m (3.0 miles) of drill string deployed was quite an impressive feat achieved by the dynamic position and drilling staff. The camera system was recovered and the hole was redrilled from 8.0 to 12.5 mbsf and swept with high-viscosity mud. The core barrel used during washing and reaming this interval (Core 2G) was recovered with 2.36 m of rubble. Our next step was to assemble a FFF cone to the 12.5 m of 10.75 inch casing hung off in the moonpool. We free-fall deployed the 10.75 inch casing with the attached FFF and dropped a core barrel to start coring ahead. The driller could not identify the normal pressure spike that occurs when the core barrel has landed at the bottom of the BHA. When the pump pressure was increased to confirm the core barrel had landed properly, the rotary hose that supplies drilling fluid to the top drive suddenly burst. The hose failed on the top drive connection at 2400 psi even though the hose is rated to 5000 psi working pressure. After we installed a new hose, we reached the bottom of the hole (12.5 mbsf) at 0500 h on 29 January. We started RCB coring and Core 3R (12.5–18.1 mbsf) arrived on deck at 1225 h. We had some difficulty getting the bit through the transition from the 14.75 to 9.875 inch portion of the hole, but we were able to drill out this area (Core 4G; 12.5–16.5 mbsf). RCB coring resumed and Cores 5R–10R extended the hole from 18.1 to 45.6 mbsf and recovered 12.19 m (44%) of nicely cored pieces of gabbro. Core 11R was cut in only 45 min of rotating time. RCB coring continued to Core 18R, extending to 82.3 mbsf and recovered on deck at 0920 on 1 February. As the hole was

deepened, we experienced faster coring rates through a formation inferred to be more fractured, leading to increasingly difficult hole cleaning. Eventually, we decided to pull out of the hole for a bit change because of increasing bit hours, decreasing recovery, and extended periods of washing/reaming back to bottom after recovering core barrels. We pulled the bit out of the hole, and the bit was back on the rig floor at 1845 h 1 February. After assembling a new C-7 RCB bit, we lowered the drill string, deployed the camera system, installed the top drive, and spaced out the drill string for reentry by 0530 h on 2 February. We reentered Hole U1415P at 0553 h. During reentry, we confirmed the top of the FFF cone was at 4862.5 mbrf. The height of the FFF from base plate to rim is 1.2 m, placing the base of the FFF at 4863.7 mbrf. The seafloor tag depth was determined to be 4864.0 mbrf on 26 January at slack tide. The FFF depth was established on 2 February when the tide tables indicated a high tide of 0.2 m. Therefore, the FFF appears to be installed right at the seafloor (4863.9 versus 4864.0 m).

We washed and reamed down to the bottom of the hole (82.3 mbsf) slowly to clean out the hole in small increments as opposed to loading up the annulus with large amounts of fill/cuttings and then having to wash these out all at once. After we finished washing and reaming down to the bottom of the hole (82.3 mbsf), we recovered the core barrel used during this hole cleaning (Core 19G; 0.6 m recovered) at 1920 h. We resumed RCB coring and Core 20R was cut from 82.3 to 89.4 mbsf. Before retrieving Core 20R, the hole had to be washed and cleaned enough to attempt making a connection. At the time, several bit nozzles were also plugged. At 0030 h on 3 February, we were able to remove a drilling knobby so that Core 20R could be recovered (0130 h) with 2.42 m of nicely cored gabbro. A new core barrel was deployed, and the drillers were able to partially unplug the bit nozzles. Before coring could resume, the hole had to be washed and reamed from 79.0 to 89.4 mbsf. At 0900 h, the core barrel deployed during this reaming was retrieved (Core 21G). We had to wash and ream back to the bottom of the hole again but then continued coring from there. Cores 22R and 23R were recovered from 89.4 to 107.9 mbsf and recovered 4.87 m (26%). After retrieving Core 23R, hole conditions began deteriorating, with the hole packing off and the bit taking weight ~9 m above the bottom of the hole. As we had just added a joint of pipe and the bit was unable to pass below this depth, we had to offset the ship 100 m to reach a connection so that the driller could pull up and lay out the same piece of pipe. At this point, we raised to 76.0 mbsf, resumed hole cleaning, reamed back down to the bottom of the hole (107.9 mbsf), and recovered the core barrel used during the reaming (Core 24G). Once again, the hole packed off and circulation and rotation were lost while making the connection after laying out the barrel, so we off-

set the ship 100 m (2% of water depth) to reach a connection in order to remove more drill pipe. We raised the bit to 79.0 mbsf and started to work the bit back down. However, after making another connection the bit could not be advanced further because of high torque, packing-off, and plugged nozzles. Ultimately, we decided to stop trying to core and to conduct a wiper trip to prepare the hole for logging.

To prepare for logging, we raised the bit to 11.9 mbsf (inside the 10.75 inch casing) and then lowered it back down the hole. Problems were encountered at 41, 55–60, and 84–90 mbsf that had to be drilled through. We elected not to attempt to clean out the ~18 m of hard fill in the bottom of the hole. At 1215 h on 4 February, the bit was back up to 11.9 mbsf (inside the casing). We deployed the camera and pulled the bit clear of the hole at 1434 h. At 1449 h, we observed the bit successfully release from the BHA. The end of pipe reentered Hole U1415P at 1550 h after only 15 min of maneuvering. We recovered the camera, placed the end of pipe at 10 mbsf, and lowered the first logging string into the hole (caliper and Dipole Sonic Imager). We had decided to deploy a very short logging string because of the poor hole conditions and risk of the tools getting stuck. The logging tool string could not pass 24 mbsf (11.5 m below the 10.75 inch casing shoe). The logging tools were retrieved so that the end of pipe could be lowered past the trouble area. The drill pipe could not be lowered past 20 mbsf (7.5 m below the casing shoe), so we terminated our logging. We pulled the bit out of the hole at 0315 h on 5 February. RCB coring in Hole U1415P extended from 12.5 to 107.9 mbsf and recovered 30.57 m (32%) of gabbroic rocks. In addition, five cores were recovered from previously drilled portions of the hole during the hole cleaning operations.

Because there was not sufficient time remaining to conduct any further drilling operations as we had dropped the bit for logging, we deployed the camera and 3.5 kHz pinger to conduct a final seafloor survey across Hole U1415P. The survey was completed at 0845 h on 5 February. Although the drill string was back on board at 1745 h, the beacon retrieved at 1838 h, and the hydrophones raised by 1900 h, we delayed our departure until 2000 h so that inductively coupled plasma–atomic emission spectroscopy geochemical analyses that are sensitive to ship motion could be completed. After we raised the thrusters, we started our transit to Balboa, Panama, at 2048 h, about a half day ahead of the scheduled departure time. During the transit, ship local time was shifted ahead 1 h on 7 February (to UTC – 6) and 1 h on 9 February (to UTC – 5). The ~1467 nmi transit from Hess Deep to Balboa took 6.5 days at 9.3 nmi/h. Expedition 345 ended with the first line ashore at 1151 h on 12 February 2013.

References

Agrinier, P., Hékinian, R., Bideau, D., and Javoy, M., 1995. O and H stable isotope compositions of oceanic crust and upper mantle rocks exposed in the Hess Deep near the Galapagos triple junction. *Earth Planet. Sci. Lett.,* 136(3–4):183–196. **doi:10.1016/0012-821X(95)00159-A**

Alt, J.C., and Bach, W., 2006. Oxygen isotope composition of a section of lower oceanic crust, ODP Hole 735B. *Geochem., Geophys., Geosyst.,* 7(12):Q12008. **doi:10.1029/2006GC001385**

Alt, J.C., Laverne, C., Coggon, R.M., Teagle, D.A.H., Banerjee, N.R., Morgan, S., Smith-Duque, C.E., Harris, M., and Galli, L., 2010. Subsurface structure of a submarine hydrothermal system in ocean crust formed at the East Pacific Rise, ODP/IODP Site 1256. *Geochem., Geophys., Geosyst.*, 11(10):Q10010. **doi:10.1029/2010GC003144**

Alt, J.C., Laverne, C., Vanko, D.A., Tartarotti, P., Teagle, D.A.H., Bach, W., Zuleger, E., Erzinger, J., Honnorez, J., Pezard, P.A., Becker, K., Salisbury, M.H., and Wilkens, R.H., 1996. Hydrothermal alteration of a section of upper oceanic crust in the eastern equatorial Pacific: a synthesis of results from Site 504 (DSDP Legs 69, 70, and 83, and ODP Legs 111, 137, 140, and 148.) *In* Alt, J.C., Kinoshita, H., Stokking, L.B., and Michael, P.J. (Eds.), *Proc. ODP, Sci. Results,* 148: College Station, TX (Ocean Drilling Program), 417–434. **doi:10.2973/odp.proc.sr.148.159.1996**

Anonymous, 1972. Penrose field conference on ophiolites. *Geotimes,* 17:24–25.

Arai, S., and Matsukage, K., 1996. Petrology of gabbro-troctolite-peridotite complex from Hess Deep, equatorial Pacific: implications for mantle-melt interaction within the oceanic lithosphere. *In* Mével, C., Gillis, K.M., Allan, J.F., and Meyer, P.S. (Eds.), *Proc. ODP, Sci. Results,* 147: College Station, TX (Ocean Drilling Program), 135–155. **doi:10.2973/odp.proc.sr.147.008.1996**

Arai, S., Matsukage, K., Isobe, E., and Vysotskiy, S., 1997. Concentration of incompatible elements in oceanic mantle: effect of melt/wall interaction in stagnant or failed melt conduits within peridotite. *Geochim. Cosmochim. Acta,* 61(3):671–675. **doi:10.1016/S0016-7037(96)00389-4**

Ballu, V., Hildebrand, J.A., and Canuteson, E.L., 1999. The density structure associated with oceanic crustal rifting at the Hess Deep: a seafloor and sea-surface gravity study. *Earth Planet. Sci. Lett.,* 171(1):21–34. **doi:10.1016/S0012-821X(99)00132-6**

Bédard, J.H., Sparks, R.S.J., Renner, R., Cheadle, M.J., and Hallworth, M.A., 1988. Peridotite sills and metasomatic gabbros in the eastern layered series of the Rhum complex. *J. Geol. Soc. (London, U. K.),* 145(2):207–224. **doi:10.1144/gsjgs.145.2.0207**

Bickle, M.J., and Teagle, D.A.H., 1992. Strontium alteration in the Troodos ophiolite: implications for fluid fluxes and geochemical transport in mid-ocean ridge hydrothermal systems. *Earth Planet. Sci. Lett.,* 113(1–2):219–237. **doi:10.1016/0012-821X(92)90221-G**

Blackman, D.K., Ildefonse, B., John, B.E., Ohara, Y., Miller, D.J., MacLeod, C.J., and the Expedition 304/305 Scientists, 2006. *Proc IODP,* 304/305: College Station, TX (Integrated Ocean Drilling Program Management International, Inc.). **doi:10.2204/iodp.proc.304305.2006**

Blum, N., 1991. Structure and composition of oceanic crust and upper mantle exposed in Hess Deep of the Galapagos microplate (equatorial east Pacific) [Ph.D.dissert.]. Univ. Karlsruhe, Germany.

Boudier, F., Nicolas, A., and Ildefonse, B., 1996. Magma chambers in the Oman ophiolite: fed from the top and the bottom. *Earth Planet. Sci. Lett.,* 144(1–2):239–250. **doi:10.1016/0012-821X(96)00167-7**

Brown, G.M., 1956. The layered ultrabasic rocks of Rhum, Inner Hebrides. *Philos. Trans. R. Soc., B,* 240(668):1–54. **doi:10.1098/rstb.1956.0011**

Canales, J.P., Nedimovic, M.R., Kent, G.M., Carbotte, S.M., and Detrick, R.S., 2009. Seismic reflection images of a near-axis melt sill within the lower crust at the Juan de Fuca Ridge. *Nature (London, U. K.),* 460(7251):89–93. **doi:10.1038/nature08095**

Cann, J.R., 1974. A model for oceanic crystal structure developed. *Geophys. J. R. Astron. Soc.,* 39(1):169–187. **doi:10.1111/j.1365-246X.1974.tb05446.x**

Cannat, M., Karson, J.A., Miller, D.J., et al., 1995. *Proc. ODP, Init. Repts.,* 153: College Station, TX (Ocean Drilling Program). **doi:10.2973/odp.proc.ir.153.1995**

Cannat, M., Mével, C., Maia, M., Deplus, C., Durand, C., Gente, P., Agrinier, P., Belarouchi, A., Dubuisson, G., Humler, E., and Reynolds, J., 1995. Thin crust, ultramafic exposures, and rugged faulting patterns at the Mid-Atlantic Ridge (22°–24°N). *Geology,* 23(1):49–52. **doi:10.1130/0091-7613(1995)023<0049:TCUEAR>2.3.CO;2**

Chen, Y.J., 2001. Thermal effects of gabbro accretion from a deeper second melt lens at the fast spreading East Pacific Rise. *J. Geophys. Res., [Solid Earth],* 106(B5):8581–8588. **doi:10.1029/2000JB900420**

Cherkaoui, A.S.M., Wilcock, W.S.D., Dunn, R.A., and Toomey, D.R., 2003. A numerical model of hydrothermal cooling and crustal accretion at a fast spreading mid-ocean ridge. *Geochem., Geophys., Geosyst.,* 4(9):8616. **doi:10.1029/2001GC000215**

Coogan, L.A., 2007. The lower oceanic crust. *In* Rudnick, R.L. (Ed.), *Treatise on Geochemistry: The Crust* (Vol. 3). Holland, H.D., and Turekian, K.K. (Series Eds.): New York (Elsevier), 1–45. **doi:10.1016/B978-008043751-4/00230-3**

Coogan, L.A., Gillis, K.M., MacLeod, C.J., Thompson, G.M., and Hékinian, R., 2002a. Petrology and geochemistry of the lower ocean crust formed at the East Pacific Rise and exposed at Hess Deep: a synthesis and new results. *Geochem., Geophys., Geosyst.,* 3(11):8604. **doi:10.1029/2001GC000230**

Coogan, L.A., and Hinton, R.W., 2006. Do the trace element compositions of detrital zircons require Hadean continental crust? *Geology,* 34(8):633–636. **doi:10.1130/G22737.1**

Coogan, L.A., Jenkin, G.R.T., and Wilson, R.N., 2007. Contrasting cooling rates in the lower oceanic crust at fast- and slow-spreading ridges revealed by geospeedometry. *J. Petrol.,* 48(11):2211–2231. **doi:10.1093/petrology/egm057**

Coogan, L.A., Thompson, G., and MacLeod, C.J., 2002b. A textural and geochemical investigation of high level gabbros from the Oman ophiolite: implications for the role of the axial magma chamber at fast-spreading ridges. *Lithos,* 63(1–2):67–82. **doi:10.1016/S0024-4937(02)00114-7**

Crawford, W.C., and Webb, S.C., 2002. Variations in the distribution of magma in the lower crust and at the Moho beneath the East Pacific Rise at 9°–10°N. *Earth Planet. Sci. Lett.,* 203(1):117–130. **doi:10.1016/S0012-821X(02)00831-2**

Detrick, R.S., Buhl, P., Vera, E., Mutter, J., Orcutt, J., Madsen, J., and Brocher, T., 1987. Multichannel seismic imaging of a crustal magma chamber along the East Pacific Rise. *Nature (London, U. K.),* 326(6108):35–41. **doi:10.1038/326035a0**

Dick, H.J.B., 1989. Abyssal peridotites, very slow spreading ridges and ocean ridge magmatism. *In* Saunders, A.D., and Norry, M.J. (Eds.), *Magmatism in the Ocean Basins*. Geol. Soc. Spec. Publ., 42(1):71–105. **doi:10.1144/GSL.SP.1989.042.01.06**

Dick, H.J.B., Lin, J., and Schouten, H., 2003. An ultraslow-spreading class of ocean ridge. *Nature (London, U. K.),* 426(6965):405–412. **doi:10.1038/nature02128**

Dick, H.J.B., Natland, J.H., Miller, D.J., et al., 1999. *Proc. ODP, Init. Repts.,* 176: College Station, TX (Ocean Drilling Program). **doi:10.2973/odp.proc.ir.176.1999**

Donaldson, C.H., 1976. An experimental investigation of olivine morphology. *Contrib. Mineral. Petrol.,* 57(2):187–213. **doi:10.1007/BF00405225**

Donaldson, C.H., 1982. Origin of some of the Rhum harrisite by segregation of intercumulus liquid. *Mineral. Mag.,* 45(337):201–209. **doi:10.1180/minmag.1982.045.337.23**

Dunn, R.A., Toomey, D.R., and Solomon, S.C., 2000. Three-dimensional seismic structure and physical properties of the crust and shallow mantle beneath the East Pacific Rise at 9°30′N. *J. Geophys. Res., [Solid Earth],* 105(B10):23537–23556. **doi:10.1029/2000JB900210**

Durant, D.T., and Toomey, D.R., 2009. Evidence and implications of crustal magmatism on the flanks of the East Pacific Rise. *Earth Planet. Sci. Lett.,* 287(1–2):130–136. **doi:10.1016/j.epsl.2009.08.003**

Faak, K., Chakraborty, S., and Coogan, L.A., 2011. Evaluation of the variation in cooling rate with depth in the lower oceanic crust at fast-spreading ridges using a newly developed Mg in plagioclase geospeedometer [presented at the 2011 American Geophysical Union Fall Meeting, San Francisco, CA, 5–9 December 2011].(Abstract V13F-04) **http://www.agu.org/meetings/fm11/waisfm11.html**

Feig, S.T., Koepke, J., and Snow, J.E., 2006. Effect of water on tholeiitic basalt phase equilibria: an experimental study under oxidizing conditions. *Contrib. Mineral. Petrol.,* 152(5):611–638. **doi:10.1007/s00410-006-0123-2**

Ferrini, V.L., Shillington, D.J., Gillis, K.M., Teagle, D.A.H., MacLeod, C.J., Morris, A., Cazenaveg, P.W., Hurst, S., Tominagai, M., Party, J.S., submitted. Evidence of mass failure in the Hess Deep Rift from multiresolutional bathymetry data. *Mar. Geol.*

Francheteau, J., Armijo, R., Cheminée, J.L., Hekinian, R., Lonsdale, P., and Blum, N., 1990. 1 Ma East Pacific Rise oceanic crust and uppermost mantle exposed by rifting in Hess Deep (equatorial Pacific Ocean). *Earth Planet. Sci. Lett.,* 101:281(2–4)–295. **doi:10.1016/0012-821X(90)90160-Y**

Frost, B.R., Beard, J.S., McCaig, A., and Condliffe, E., 2008. The formation of micro-rodingites from IODP Hole U1309D: key to understanding the process of serpentinization. *J. Petrol.,* 49(9):1579–1588. **doi:10.1093/petrology/egn038**

Früh-Green, G.L., Plas, A., and Dell'Angelo, L.N., 1996. Mineralogic and stable isotope record of polyphase alteration of upper crustal gabbros of the East Pacific Rise (Hess Deep, Site 894). *In* Mével, C., Gillis, K.M., Allan, J.F., and Meyer, P.S. (Eds.), *Proc. ODP, Sci. Results,* 147: College Station, TX (Ocean Drilling Program), 235–254. **doi:10.2973/odp.proc.sr.147.015.1996**

Gao, Y., Hoefs, J., Przybilla, R., and Snow, J.E., 2006. A complete oxygen isotope profile through the lower oceanic crust, ODP Hole 735B. *Chem. Geol.,* 233(3–4):217–234. **doi:10.1016/j.chemgeo.2006.03.005**

Garmany, J., 1989. Accumulations of melt at the base of young oceanic crust. *Nature (London, U. K.),* 340(6235):628–632. **doi:10.1038/340628a0**

Gillis, K., Mével, C., Allan, J., et al., 1993. *Proc. ODP, Init. Repts.,* 147: College Station, TX (Ocean Drilling Program). **doi:10.2973/odp.proc.ir.147.1993**

Gillis, K., Snow, J.E., and Klaus, A., 2012. Hess Deep plutonic crust: exploring the plutonic crust at a fast-spreading ridge: new drilling at Hess Deep. *IODP Sci. Prosp.,* 345. **doi:10.2204/iodp.sp.345.2012**

Gillis, K.M., 1995. Controls on hydrothermal alteration in a section of fast-spreading oceanic crust. *Earth Planet. Sci. Lett.,* 134(3–4):473–489. **doi:10.1016/0012-821X(95)00137-2**

Gillis, K.M., 2008. The roof of an axial magma chamber: a hornfelsic heat exchanger. *Geology,* 36(4):299–302. **doi:10.1130/G24590A.1**

Gillis, K.M., Coogan, L.A., and Chaussidon, M., 2003. Volatile element (B, Cl, F) behaviour in the roof of an axial magma chamber from the East Pacific Rise. *Earth Planet. Sci. Lett.,* 213(3–4):447–462. **doi:10.1016/S0012-821X(03)00346-7**

Gillis, K.M., Coogan, L.A., and Pedersen, R., 2005. Strontium isotope constraints on fluid flow in the upper oceanic crust at the East Pacific Rise. *Earth Planet. Sci. Lett.,* 232(1–2):83–94. **doi:10.1016/j.epsl.2005.01.008**

Gillis, K.M., Muehlenbachs, K., Stewart, M., Gleeson, T., and Karson, J., 2001. Fluid flow patterns in fast spreading East Pacific Rise crust exposed at Hess Deep. *J. Geophys. Res., [Solid Earth],* 106(B11):26311–26329. **doi:10.1029/2000JB000038**

Grove, T.L., and Bryan, W.B., 1983. Fractionation of pyroxene-phyric MORB at low pressure: an experimental study. *Contrib. Mineral. Petrol.,* 84(4):293–309. **doi:10.1007/BF01160283**

Hanna, H.D., 2004. Geochemical variations in basaltic glasses from an incipient rift and upper level gabbros from Hess Deep, eastern equatorial Pacific [M.Sc. thesis]. Duke Univ., Durham.

Hékinian, R., Bideau, D., Francheteau, J., Cheminee, J.L., Armijo, R., Lonsdale, P., and Blum, N., 1993. Petrology of the East Pacific Rise crust and upper mantle exposed in Hess Deep (eastern equatorial Pacific). *J. Geophys. Res., [Solid Earth],* 98(B5):8069–8094. **doi:10.1029/92JB02072**

Henstock, T.J., Woods, A.W., and White, R.S., 1993. The accretion of oceanic crust by episodic sill intrusion. *J. Geophys. Res., [Solid Earth],* 98(B3):4143–4161. **doi:10.1029/92JB02661**

Hess, H.H., 1960. The AMSOC hole to the Earth's mantle. *Am. Sci.,* 48(2):254–263. **http://www.jstor.org/stable/27827541**

Hey, R., Johnson, G.L., and Lowrie, A., 1977. Recent plate motions in the Galapagos area. *Geol. Soc. Am. Bull.,* 88(10):1385–1403. **doi:10.1130/0016-7606(1977)88<1385:RPMITG>2.0.CO;2**

Hey, R.N., Deffeyes, K.S., Johnson, G.L., and Lowrie, A., 1972. The Galapagos triple junction and plate motions in the East Pacific. *Nature (London, U. K.),* 237(5349)20–22. **doi:10.1038/237020a0**

Holden, J.C., and Dietz, R.S., 1972. Galapagos gore, NazCoPac triple junction and Carnegie/Cocos Ridges. *Nature (London, U. K.),* 235(5336):266–269. **doi:10.1038/235266a0**

Hooft, E.E.E., Detrick, R.S., and Kent, G.M., 1997. Seismic structure and indicators of magma budget along the southern East Pacific Rise. *J. Geophys. Res., [Solid Earth],* 102(B12):27319–27340. **doi:10.1029/97JB02349**

John, B.E., Foster, D.A., Murphy, J.M., Cheadle, M.J., Baines, A.G., Fanning, C.M., and Copeland, P., 2004. Determining the cooling history of in situ lower oceanic crust—Atlantis Bank, SW Indian Ridge. *Earth Planet. Sci. Lett.,* 222(1):145–160. **doi:10.1016/j.epsl.2004.02.014**

Karson, J.A., Hurst, S.D., and Lonsdale, P., 1992. Tectonic rotations of dikes in fast-spread oceanic crust exposed near Hess Deep. *Geology,* 20(8):685–688. **doi:10.1130/0091-7613(1992)020<0685:TRODIF>2.3.CO;2**

Karson, J.A., Klein, E.M., Hurst, S.D., Lee, C.E., Rivizzigno, P.A., Curewitz, D., Morris, A.R., Miller, D.J., Varga, R.G., Christeson, G.L., Cushman, B., O'Neill, J.M., Brophy, J.G., Gillis, K.M., Stewart, M.A., and Sutton, A.L., 2002. Structure of uppermost fast-spread oceanic crust exposed at the Hess Deep Rift: implications for subaxial processes at the East Pacific Rise. *Geochem., Geophys., Geosyst.,* 3(1):1002. **doi:10.1029/2001GC000155**

Kelemen, P.B., and Aharonov, E., 1998. Periodic formation of magma fractures and generation of layered gabbros in the lower crust beneath oceanic spreading ridges. *In* Buck, R., Delaney, P.T., Karson, J.A., and Lagabrielle, Y. (Eds.), *Faulting and Magmatism at Mid-Ocean Ridges*. Geophys. Monogr., 106:267–289. **doi:10.1029/GM106p0267**

Kelemen, P.B., Kikawa, E., Miller, D.J., et al., 2004. *Proc. ODP, Init. Repts.,* 209: College Station, TX (Ocean Drilling Program). **doi:10.2973/odp.proc.ir.209.2004**

Kelemen, P.B., Koga, K., and Shimizu, N., 1997. Geochemistry of gabbro sills in the crust-mantle transition zone of the Oman ophiolite: implications for the origin of the oceanic lower crust. *Earth Planet. Sci. Lett.,* 146(3–4):475–488. **doi:10.1016/S0012-821X(96)00235-X**

Kent, G.M., Harding, A.J., and Orcutt, J.A., 1990. Evidence for a smaller magma chamber beneath the East Pacific Rise at 9°30′N. *Nature (London, U. K.),* 344(6267):650–653. **doi:10.1038/344650a0**

Kirchner, T.M., and Gillis, K.M., 2012. Mineralogical and strontium isotopic record of hydrothermal processes in the lower ocean crust at and near the East Pacific Rise. *Contrib. Mineral. Petrol.,* 164(1):123–141 **doi:10.1007/s00410-012-0729-5**

Klein, E.M., 2007. Geochemistry of the igneous oceanic crust. *Treatise Geochem.,* 3:433–463. **doi:10.1016/B0-08-043751-6/03030-9**

Koepke, J., Berndt, J., Feig, S.T., and Holtz, F., 2007. The formation of SiO_2-rich melts within the deep ocean crust by hydrous partial melting of gabbros. *Contrib. Mineral. Petrol.,* 153(1):67–84. **doi:10.1007/s00410-006-0135-y**

Koepke, J., France, L., Müller, T., Faure, F., Goetze, N., Dziony, W., and Ildefonse, B., 2011. Gabbros from IODP Site 1256, equatorial Pacific: insight into axial magma chamber processes at fast spreading ocean ridges. *Geochem., Geophys., Geosyst.,* 12(9):Q09014. **doi:10.1029/2011GC003655**

Korenaga, J., and Kelemen, P.B., 1997. Origin of gabbro sills in the Moho transition zone of the Oman ophiolite: implications for magma transport in the oceanic lower crust. *J. Geophys. Res., [Solid Earth],* 102(B12):27729–27749. **doi:10.1029/97JB02604**

Korenaga, J., and Kelemen, P.B., 1998. Melt migration through the oceanic lower crust: a constraint from melt percolation modeling with finite solid diffusion. *Earth Planet. Sci. Lett.,* 156(1–2):1–11. **doi:10.1016/S0012-821X(98)00004-1**

Lécuyer, C., and Gruau, G., 1996. Oxygen and strontium isotope compositions of Hess Deep gabbros (Holes 894F and 894G): high-temperature interaction of seawater with the oceanic crust Layer 3. *In* Mével, C., Gillis, K.M., Allan, J.F., and Meyer, P.S. (Eds.), *Proc. ODP, Sci. Results,* 147: College Station, TX (Ocean Drilling Program), 227–234. **doi:10.2973/odp.proc.sr.147.014.1996**

Lecuyer, C., and Reynard, B., 1996. High-temperature alteration of oceanic gabbros by seawater (Hess Deep, Ocean Drilling Program Leg 147): evidence from oxygen isotopes and elemental fluxes. *J. Geophys. Res., [Solid Earth],* 101(B7):15883–15897. **doi:10.1029/96JB00950**

Lissenberg, C.J., MacLeod, C.J., Howard, K.A., and Godard, M., 2013. Pervasive reactive melt migration through fast-spreading lower oceanic crust (Hess Deep, equatorial Pacific Ocean). *Earth Planet. Sci. Lett.,* 361:436–447. **doi:10.1016/j.epsl.2012.11.012**

Lonsdale, P., 1988. Structural pattern of the Galapagos microplate and evolution of the Galapagos triple junctions. *J. Geophys. Res. [Solid Earth],* 93(B11):13551–13574. **doi:10.1029/JB093iB11p13551**

Lonsdale, P., 1989. Segmentation of the Pacific-Nazca spreading center, 1°N–20°S. *J. Geophys. Res., [Solid Earth],* 94(B9):12197–12225. **doi:10.1029/JB094iB09p12197**

Maclennan, J., Hulme, T., and Singh, S.C., 2004. Thermal models of oceanic crustal accretion: linking geophysical, geological, and petrological observations. *Geochem., Geophys., Geosyst.,* 5(2):Q02F25. **doi:10.1029/2003GC000605**

MacLeod, C.J., Boudier, F., Yaouancq, G., and Richter, C., 1996a. Gabbro fabrics from Site 894, Hess Deep: implications for magma chamber processes at the East Pacific Rise. *In* Mével, C., Gillis, K.M., Allan, J.F., and Meyer, P.S. (Eds.), *Proc. ODP, Sci. Results,* 147: College Station, TX (Ocean Drilling Program), 317–328. **doi:10.2973/odp.proc.sr.147.018.1996**

MacLeod, C.J., Célérier, B., Früh-Green, G.L., and Manning, C.E., 1996b. Tectonics of Hess Deep: a synthesis of drilling results from Leg 147. *In* Mével, C., Gillis, K.M., Allan, J.F., and Meyer, P.S. (Eds.), *Proc. ODP, Sci. Results,* 147: College Station, TX (Ocean Drilling Program), 461–475. **doi:10.2973/odp.proc.sr.147.032.1996**

MacLeod, C.J., Teagle, D.A., Gillis, K.M., Shillington, D.J., and Scientific Party, 2008. Morphotectonics of Hess Deep: preliminary results of RSS *James Cook* Cruise JC21. *Eos, Trans. Am. Geophys. Union,* 89(53)(Suppl.):V43I-408 (Abstract). **http://www.agu.org/meetings/fm08/waisfm08.html**

MacLeod, C.J., and Yaouancq, G., 2000. A fossil melt lens in the Oman ophiolite: implications for magma chamber processes at fast spreading ridges. *Earth Planet. Sci. Lett.,* 176(3–4):357–373. **doi:10.1016/S0012-821X(00)00020-0**

Manning, C.E., and MacLeod, C.J., 1996. Fracture-controlled metamorphism of Hess Deep gabbros, Site 894: constraints on the roots of mid-ocean-ridge hydrothermal systems at fast-spreading centers. *In* Mével, C., Gillis, K.M., Allan, J.F., and Meyer, P.S. (Eds.), *Proc. ODP, Sci. Results,* 147: College Station, TX (Ocean Drilling Program), 189–212. **doi:10.2973/odp.proc.sr.147.011.1996**

Manning, C.E., Weston, P.E., and Mahon, K.I., 1996. Rapid high-temperature metamorphism of East Pacific Rise gabbros from Hess Deep. *Earth Planet. Sci. Lett.,* 144(1–2):123–132. **doi:10.1016/0012-821X(96)00153-7**

Mathison, C.I., 1987. Cyclic units in the Somerset Dam layered gabbro intrusion, southeastern Queensland, Australia. *Lithos,* 20(3):187–205. **doi:10.1016/0024-4937(87)90008-9**

McCollom, T.M., and Shock, E.L., 1998. Fluid-rock interactions in the lower oceanic crust: thermodynamic models of hydrothermal alteration. *J. Geophys. Res., [Solid Earth],* 103(B1):547–575. **doi:10.1029/97JB02603**

Melson, W.G., and Thompson, G., 1970. Layered basic complex in oceanic crust, Romanche fracture, equatorial Atlantic Ocean. *Science,* 168(3933):817–820. **doi:10.1126/science.168.3933.817**

Morton, J.L., and Sleep, N.H., 1985. A mid-ocean ridge thermal model: constraints on the volume of axial hydrothermal heat flux. *J. Geophys. Res., [Solid Earth],* 90(B13):11345–11353. **doi:10.1029/JB090iB13p11345**

Natland, J.H., and Dick, H.J.B., 1996. Melt migration through high-level gabbroic cumulates of the East Pacific Rise at Hess Deep: the origin of magma lenses and the deep crustal structure of fast-spreading ridges. *In* Mével, C., Gillis, K.M., Allan, J.F., and Meyer, P.S. (Eds.), *Proc. ODP, Sci. Results,* 147: College Station, TX (Ocean Drilling Program), 21–58. **doi:10.2973/odp.proc.sr.147.002.1996**

Nicolas, A., 1989. *Structure of Ophiolites and Dynamics of the Oceanic Lithosphere:* Dordrecht (Springer).

Nicolas, A., Reuber, I., and Benn, K., 1988. A new magma chamber model based on structural studies in the Oman ophiolite. *Tectonophysics,* 151(1–4):87–105. **doi:10.1016/0040-1951(88)90242-9**

Nozaka, T., and Fryer, P., 2011. Alteration of the oceanic lower crust at a slow-spreading axis: insight from vein-related zoned halos in olivine gabbro from Atlantis Massif, Mid-Atlantic Ridge. *J. Petrol.,* 52(4):643–664. **doi:10.1093/petrology/egq098**

O'Driscoll, B., Donaldson, C.H., Troll, V.R., Jerram, D.A., and Emeleus, C.H., 2007. An origin for harrisitic and granular olivine in the Rum Layered Suite, NW Scotland: a crystal size distribution study. *J. Petrol.,* 48(2):253–270. **doi:10.1093/petrology/egl059**

O'Hara, M.J., 1968. Are ocean floor basalts primary magma? *Nature (London, U. K.),* 220(5168):683–686. **doi:10.1038/220683a0**

Pallister, J.S., and Hopson, C.A., 1981. Samail ophiolite plutonic suite: field relations, phase variation, cryptic variation and layering, and a model of a spreading ridge magma chamber. *J. Geophys. Res., [Solid Earth],* 86(B4):2593–2644. **doi:10.1029/JB086iB04p02593**

Pariso, J.E., Kelso, P., and Richter, C., 1996. Paleomagnetism and rock magnetic properties of gabbro from Hole 894G, Hess Deep. *In* Mével, C., Gillis, K.M., Allan, J.F., and Meyer, P.S. (Eds.), *Proc. ODP, Sci. Results,* 147: College Station, TX (Ocean Drilling Program), 373–381. **doi:10.2973/odp.proc.sr.147.023.1996**

Pedersen, R.B., Malpas, J., and Falloon, T., 1996. Petrology and geochemistry of gabbroic and related rocks from Site 894, Hess Deep. *In* Mével, C., Gillis, K.M., Allan, J.F., and Meyer, P.S. (Eds.), *Proc. ODP, Sci. Results,* 147: College Station, TX (Ocean Drilling Program), 3–19. **doi:10.2973/odp.proc.sr.147.001.1996**

Perk, N.W., Coogan, L.A., Karson, J.A., Klein, E.M., and Hanna, H.D., 2007. Petrology and geochemistry of primitive lower oceanic crust from Pito Deep: implications for the accretion of the lower crust at the southern East Pacific Rise. *Contrib. Mineral. Petrol.,* 154(5):575–590. **doi:10.1007/s00410-007-0210-z**

Phipps Morgan, J., and Chen, Y.J., 1993. The genesis of oceanic crust: magma injection, hydrothermal circulation, and crustal flow. *J. Geophys. Res., [Solid Earth],* 98(B4):6283–6297. **doi:10.1029/92JB02650**

Quick, J.E., and Denlinger, R.P., 1993. Ductile deformation and the origin of layered gabbro in ophiolites. *J. Geophys. Res., [Solid Earth],* 98(B8):14015–14027. **doi:10.1029/93JB00698**

Richter, C., Kelso, P.R., and MacLeod, C.J., 1996. Magnetic fabrics and sources of magnetic susceptibility in lower crustal and upper mantle rocks from Hess Deep. *In* Mével, C., Gillis, K.M., Allan, J.F., and Meyer, P.S. (Eds.), *Proc. ODP, Sci. Results,* 147: College Station, TX (Ocean Drilling Program), 393–403. **doi:10.2973/odp.proc.sr.147.025.1996**

Rioux, M., Lissenberg, C.J., McLean, N.M., Bowring, S.A., MacLeod, C.J., Hellebrand, E., and Shimizu, N., 2012. Protracted timescales of lower crustal growth at the fast-spreading East Pacific Rise. *Nat. Geosci.,* 5(4):275–278. **doi:10.1038/ngeo1378**

Robinson, P.T., Von Herzen, R., et al., 1989. *Proc. ODP, Init. Repts.,* 118: College Station, TX (Ocean Drilling Program). **doi:10.2973/odp.proc.ir.118.1989**

Ryan, W.B.F., Carbotte, S.M., Coplan, J.O., O'Hara, S., Melkonian, A., Arko, R., Weissel, R.A., Ferrini, V., Goodwillie, A., Nitsche, F., Bonczkowski, J., and Zemsky, R., 2009. Global multi-resolution topography synthesis. *Geochem., Geophys., Geosyst.,* 10(3):Q03014. **doi:10.1029/2008GC002332**

Schouten, H., Smith, D.K., Montési, L.G.J., Zhu, W., and Klein, E.M., 2008. Cracking of lithosphere north of the Galapagos triple junction. *Geology,* 36(5):339–342. **doi:10.1130/G24431A.1**

Singh, S.C., Kent, G.M., Collier, J.S., Harding, A.J., and Orcutt, J.A., 1998. Melt to mush variations in crustal magma properties along the ridge crest at the southern East Pacific Rise. *Nature (London, U. K.),* 394(6696):874–878. **doi:10.1038/29740**

Sleep, N.H., 1975. Formation of oceanic crust: some thermal constraints. *J. Geophys. Res., [Solid Earth],* 80(29):4037–4042. **doi:10.1029/JB080i029p04037**

Smith, D.K., Schouten, H., Zhu, W., Montési, L.G.J., and Cann, J.R., 2011. Distributed deformation ahead of the Cocos-Nazca Rift at the Galapagos triple junction. *Geochem., Geophys., Geosyst.,* 12(6):Q11003. **doi:10.1029/2011GC003689**

Stewart, M.A., Klein, E.M., and Karson, J.A., 2002. Geochemistry of dikes and lavas from the north wall of the Hess Deep Rift: insights into the four-dimensional character of crustal construction at fast-spreading mid-ocean ridges. *J. Geophys. Res., [Solid Earth],* 107(B10):2238. **doi:10.1029/2001JB000545**

Stolper, E., and Walker, D., 1980. Melt density and the average composition of basalt. *Contrib. Mineral. Petrol.,* 74(1):7–12. **doi:10.1007/BF00375484**

Teagle, D.A.H., Alt, J.C., and Halliday, A.N., 1998. Tracing the chemical evolution of fluids during hydrothermal recharge: constraints from anhydrite recovered in ODP Hole 504B. *Earth Planet. Sci. Lett.,* 155(3–4):167–182. **doi:10.1016/S0012-821X(97)00209-4**

Teagle, D.A.H., Bickle, M.J., and Alt, J.C., 2003. Recharge flux to ocean-ridge black smoker systems: a geochemical estimate from ODP Hole 504B. *Earth Planet. Sci. Lett.,* 210(1–2):81–89. **doi:10.1016/S0012-821X(03)00126-2**

Wager, L.R., and Brown, G.M., 1967. *Layered Igneous Rocks:* San Francisco (W.H. Freeman).

Wager, L.R., Brown, G.M., and Wadsworth, W.J., 1960. Types of igneous cumulates. *J. Petrol.,* 1(1):73–85. **http://petrology.oxfordjournals.org/content/1/1/73.abstract**

Wiggins, S.M., Dorman, L.M., Cornuelle, B.D., and Hildebrand, J.A., 1996. Hess Deep rift valley structure from seismic tomography. *J. Geophys. Res., [Solid Earth],* 101(B10):22335–22353. **doi:10.1029/96JB01230**

Wilson, D.S., Teagle, D.A.H., Alt, J.C., Banerjee, N.R., Umino, S., Miyashita, S., Acton, G.D., Anma, R., Barr, S.R., Belghoul, A., Carlut, J., Christie, D.M., Coggon, R.M., Cooper, K.M., Cordier, C., Crispini, L., Durand, S.R., Einaudi, F., Galli, L., Gao, Y., Geldmacher, J., Gilbert, L.A., Hayman, N.W., Herrero-Bervera, E., Hirano, N., Holter, S., Ingle, S., Jiang, S., Kalberkamp, U., Kerneklian, M., Koepke, J., Laverne, C., Vasquez, H.L.L., Maclennan, J., Morgan, S., Neo, N., Nichols, H.J., Park, S.-H., Reichow, M.K., Sakuyama, T., Sano, T., Sandwell, R., Scheibner, B., Smith-Duque, C.E., Swift, S.A., Tartarotti, P., Tikku, A.A., Tominaga, M., Veloso, E.A., Yamasaki, T., Yamazaki, S., and Ziegler, C., 2006. Drilling to gabbro in intact ocean crust. *Science,* 312(5776):1016–1020. **doi:10.1126/science.1126090**

Zonenshain, L.P., Kogan, L.I., Savostin, L.A., Golmstock, A.J., and Gorodnitskii, A.M., 1980. Tectonics, crustal structure and evolution of the Galapagos triple junction. *Mar. Geol.,* 37(3–4):209–230. **doi:10.1016/0025-3227(80)90102-4**

Table T1. Expedition 345 operations summary.

Hole	Location	Water depth (mbsl)	Total penetration (mbsf)	Interval cored (m)	Core recovery* (m)	Core recovery (%)	Time on hole (d)	Operations
U1415A	2°15.1757'N, 101°32.5695'W	4837	10.3	—	—	—	1.2	Jet-in test
U1415B	2°15.1355'N, 101°32.8671'W	4845	11.7	—	—	—	0.2	Jet-in test
U1415C	2°15.1349'N, 101°32.8669'W	4845	BHA bent during penetration				0.8	Jet-in test; bent BHA
U1415D	2°15.1437'N, 101°32.7441'W	4840	4.2	—	—	—	0.9	Jet-in test
U1415E	2°15.1461'N, 101°32.7424'W	4840	15.3	15.3	0.84	5	1.1	RCB coring
U1415F	2°15.1394'N, 101°32.6261'W	4846	1.5	—	—	—	0.8	Jet-in test
U1415G	2°15.1390'N, 101°32.6263'W	4846	12.9	12.9	0.29	2	0.3	RCB coring
U1415H	2°15.1317'N, 101°32.6370'W	4846	12.9	12.9	0.44	3	1.0	RCB coring
U1415I	2°15.1547'N, 101°32.6622'W	4842	35.2	35.2	7.12	20	2.9	RCB coring
U1415J	2°15.1604'N, 101°32.6622'W	4839	111.8	91.8	14.35	16	16.0	Installed nested FFFs and casing to 15 mbsf; RCB coring
U1415K	2°15.3307'N, 101°32.8527'W	4687	35.3	—	—	—	3.6	Failed attempt to establish reentry capability
U1415L	2°15.3300'N, 101°32.8041'W	4675	4.0	—	—	—	0.7	Jet-in test
U1415M	2°15.3304'N, 101°32.8040'W	4675	25.9	—	—	—	2.6	Failed attempt to establish reentry capability
U1415N	2°15.3304'N, 101°32.8121'W	4675	37.0	37.0	1.56	4	2.1	RCB coring
U1415O	2°15.1516'N, 101°32.5848'W	4850	17.0	—	—	—	1.2	Failed attempt to establish reentry capability
U1415P	2°15.1486'N, 101°32.6102'W	4853	107.9	95.4	30.57	32		Installed FFF and casing to 12.5 mbsf; RCB coring; failed attempt to log
		Totals*:	442.9	300.5	55.17	18	35.4	

* = excludes cores recovered during hole-cleaning operations (ghost cores). — = no data. RCB = rotary core barrel. BHA = bottom-hole assembly. FFF = free-fall funnel.

Figure F1. Schematic models for the ocean crust showing how its structure changes with decreasing magmatism and increasing faulting from A to D. Modified after Dick et al. (2007). **A.** Fast-spreading crust, after the Penrose standard layered model (Anonymous, 1972). Red bars = major deep drilling sites, dashed blue bar = drilling target area for Expedition 345. Moho = Mohorovicic discontinuity. **B.** Slow-spreading crust formed at a segment center (Cannat et al., 1995). **C.** Slow-spreading crust formed at a segment end (Cannat et al., 1995). **D.** Ultraslow-spreading crust, which is the nearly nonvolcanic end-member of crustal construction (Dick et al., 2007).

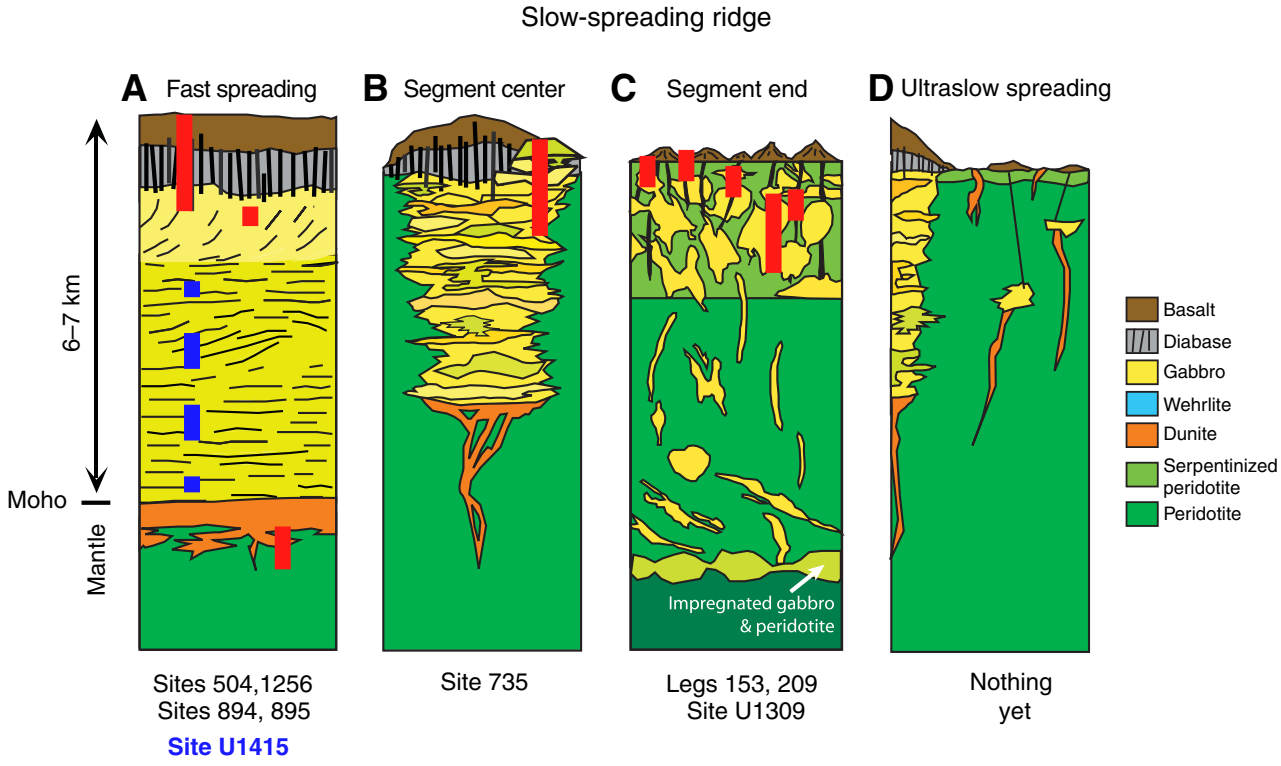

Figure F2. Schematic drawings of crustal accretion models (modified from Korenaga and Kelemen, 1997). Black arrows = movement of the crystal mush, blue arrows = dominant zones where hydrothermal circulation removes latent and sensible heat. **A.** Gabbro glacier in which the lower oceanic crust crystallizes in a thin magma lens at the base of the sheeted dike complex from which cumulates subside downward and outward to form the lower crust (e.g., Henstock et al., 1993; Phipps Morgan and Chen, 1993; Quick and Denlinger, 1993). **B.** Hybrid model in which some crystallization occurs in an upper melt lens and some within sill-like bodies in the lower crust (e.g., Boudier et al., 1996). **C.** "Sheeted" or "stacked" sill model in which the lower ocean crust forms by crystallization of multiple sill-like intrusions (e.g., Bédard et al., 1988; Kelemen and Aharonov, 1998; Kelemen et al., 1997).

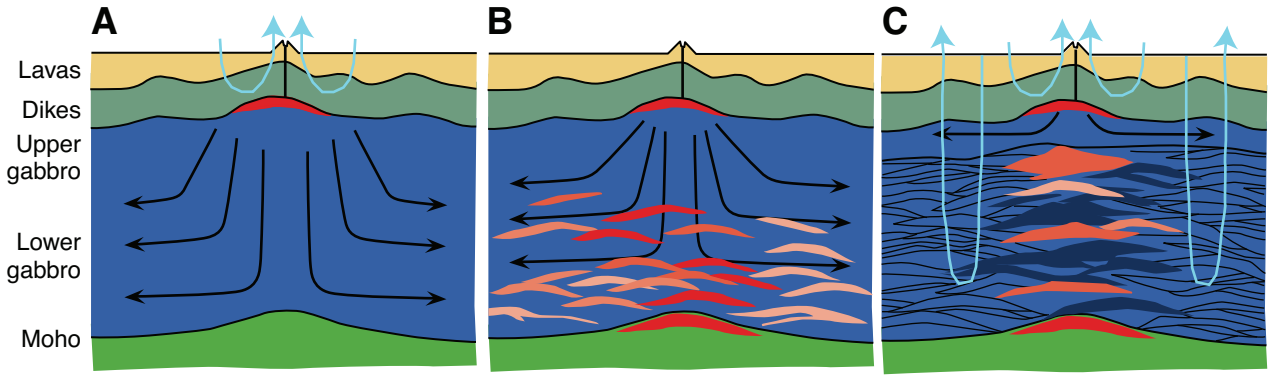

Figure F3. Schematic representation of the predictions of the general depth trends of latent heat release, bulk Mg#, strain rate, cooling rate, hydrothermal fluid flux, fluid temperature, and intensity of high-temperature (HT) alteration for the end-member "gabbro glacier" (with mainly conductive cooling of the lower crust) and "sheeted sill" (with convective cooling of the lower crust) models (from Gillis et al., 2012).

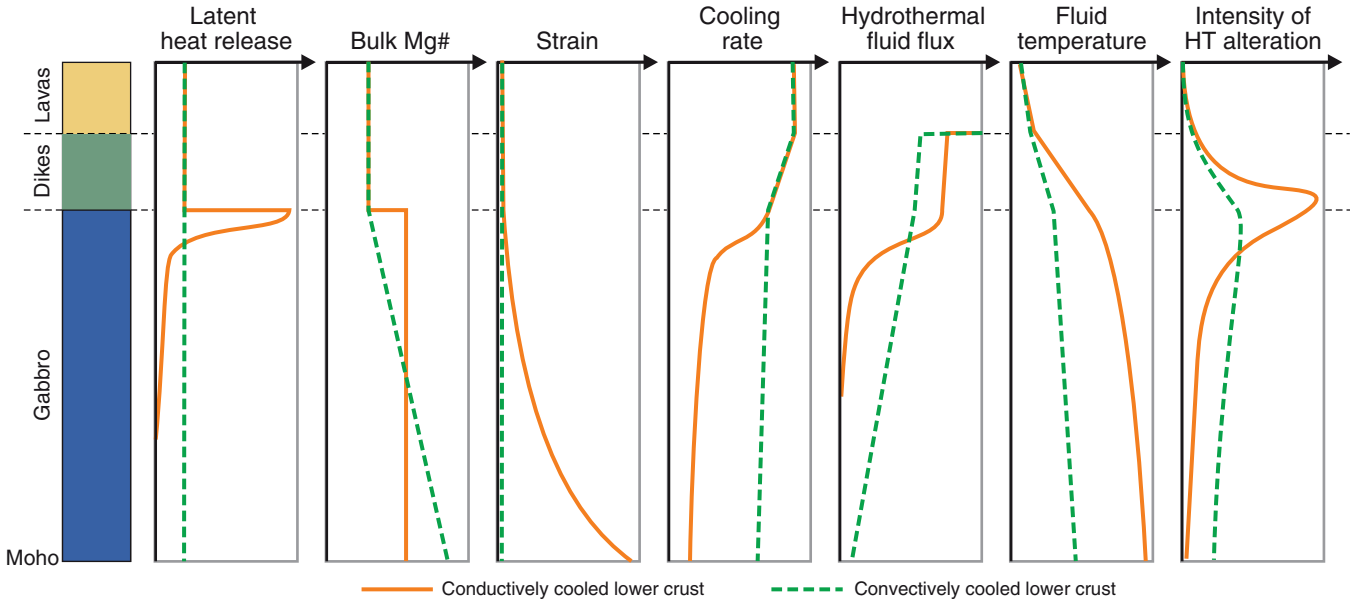

Figure F4. Map of the Galapagos triple junction in the eastern equatorial Pacific Ocean showing bathymetry derived from satellite altimetry data and archived multibeam bathymetry data available from the Global MultiResolution Topography Data Portal at Lamont-Doherty Earth Observatory. The map was generated using GeoMapApp (Ryan et al., 2009). Tectonic boundaries modified from Smith et al. (2011). EPR = East Pacific Rise, TJ = triple junction. Red box with dashed lines indicates location of the map in Figure F5.

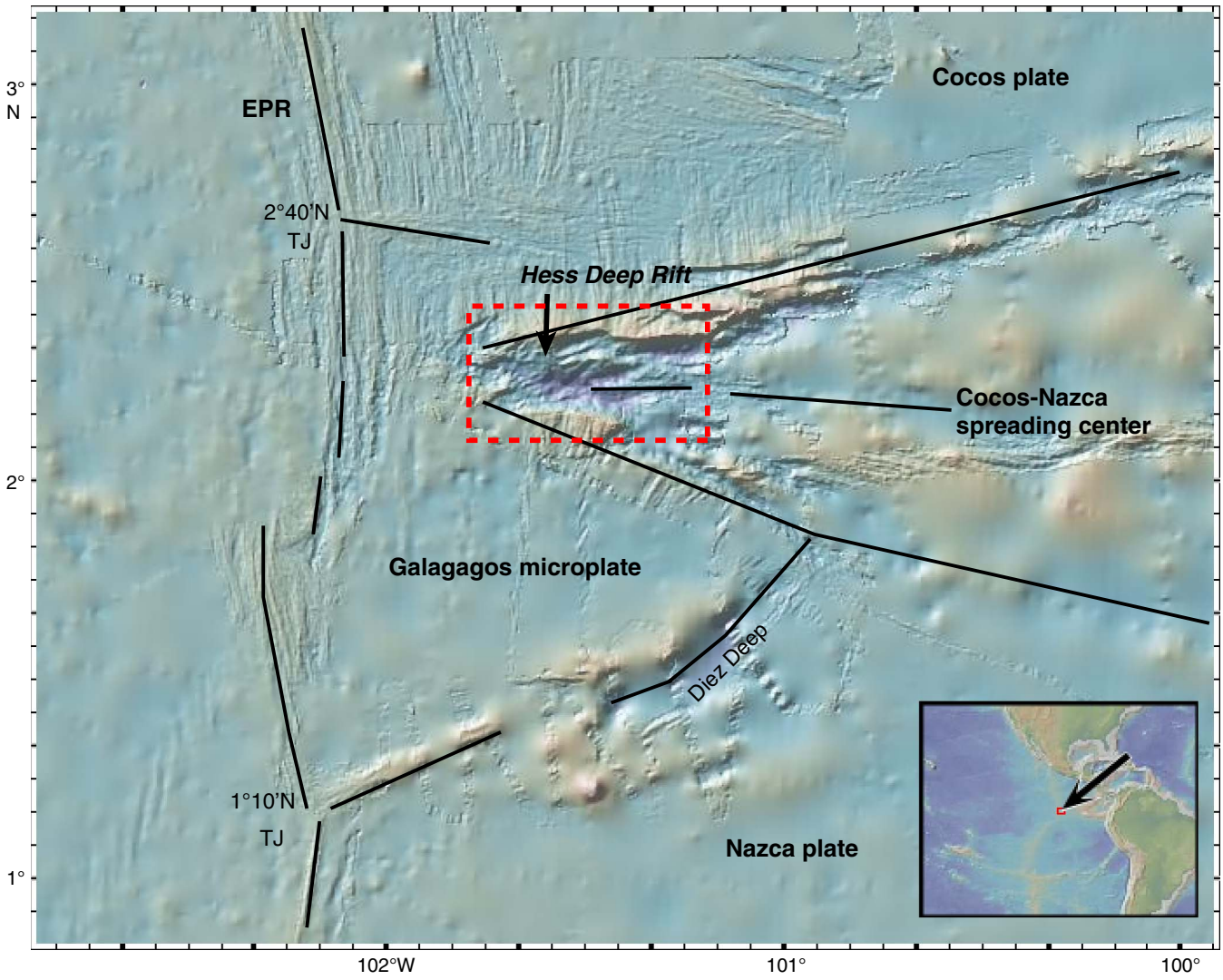

Figure F5. Regional bathymetric map of the Hess Deep Rift showing key morphological features and locations of IODP Expedition 345 Site U1415 and ODP Site 895. Regional multibeam bathymetry data were acquired using the hull-mounted Kongsberg Simrad EM120/SBP120 system (12 kHz). Swath data were gridded at between 50 and 150 m depending on the density of data coverage, with the smallest grid spacing in the center of Hess Deep, and combined with existing swath data in this region available from the Marine Geoscience Data System (**www.marine-geo.org**). Existing data were from cruises aboard the R/V *Thomas Washington* in 1982 (PI: P. Lonsdale), 1985 (PI: Lonsdale), and 1992 (PI: L. Dorman) and aboard the R/V *Melville* in 2000 (PI: D. Fornari) and 2002 (PI: E. Klein).

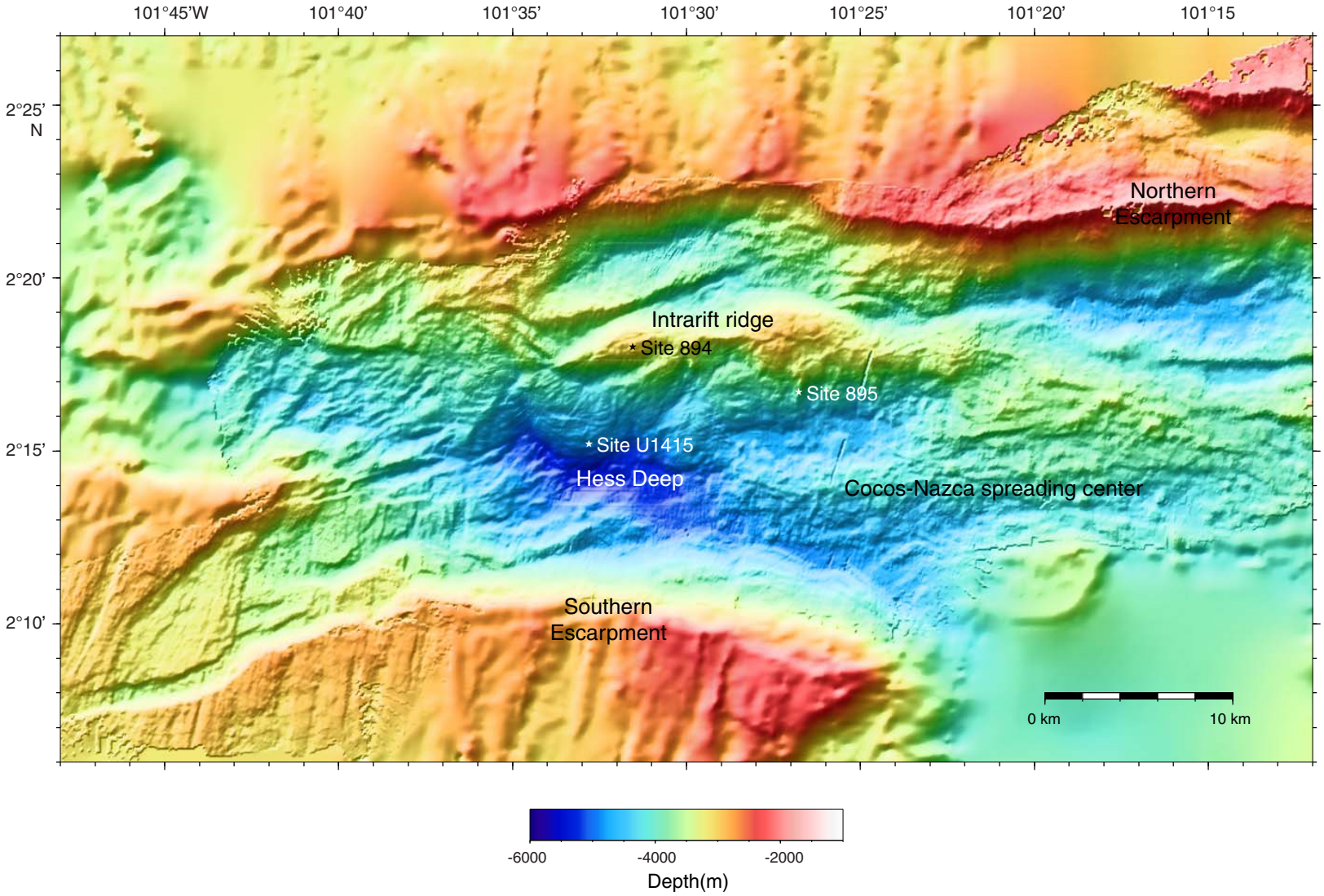

Figure F6. Bathymetric map of the western end of the intrarift ridge and its southern slope showing the distribution of rock types recovered during the Nacopac submersible cruise (Francheteau et al., 1990; Hékinian et al., 1993) and the JC-21 site survey cruise (MacLeod et al., unpubl. cruise report, 2008). Box indicates where a smaller scale map of the southern slope are shown in Figure F8. See Figure F5 for bathymetric data sources. Contour interval = 100 m.

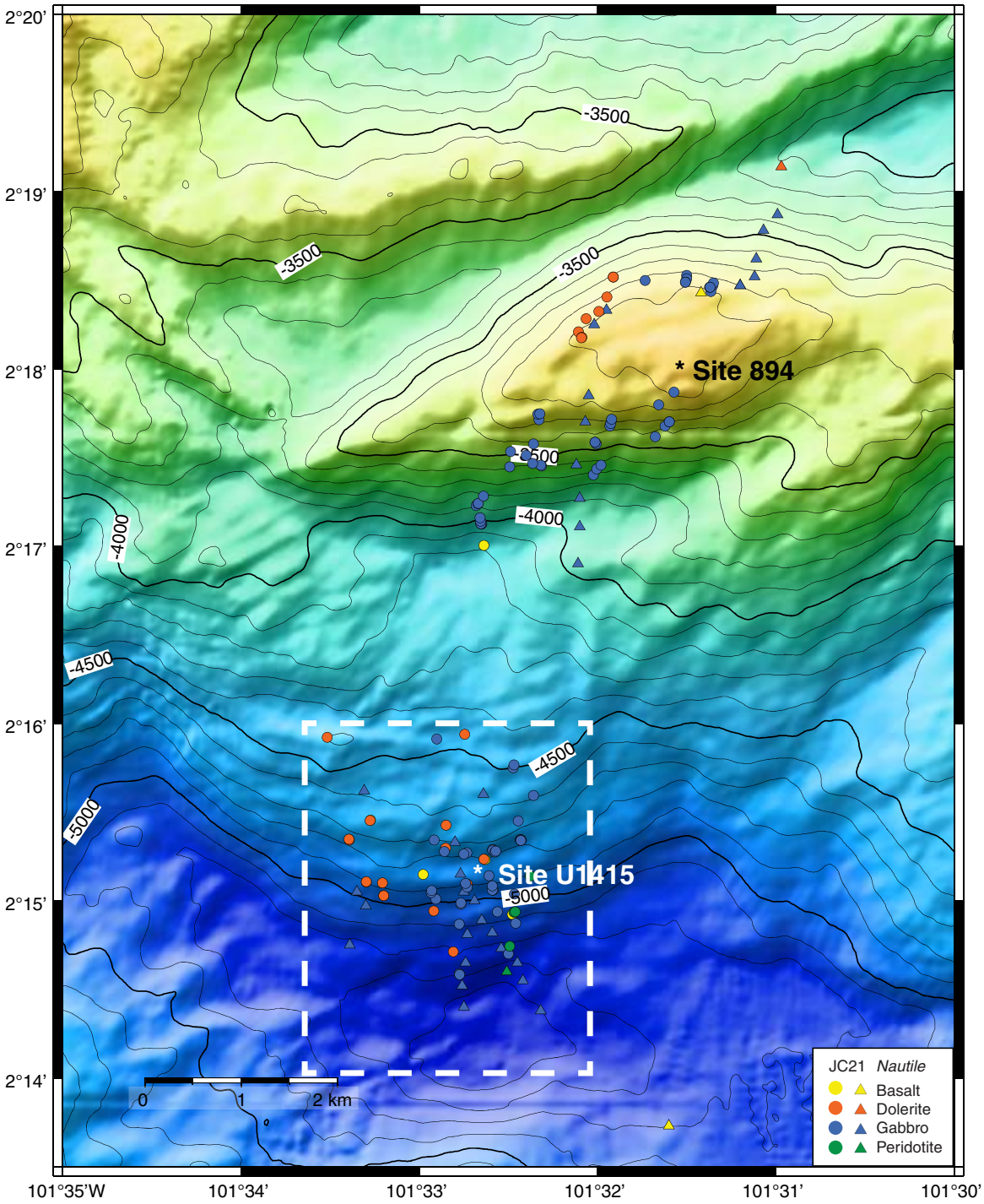

Figure F7. Contoured microbathymetry map for southern slope of the intrarift ridge between 4300 and 5400 mbsl showing the location and rock type for samples recovered during the JC21 site survey cruise by the ROV *Isis* (MacLeod et al., unpubl. cruise report, 2008) and the submersible Nautile during the NazCoPac cruise (Francheteau et al., 1990). Rock types were determined by shore-based petrographic analysis (MacLeod, unpubl. data, 2009; Hékinian et al., 1993). Microbathymetry data were acquired at a nominal altitude of ~100 m and speed of 0.3 kt by a Simrad SM2000 (200 kHz) multibeam sonar system mounted on the *Isis*. Swath widths during *Isis* surveys were ~200–350 m depending on noise and seabed characteristics (dip and reflectivity). See Figure **F6** for location within the Hess Deep Rift. The dashed line outlines the area surrounding Site U1415 shown in Figure **F18.** Note that the NazCoPac samples are not precisely located, as the dive tracks were not transponder navigated. Map prepared by D. Shillington and V. Ferrini. Contour interval = 20 m.

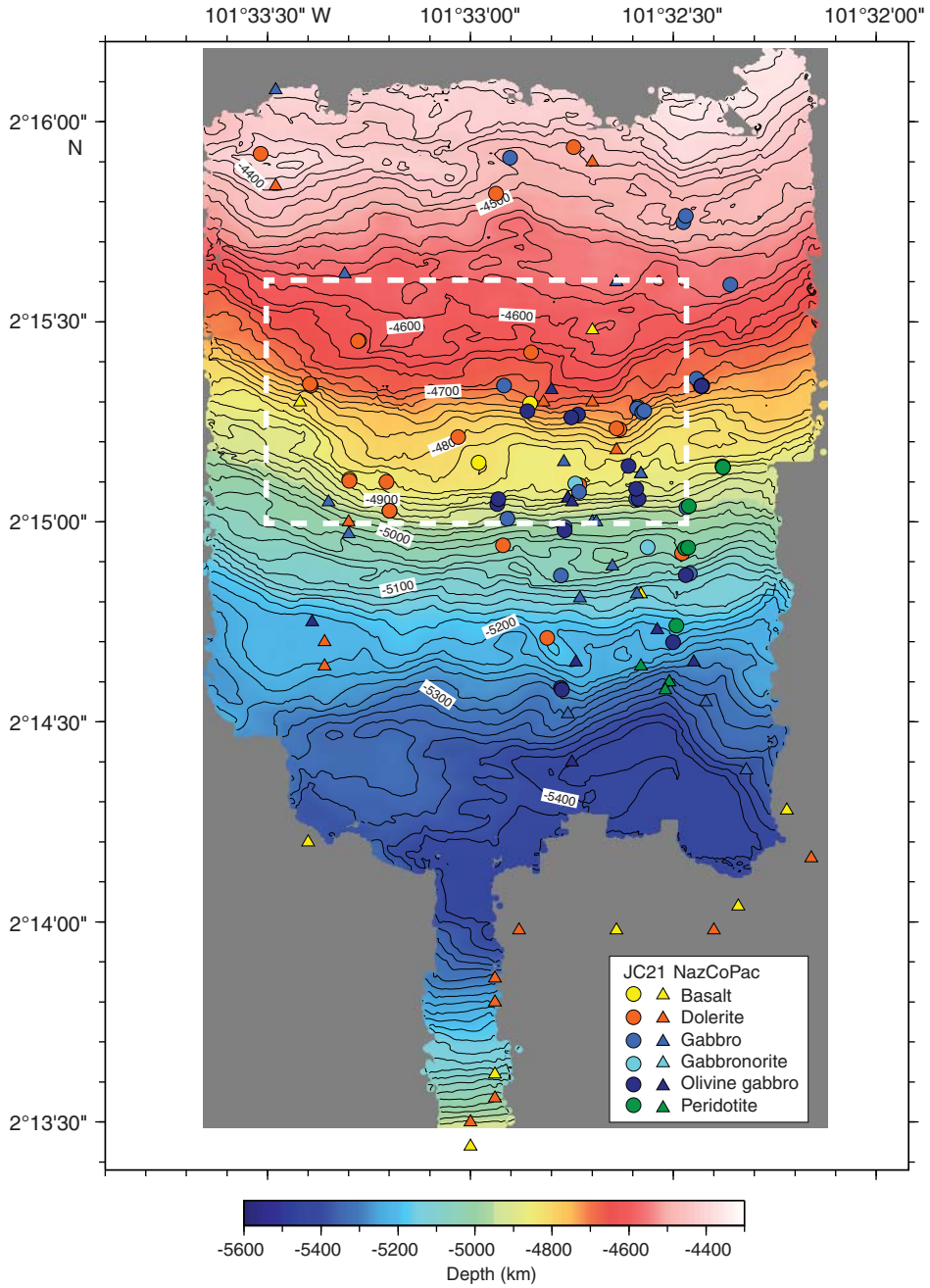

Figure F8. Bathymetric map with locations of Site U1415 drill holes. See Figure F10 for close-up of outlined area at the eastern end of the bench.

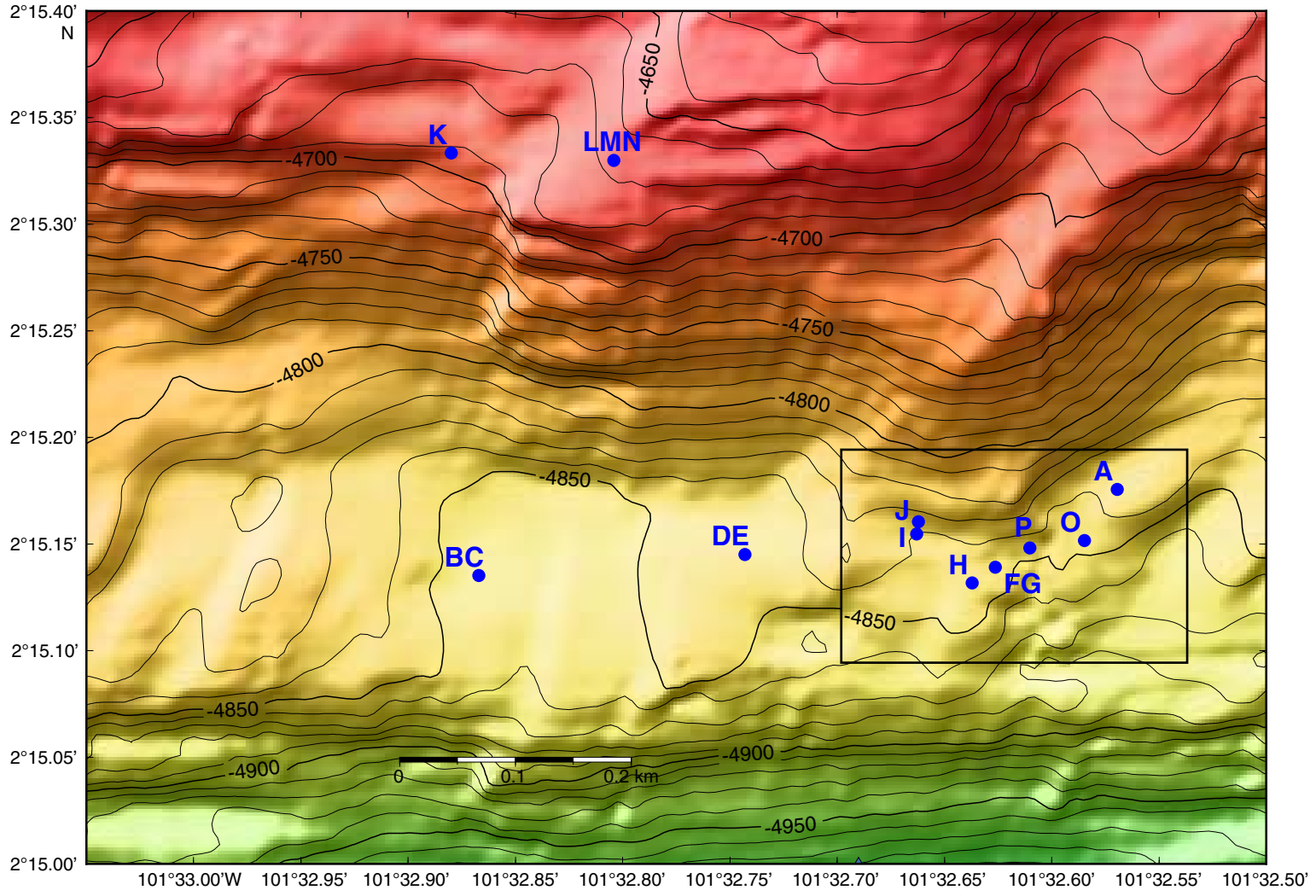

Figure F9. Bathymetric map detail of Site U1415 drill hole locations at the eastern end of the bench outlined in Figure F8.

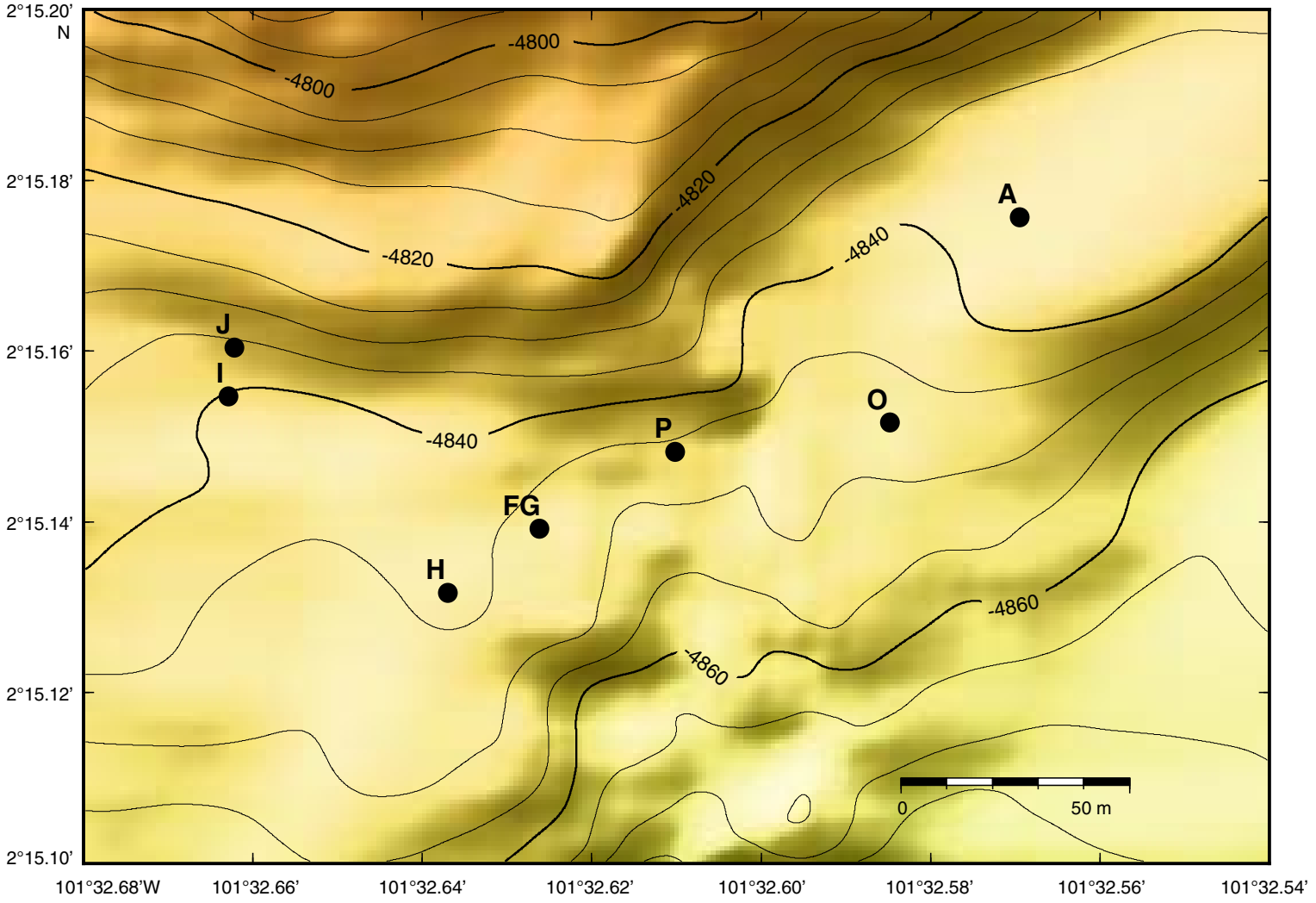

Figure F10. Pie chart showing the relative proportions of all recovered igneous lithologies except samples from ghost cores, Site 1415.

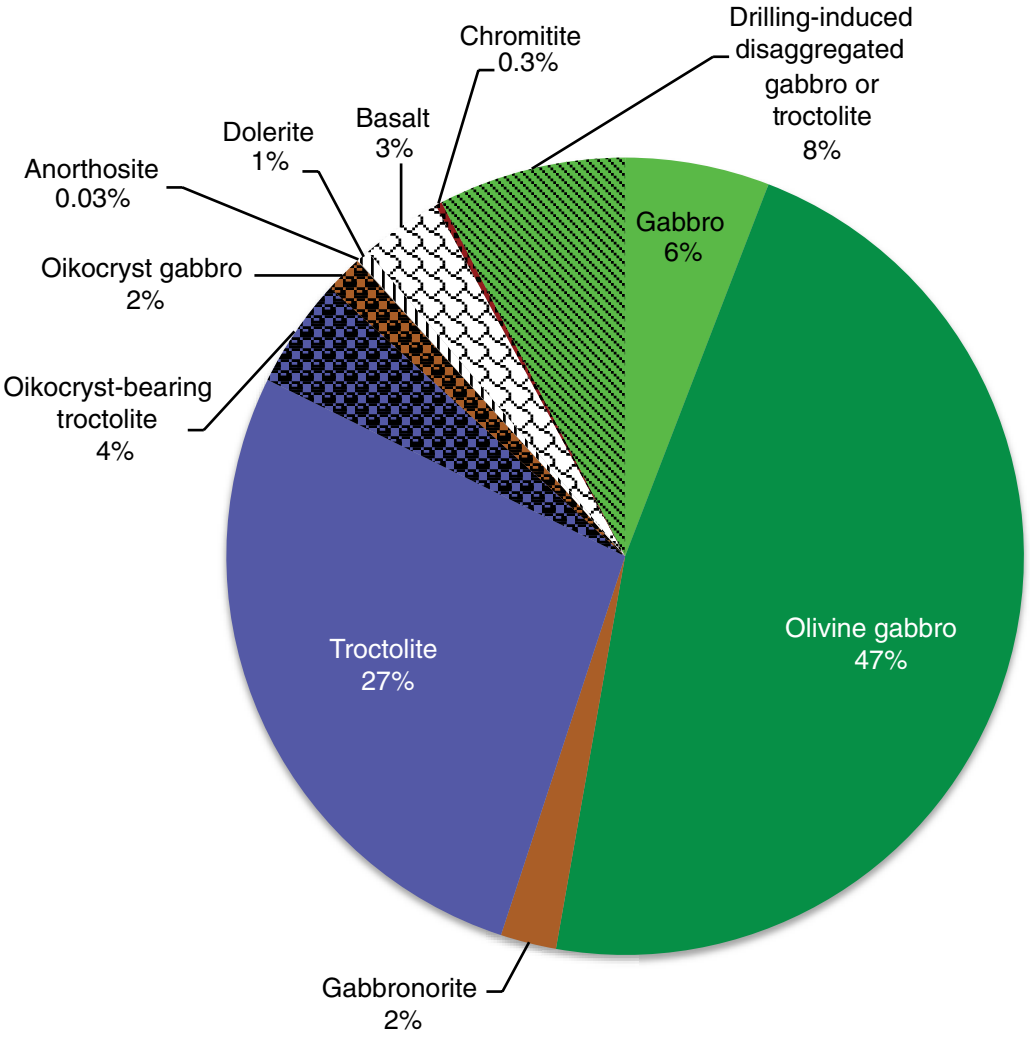

Figure F11. Summary of shipboard results, Hole U1415J. Cored intervals are shaded gray. "Others" include dolerite, basalt, altered chromitite, and cataclasite. Ghost core cluster 1 includes Cores 6G, 7G, and 15G and ghost core cluster 2 includes Cores 14G, 17G, 22G, 24G, and 25G. In dip of magmatic structures, foliations and modal layers are always subparallel. Inclination of magnetic remanence (only well-constrained values) and *P*-wave velocity were measured on discrete shipboard samples. Note that the horizontal scale for orthopyroxene (Opx) percentage is logarithmic. TS = shipboard thin sections.

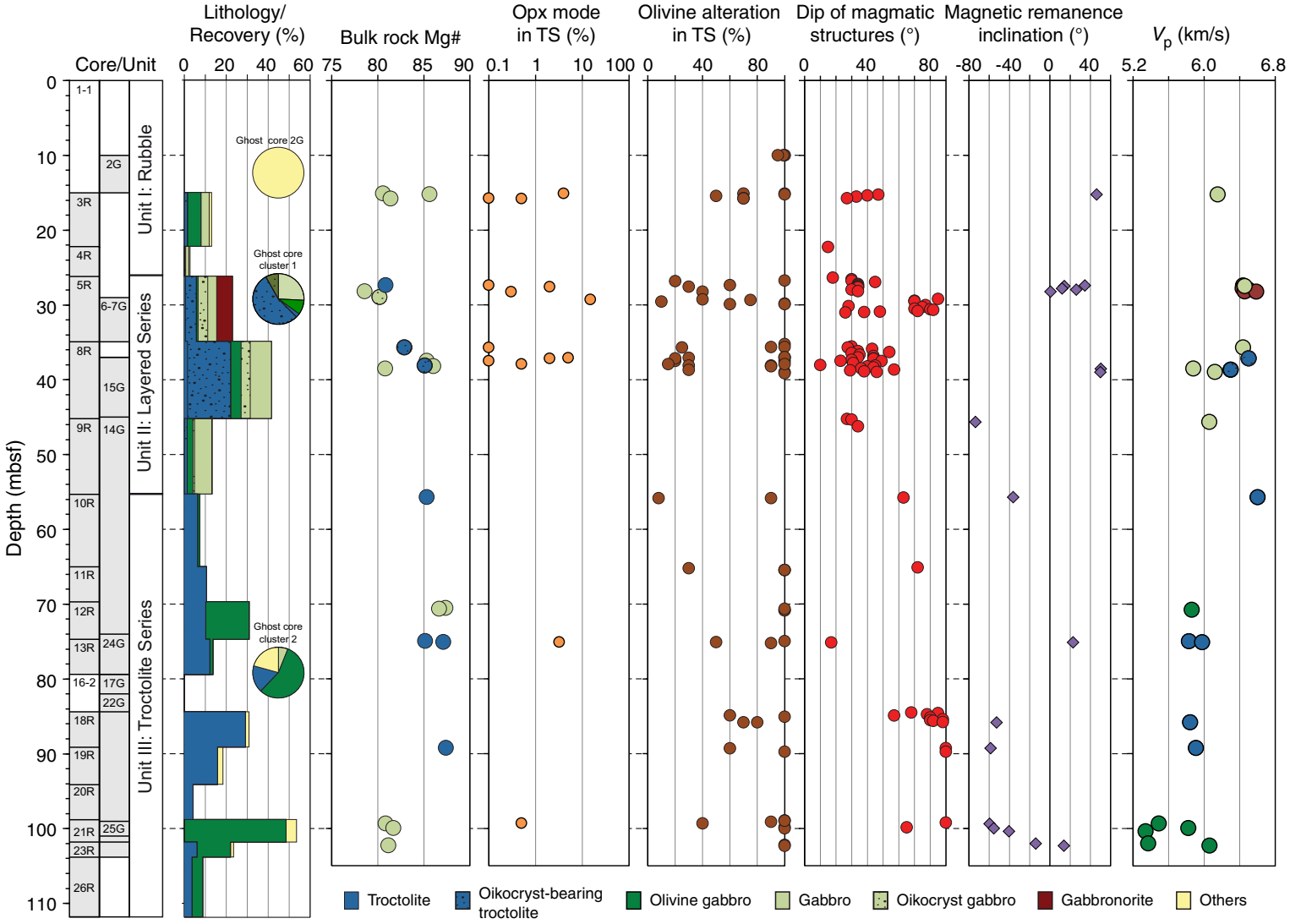

Figure F12. Summary of shipboard results, Hole U1415P. Cored intervals are shaded gray. "Others" include sand and cuttings (in core Core 2G). Inclination of magnetic remanence (only well-constrained values) and *P*-wave velocity were measured on discrete shipboard samples. Note that the horizontal scale for orthopyroxene (Opx) percentage is logarithmic. TS = shipboard thin sections.

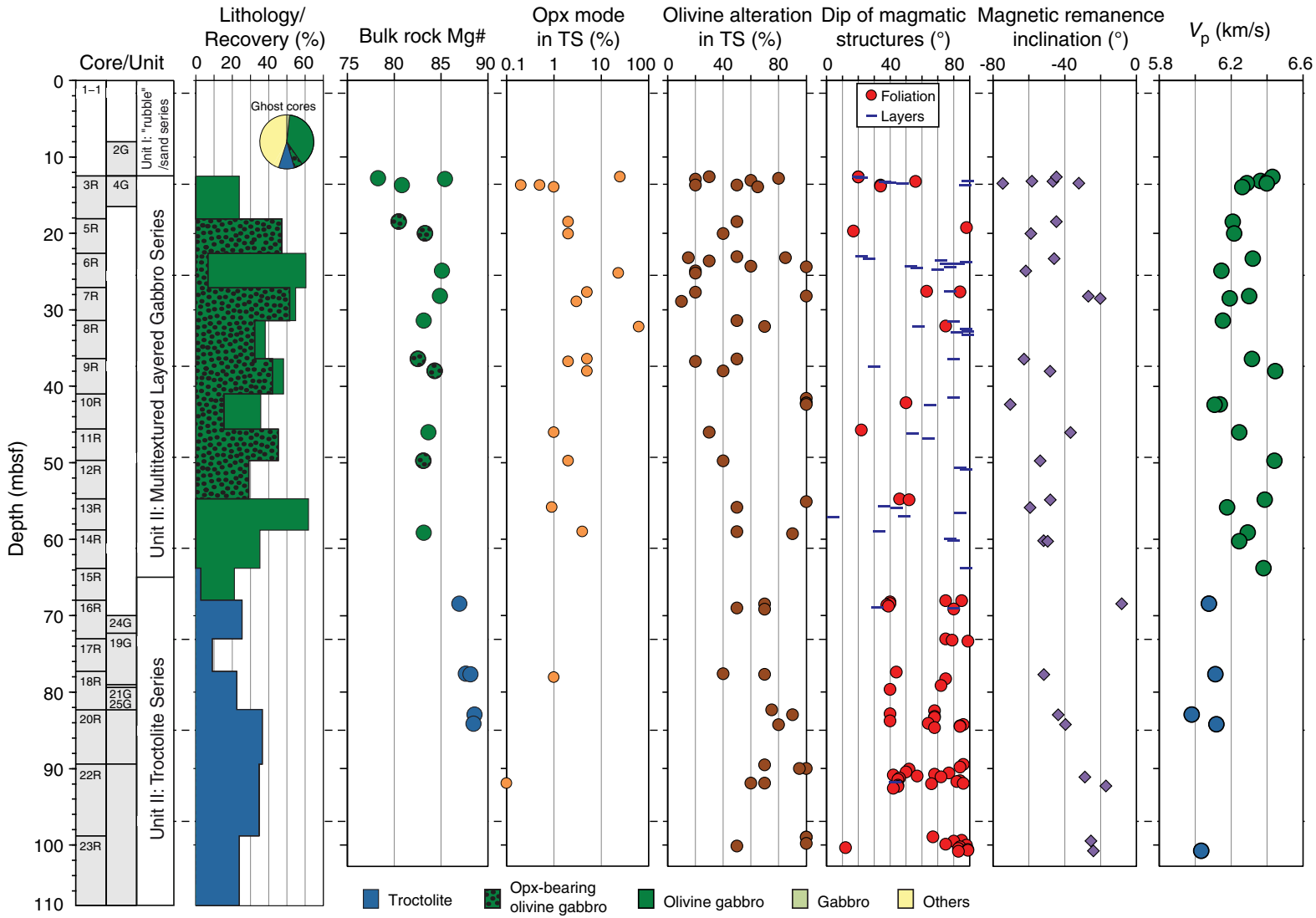

Figure F13. Core images and thin section photomicrographs of an olivine-bearing gabbronorite, Sample 345-U1415I-4R-1 (Piece 8a, 48–50 cm); Thin Section 22. **A.** Position from which the thin section was cut is marked. **B.** Plane-polarized light thin section image. **C.** Cross-polarized light thin section image. Note the subparallel alignment of tabular plagioclase and clinopyroxene following the foliation of the rock in B and C. Cpx = clinopyroxene, Ol = olivine, Opx = orthopyroxene.

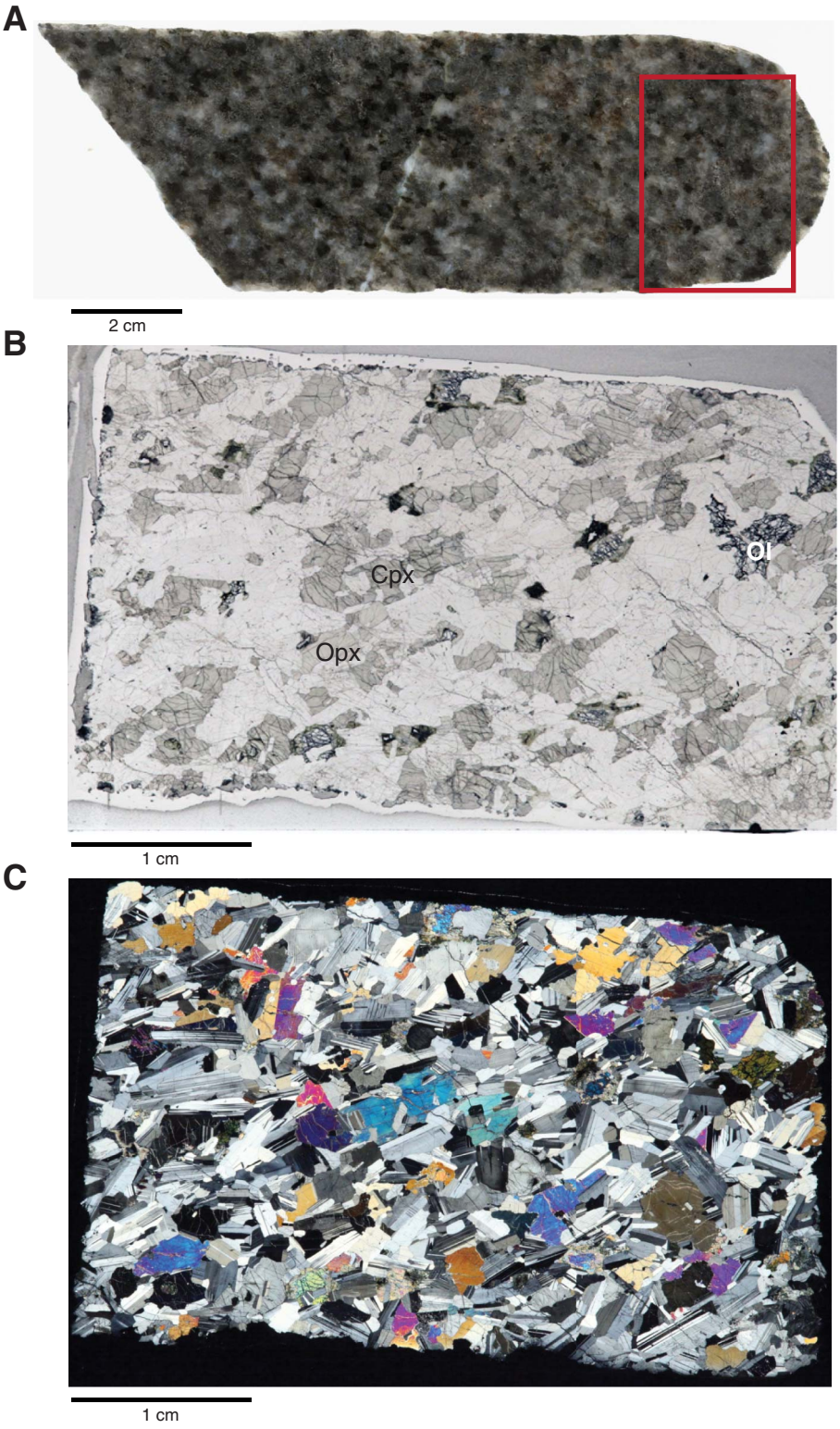

Figure F14. Photomicrographs of orthopyroxene-bearing olivine gabbro illustrating the crystallization order for olivine (Ol), orthopyroxene (Opx)/plagioclase, and clinopyroxene (Cpx) (Thin Section 118; Sample 345-U1415P-9R-1 [Piece 3, 36–41 cm]). **A.** Plane-polarized light. **B.** Cross-polarized light. White boxes indicate the locations of C and D. **C.** Skeletal olivine (Ol) is intergrown with orthopyroxene (gray) and plagioclase. **D.** Late clinopyroxene (orange) is interstitial to all phases.

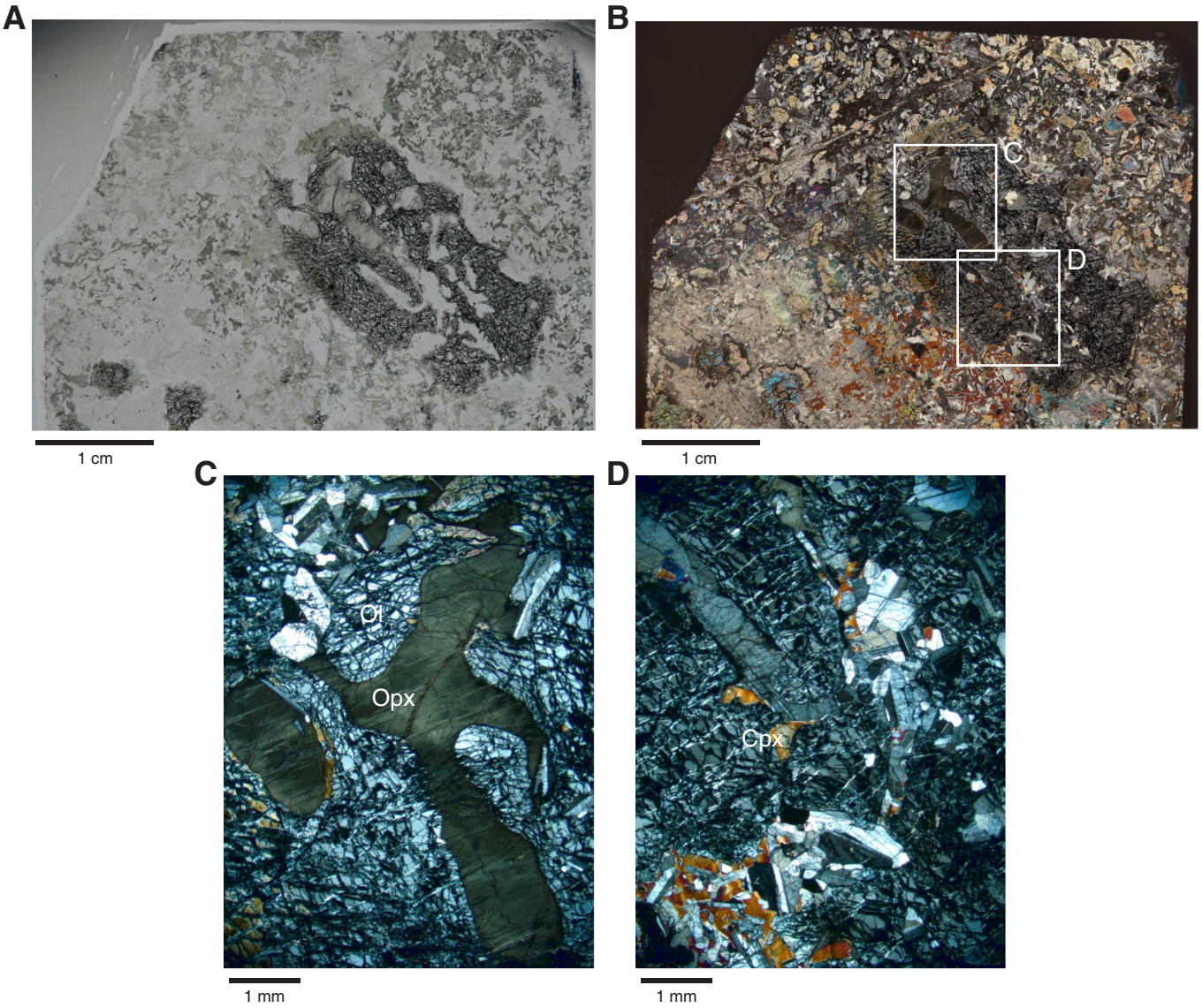

Figure F15. Core images of the typical appearance of troctolites from the Troctolite Series, Site U1415. **A.** Typical troctolite (Sample 345-U1415J-13R-1 [Piece 6, 45–52 cm]). **B.** Typical troctolite (Sample 345-U1415P-16R-1 [Piece 9, 85–94 cm]). **C.** Typical olivine-rich troctolite (Sample 345-U1415P-20R-2 [Piece 1, 3–12 cm]).

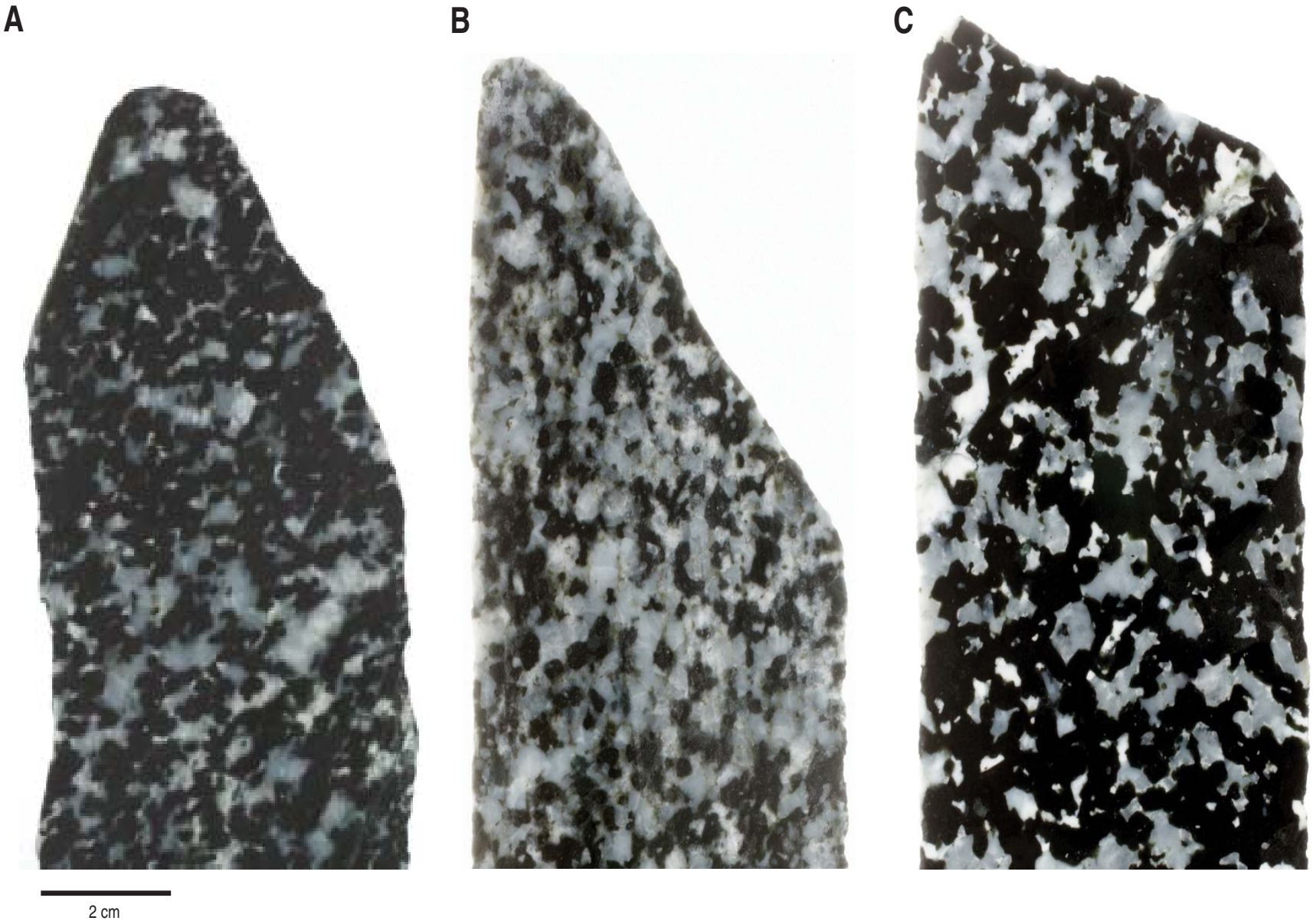

Figure F16. Core images and thin section photomicrographs of mineral textures in the Layered Series, Site U1415. **A.** Clinopyroxene oikocryst-bearing troctolite (Sample 345-U1415J-8R-3 [Piece 4b, 79–91 cm]). Box in the core image shows location of the thin section photomicrograph to the right. **B.** Close-up of skeletal olivine (arrow) in a coarse-grained, multitextured orthopyroxene-bearing olivine gabbro (Sample 345-U1415P-10R-1 [Piece 7, 56–69 cm]). Thin section photomicrograph of skeletal olivine in medium-grained troctolite (Sample 345-U1415J-10R-1 [Piece 6b, 53–55 cm]).

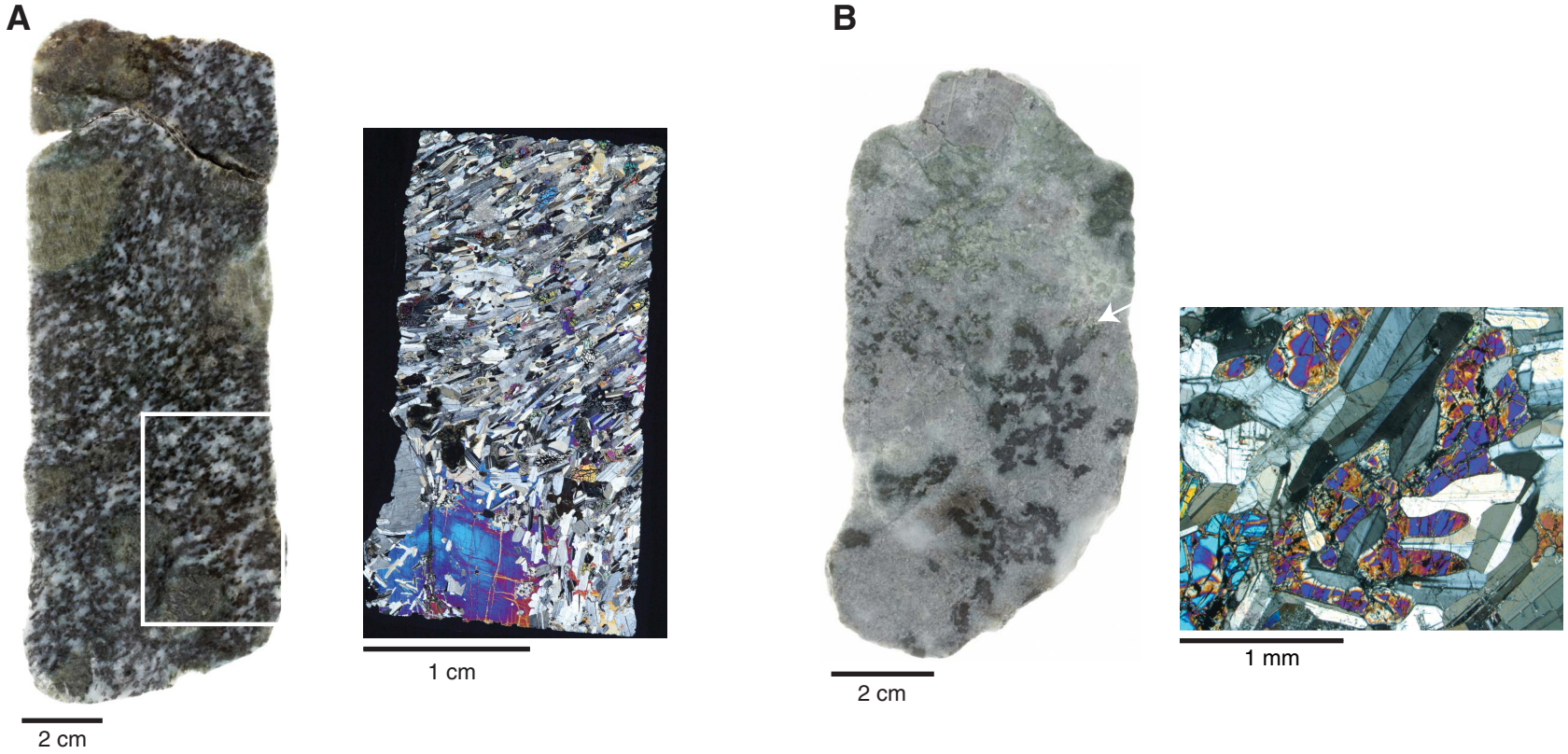

Figure F17. A. Close-up core image of clinopyroxene oikocryst-bearing troctolite (Sample 345-U1415J-8R-3 [Piece 5, 23–29 cm]). **B, C.** Thin section photomicrographs of clinopyroxene oikocryst-bearing troctolite (Thin Section 53; Sample 345-U1415J-8R-3 [Piece 5, 23–29 cm]) showing the strongly foliated troctolite with a single large clinopyroxene oikocryst with abundant randomly orientated subhedral to resorbed deformed to undeformed plagioclase chadacrysts. Ol = olivine, Cpx = clinopyroxene, Pl = plagioclase. B is under plane-polarized light, and C is under cross-polarized light.

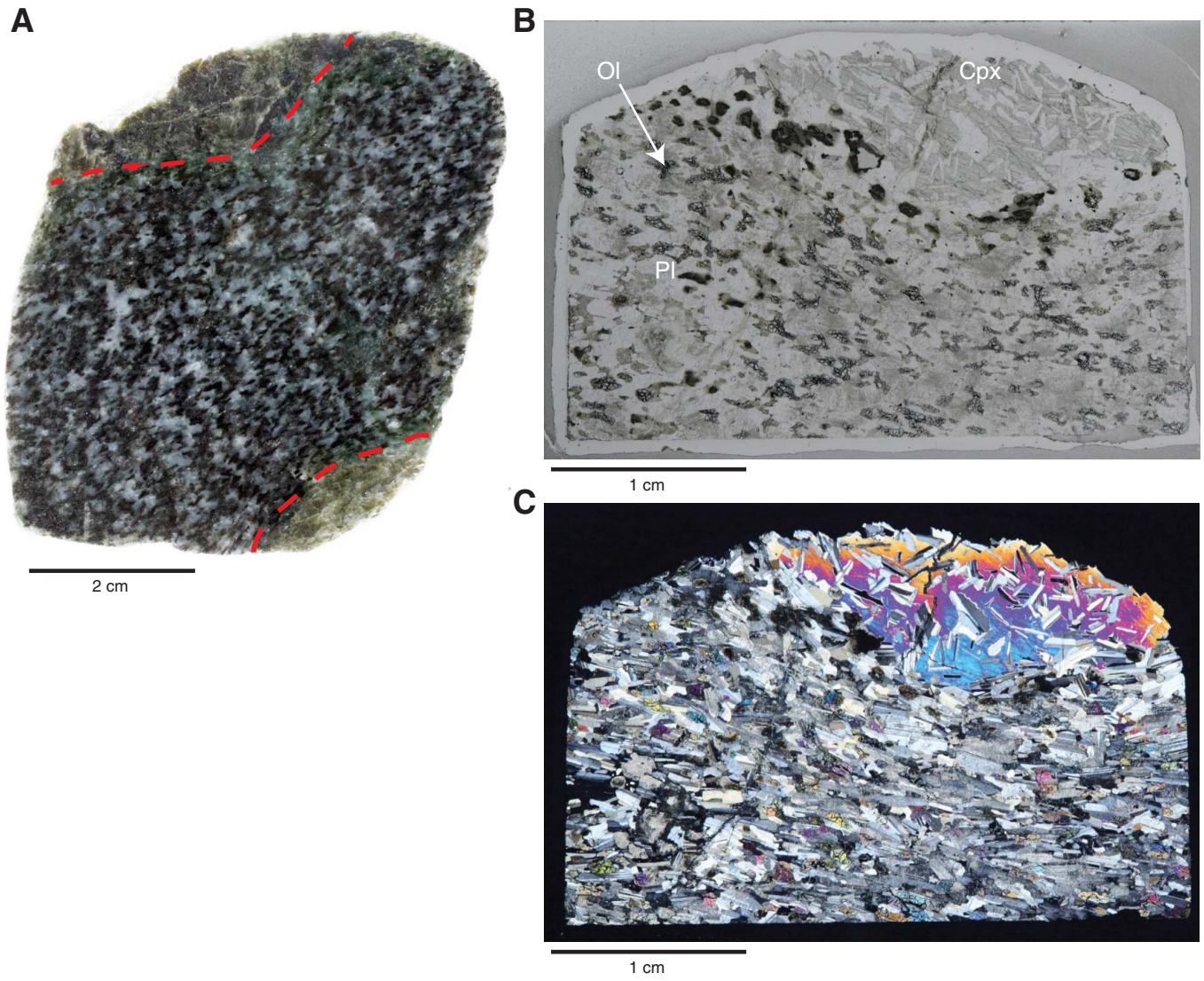

Figure F18. Core images and thin section photomicrographs of the sutured boundary between gabbro and olivine gabbro intervals in the Layered Series, Hole U1415J. Contacts are shown with red dashed lines. The boundary is defined by differences in grain size and modal mineralogy (Sample U1415J-8R-3 [Piece 7, 31–41 cm]). **A.** Close-up core image. **B, C.** Photomicrographs of Piece 7 (35–38 cm); Thin Section 54, under (B) plane-polarized and (C) cross-polarized light.

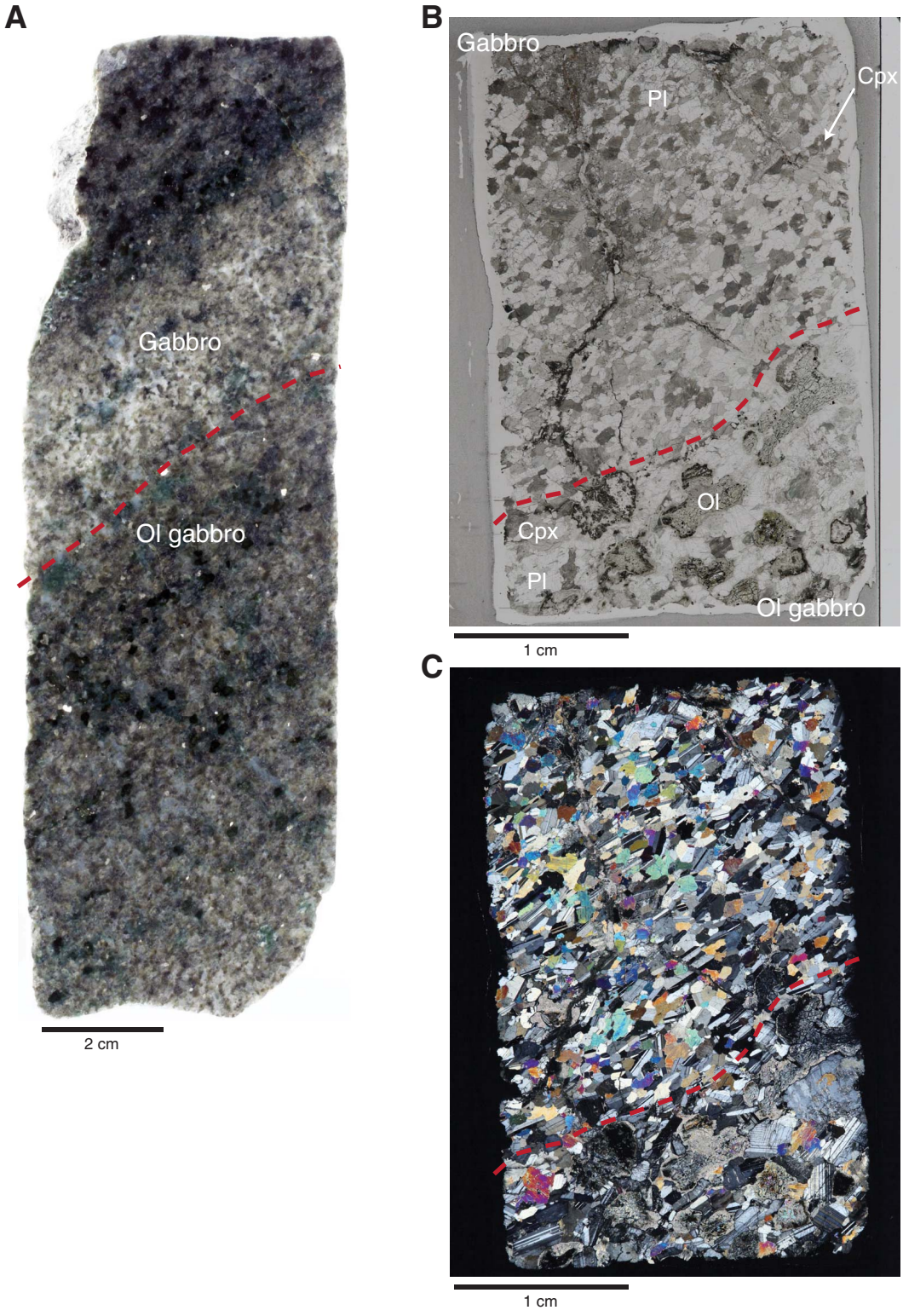

Figure F19. Plot of compositions of Cr vs. Mg# in gabbroic rocks recovered at Site U1415. For comparison, a compilation of the plutonic rocks sampled from Hess Deep (Hékinian et al., 1993; Mével, Gillis, Allan, and Meyer, 1996; Miller et al., 1996; Natland and Dick, 1996; Pedersen et al., 1996; Hanna, 2004; Kirchner and Gillis, 2012), Pito Deep (Perk et al., 2007), and other locations (Saunders et al., 1982) along the East Pacific Rise (EPR) is shown.

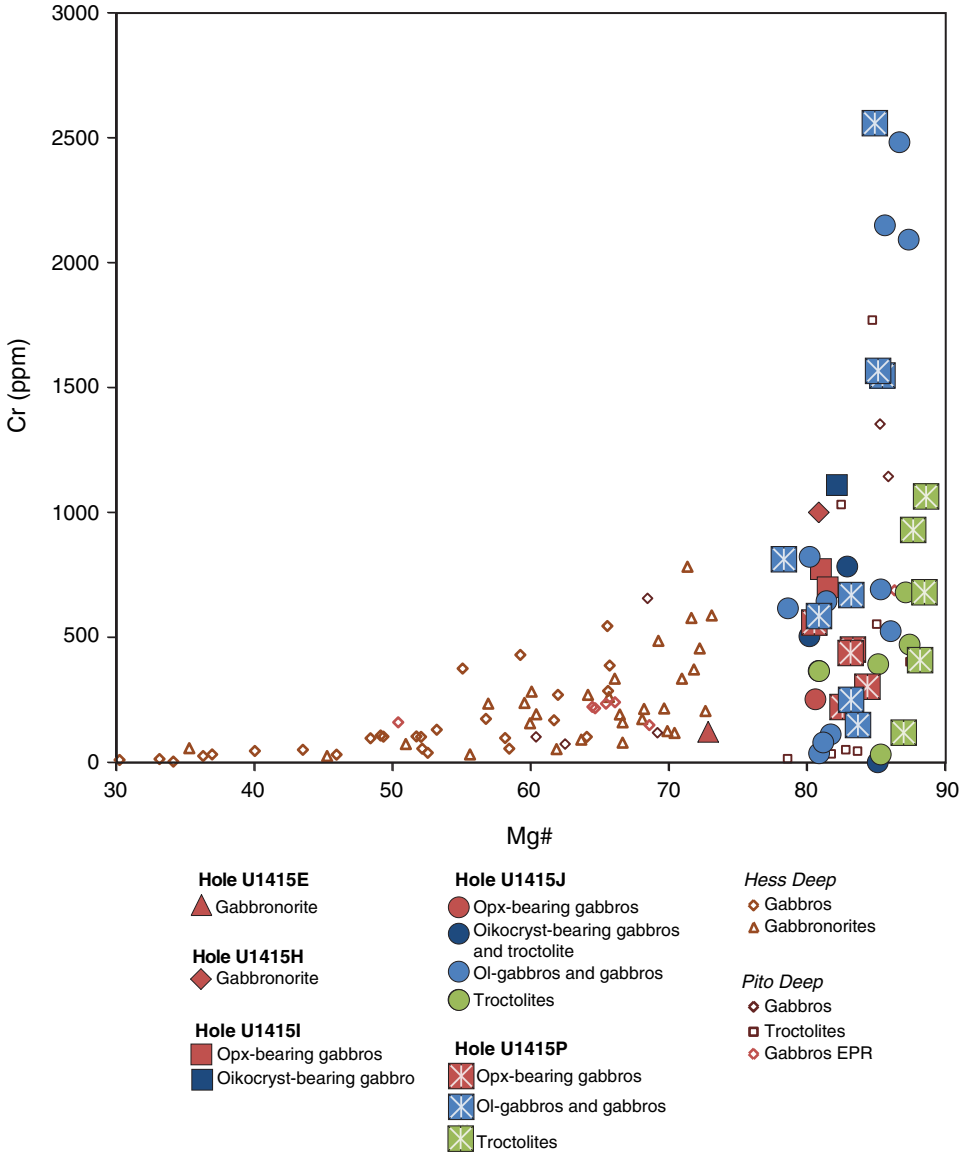

Figure F20. Core images (dry) showing styles of magmatic layering and foliation in the Layered Series, Hole U1415J and U1415P. **A.** Simple, centimeter-scale modal layering with an olivine-bearing gabbronorite layer between a troctolite layer at the top and a second, thin troctolite layer in turn overlying an olivine-bearing gabbro layer at the bottom. Olivine-plagioclase magmatic foliation is also shown (Sample 345-U1415J-5R-2 [Piece 1, 2.0–17.5 cm]). **B.** Simple, centimeter-scale modal layering consisting of a 2 cm thick olivine-bearing gabbro layer within a clinopyroxene oikocryst-bearing troctolite layer (Sample 345-U1415J-8R-2 [Piece 9, 105.5–121.0 cm]). **C.** Diffuse, subvertical (in the core reference frame) layering orthopyroxene-bearing olivine gabbro (Sample 345-U1415P-8R-2 [Piece 1, 0–16 cm]).

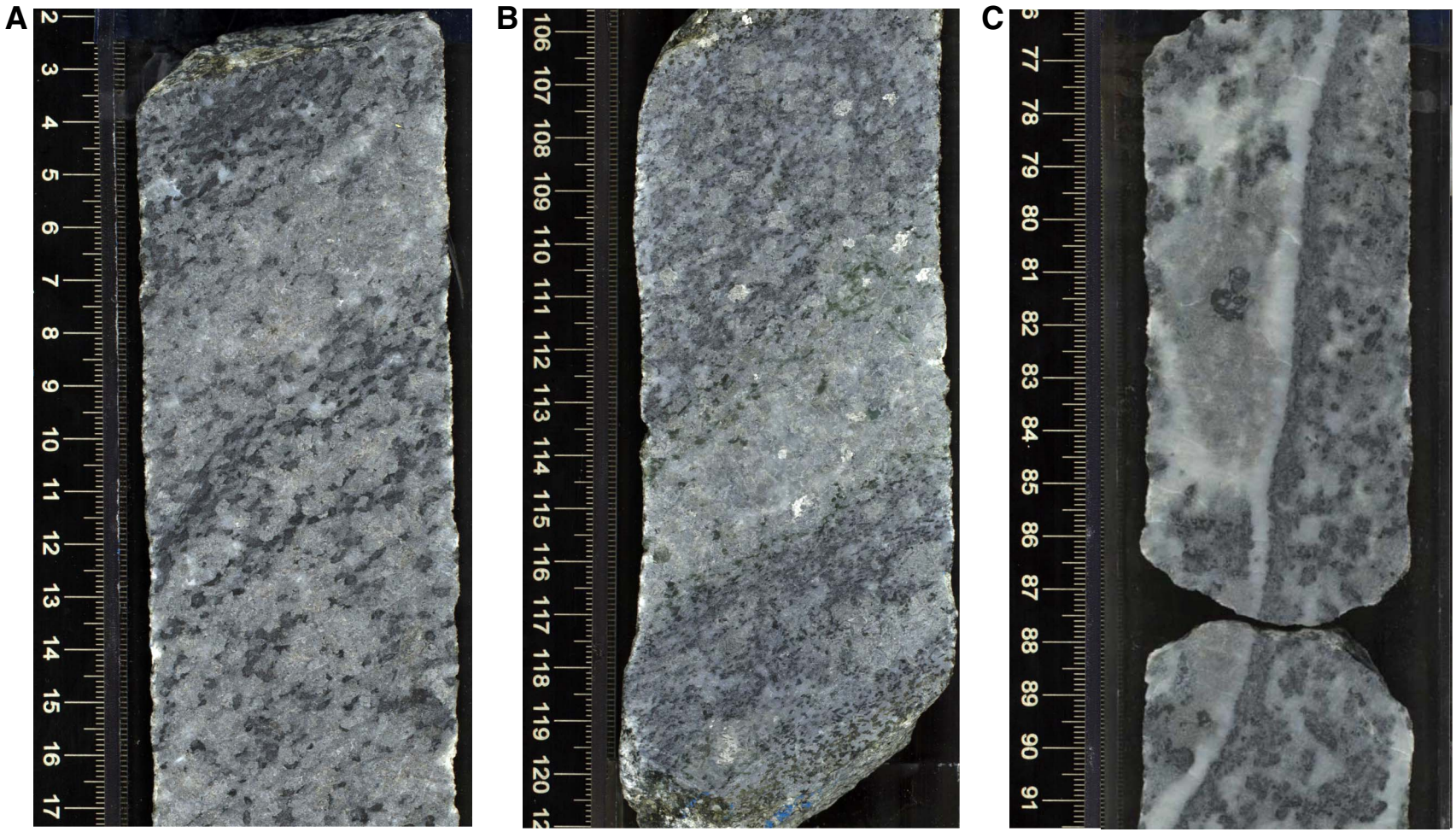

Figure F21. Plane-polarized (left) and cross-polarized (right) light photomicrographs showing variability of olivine and plagioclase replacement across different lithologies, Site U1415. Cpx = clinopyroxene, Chl = chlorite, Ol = olivine, Pl = plagioclase, Pr = prehnite, Serp = serpentine. **A.** Serpentinized olivine with a moderately well developed corona texture. Olivine is altered to chlorite along the edge of the grain in gabbro. The surrounding plagioclase is minimally fractured and slightly altered to prehnite along microfractures (Sample 345 U1415J-5R-1 [Piece 18, 138–141 cm]; Thin Section 38). **B.** Similar olivine alteration in the olivine gabbro in the Layered Series (Unit II), Hole U1415P. Coronitic textures are moderately well developed, but clinopyroxene and plagioclase are nearly fresh (Sample 345-U1415P-3R-1 [Piece 7, 113–115 cm]; Thin Section 96). **C.** Complete pseudomorphic replacement of plagioclase in association with strongly serpentinized olivine and prehnite veins in the Troctolitic Series (Unit III), Hole U1415P. Coronitic textures are absent from these relict olivine grains. (Sample 345 U1415P-22R-1 [Piece 7, 113–115 cm]; Thin Section 140).

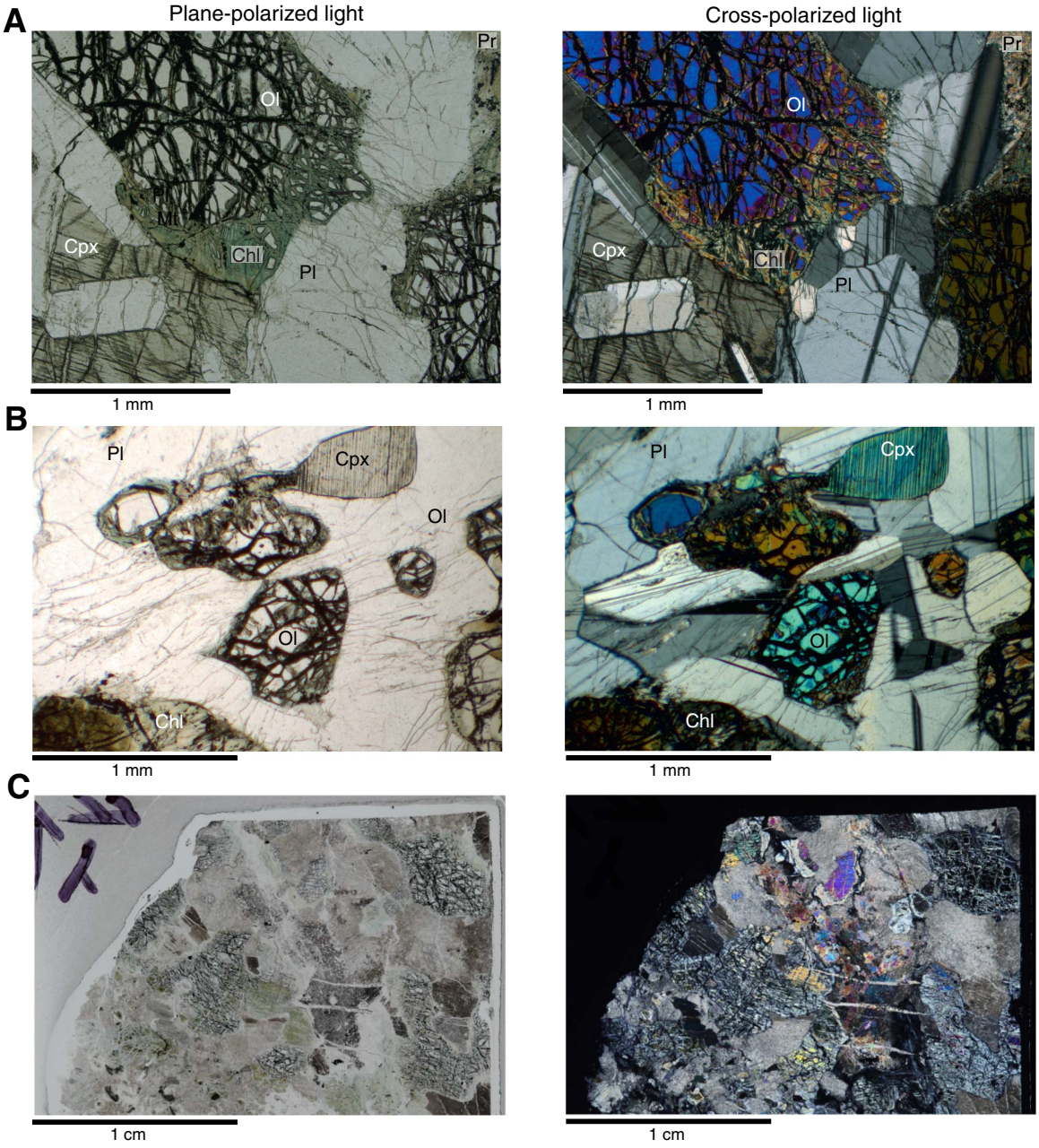

Figure F22. Schematic pressure-temperature diagram showing conditions for representative background alteration mineral assemblages in the Site U1415 gabbroic rocks. Temperature conditions are estimated from thermodynamic calculations of reaction curves using simplified bulk compositions. Reaction curves were drawn using the TWQ software (version 2.3) with the database version 1.02 (Berman, 1988, 1991). Dotted curves = displacement caused by the substitution of Mg by Fe in mafic minerals coexisting with Fo^{80} olivine, calculated using the distribution coefficients of Trommsdorff and Evans (1974). Because of the lack of appropriate constraints, pressure conditions were inferred from the assumption that gabbros originated at a normal lower crustal level and were exposed at the present position by a tectonic event under a low-temperature condition. This uncertainty is indicated by the question marks on the pressure scale. **A.** CaO- Al_2O_3-SiO_2-H_2O system with additional reactions forming prehnite + chlorite assemblage. **B.** CaO-MgO-Al_2O_3-SiO_2-H_2O system (modified after Nozaka and Fryer, 2011).

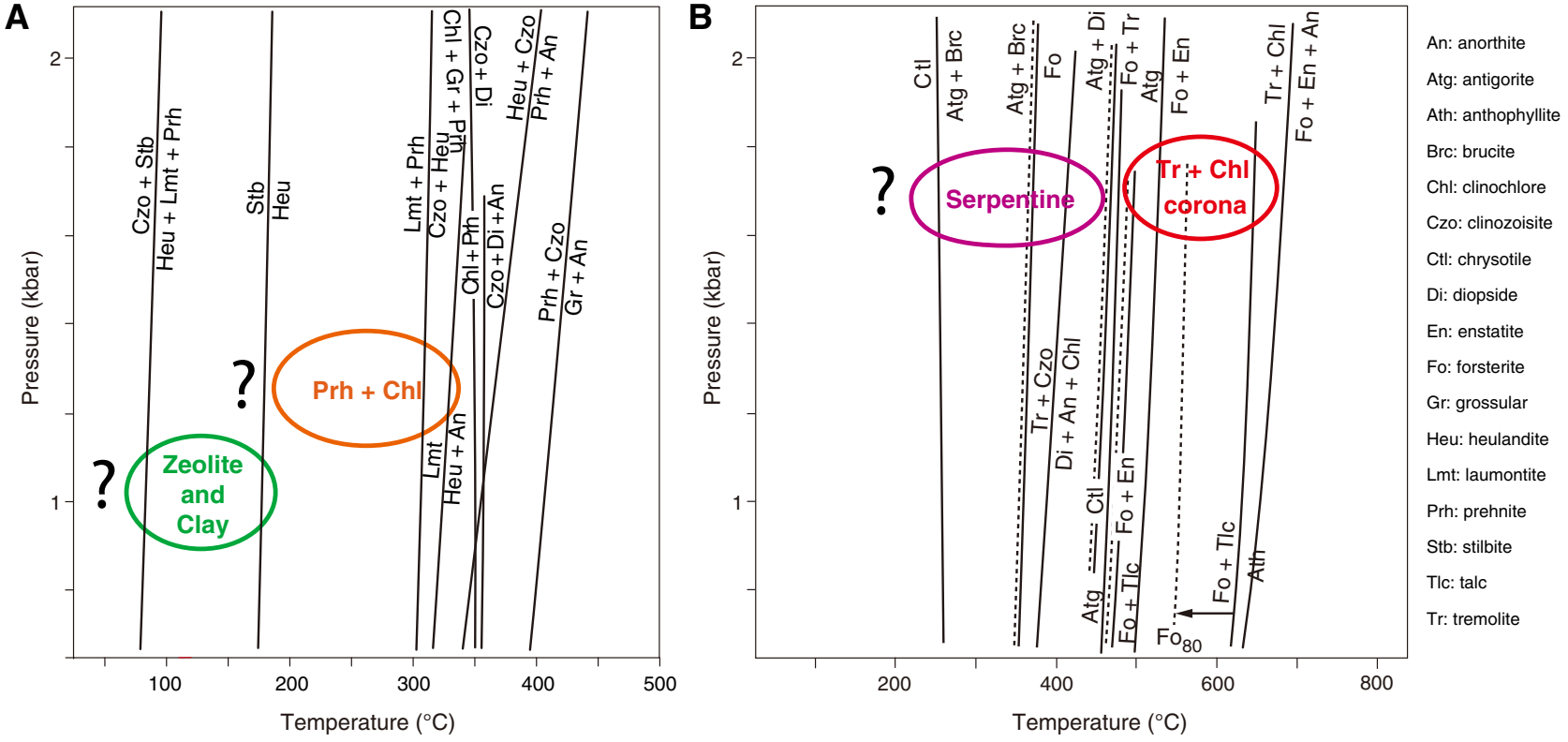

Figure F23. Plots of variation with depth of the inclination of high unblocking temperature components of magnetization in discrete samples, Holes U1415J and U1415P. Data from Hole U1415J show a downhole change from an upper unit with downward-directed magnetization to a lower unit with upward-directed magnetization, suggesting sampling of blocks that have been inverted relative to each other. More extensive data from Hole U1415P allow definition of statistically different mean inclinations from petrologically defined Units I (Layered Series) and III (Troctolitic Series), again consistent with sampling of two blocks with independent rotation histories.

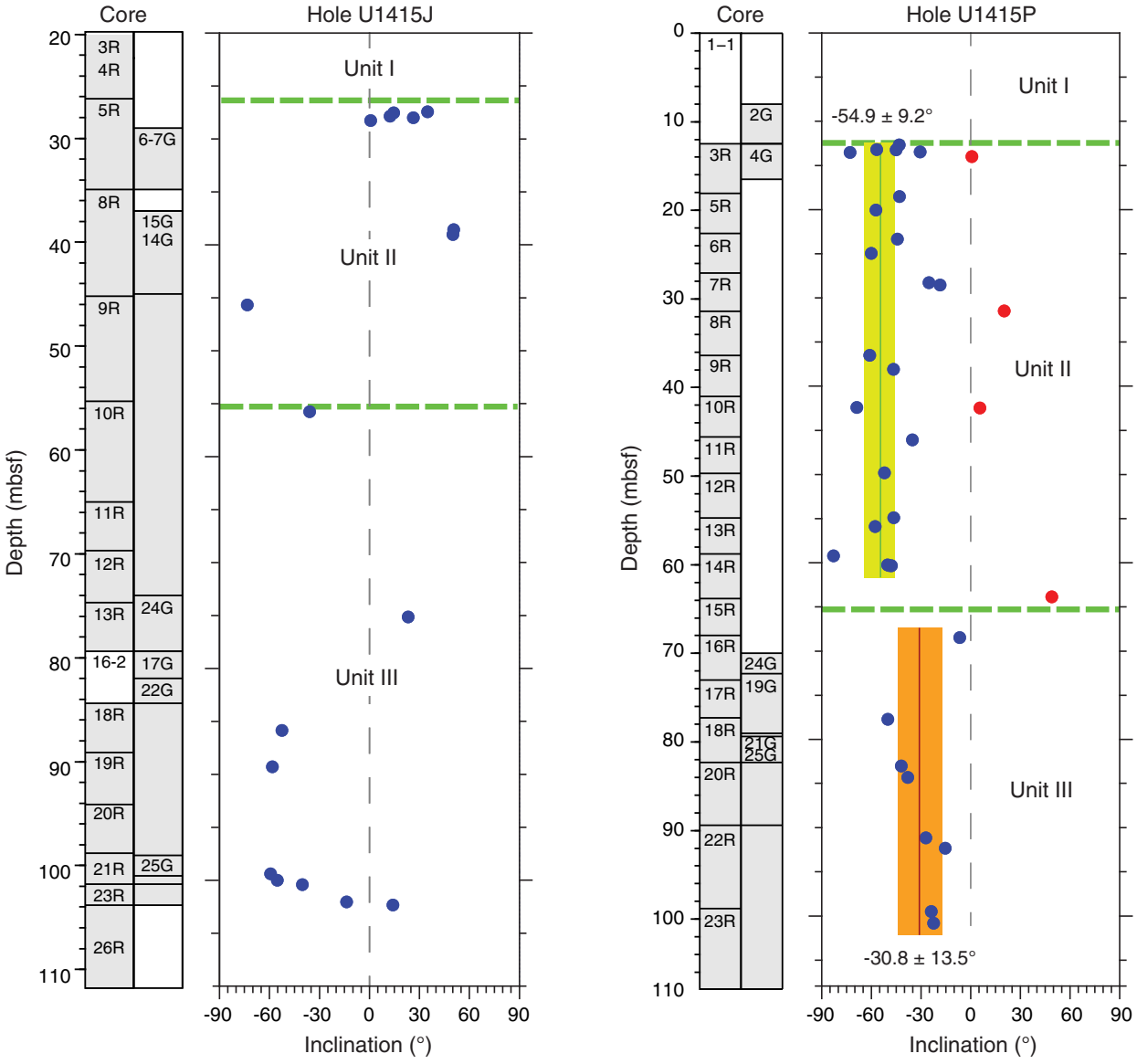

Figure F24. Examples of high-quality thermal demagnetization data, Expedition 345. **A.** Most samples displayed stable, high unblocking temperature components of magnetization after removal of drilling-induced components by low-temperature demagnetization (LTD) and of lower temperature components (probably related to alteration in some samples). **B.** Several samples from Hole U1415J were found to hold complex remanences consisting of two or three nearly antipodal components, suggesting that magnetization was acquired in different geomagnetic polarity periods. Blue arrow = drilling-induced magnetization, red/orange/green arrows = high/middle/low unblocking temperature components, solid circles = projection on to the horizontal plane, open circles = projection on to the vertical *y*-*z* plane. Inset is equal-area stereographic projection in B (solid/open symbols = lower/upper hemisphere).

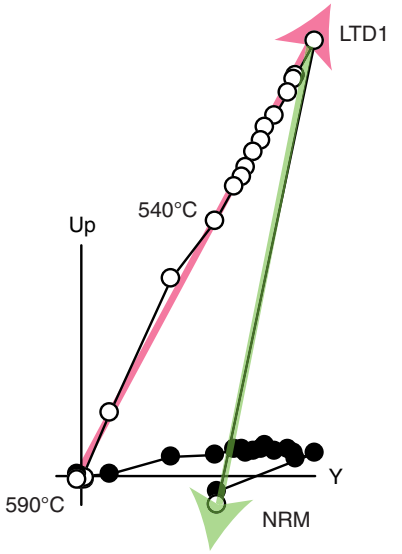

Troctolitic olivine gabbro
345-U1415P-6R-2, 92 cm
NRM = 906 m/Am

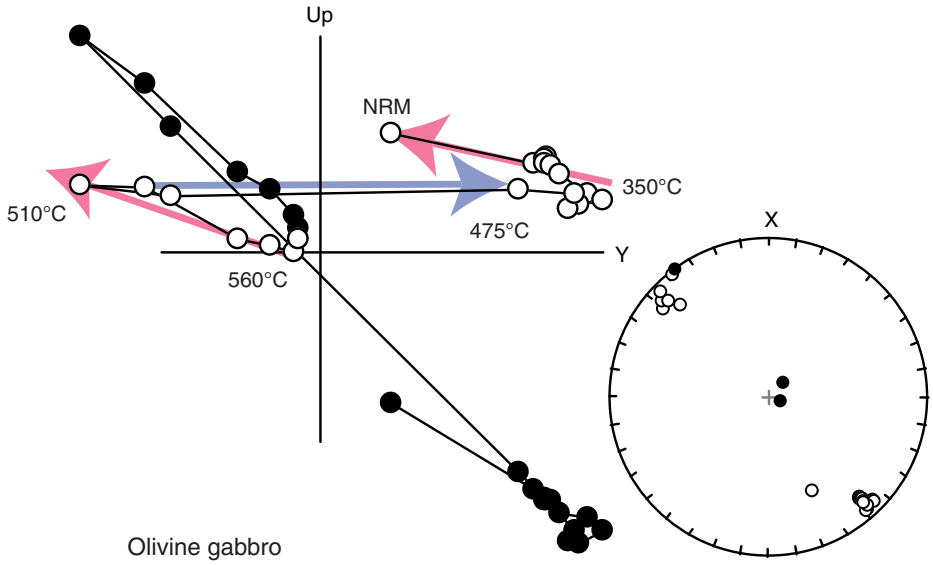

Olivine gabbro
345-U1415J-23R-1, 22 cm
NRM = 3.2 m/Am